AD-A115 805   ILLINOIS UNIV AT CHICAGO CIRCLE ELECTROMAGNETIC IMAGI--ETC   F/G 20/14
A HIGH FREQUENCY INVERSE SCATTERING MODEL TO RECOVER THE SPECUL--ETC(U)
MAY 82   B FOO   N00014-80-C-0708
UNCLASSIFIED   EMID-CL-1982-05-21-01   NL

1 OF 2
AD A
115805

COMMUNICATIONS LABORATORY

Department of Information Engineering
University of Illinois at Chicago Circle
Box 4348, Chicago IL 60680, USA

1

82

Acoustics, Electromagnetics, Optics - Circuits and Networks
Communication Theory and Systems - Electronic Devices

COMMUNICATIONS LABORATORY
Department of Information Engineering
University of Illinois at Chicago Circle
Box 4348, Chicago IL 60680, USA

A HIGH FREQUENCY INVERSE SCATTERING MODEL TO RECOVER THE SPECULAR POINT CURVATURE FROM POLARIMETRIC SCATTERING DATA

by

Bing-Yuen Foo

Communications Laboratory Report Number
EMID-CL-1982-05-21-01
M.Sc. Thesis
May 21, 1982

UNCLASSIFIED

SECURITY CLASSIFICATION OF THIS PAGE (When Data Entered)

REPORT DOCUMENTATION PAGE		READ INSTRUCTIONS BEFORE COMPLETING FORM
1. REPORT NUMBER EMID-CL-1982-05-21-01	2. GOVT ACCESSION NO. AD-A115 [illegible]	3. RECIPIENT'S CATALOG NUMBER
4. TITLE (and Subtitle) A High Frequency Inverse Scattering Model to Recover the Specular Point Curvature from Polarimetric Scattering Data		5. TYPE OF REPORT & PERIOD COVERED M.S. Thesis 6. PERFORMING ORG. REPORT NUMBER EMID-CL-82-05-18-01
7. AUTHOR(s) Bing-Yuen (Thomas) Foo		8. CONTRACT OR GRANT NUMBER(s) US ONR N00014-80-C-0708 US ARMY DAAG 29-80-K-0027 US ONR N00014-80-C-0773
9. PERFORMING ORGANIZATION NAME AND ADDRESS Electromagnetic Imaging Division Communications Laboratory, UIC P.O. Box 4348, SEO-1141, Chicago, IL. 60680		10. PROGRAM ELEMENT, PROJECT, TASK AREA & WORK UNIT NUMBERS
11. CONTROLLING OFFICE NAME AND ADDRESS Naval Air Systems Command Headquarters, AIR-310B, Washington DC 20361 Attn: Mr. James Willis		12. REPORT DATE May 21, 1982 13. NUMBER OF PAGES 16 + 145 = 161
14. MONITORING AGENCY NAME & ADDRESS (if different from Controlling Office) Chicago Branch Office, Office of Naval Research 536 S. Clark St., Chicago IL 60605 Attn: Mr. Gordon I. Lovitt		15. SECURITY CLASS. (of this report) UNCLASSIFIED 15a. DECLASSIFICATION/DOWNGRADING SCHEDULE

16. DISTRIBUTION STATEMENT (of this Report)

UNLIMITED

17. DISTRIBUTION STATEMENT (of the abstract entered in Block 20, if different from Report)

UNLIMITED

18. SUPPLEMENTARY NOTES

The findings of this report are not to be construed as an official Department of the Navy position unless so designated by other authorized documents.

19. KEY WORDS (Continue on reverse side if necessary and identify by block number)

Specular point curvature, scattering matrix element, phase difference of like polarized terms, circular polarization.

20. ABSTRACT (Continue on reverse side if necessary and identify by block number)

Based on the time-domain first order correction to the physical optics current approximation, a relationship between the phase factors of the polarimetric scattering matrix elements and the principal curvatures at the specular point of a scatterer is established.

(Continued on next page)

DD FORM 1 JAN 73 1473 EDITION OF 1 NOV 65 IS OBSOLETE
S/N 0102-LF-014-6601

UNCLASSIFIED

SECURITY CLASSIFICATION OF THIS PAGE (When Data Entered)

The above phase-curvature relationship is tested by applying it to theoretical as well as experimental backscattering data obtained for a prolate spheroidal scatterer. The results of these tests not only determine the acceptability of the phase-curvature relationship, they also point out the range of kb values over which the first order correction to the physical optics currents is valid, and which serves as a compromise range between the high frequency condition required by the curvature recovery model and the drawback to lower frequencies required to prevent critical magnification of measurement errors.

Another curvature recovery equation is derived by transforming the linear polarization basis to the circular polarization basis. The curvature recovery model is proven to satisfy the image reconstruction identities of invariant transformation. A scattering ratio is defined and its behavior is investigated at high frequencies. Its plot on the complex plane provides a simple way to help judge the accuracy of polarimetric scattering measurement, regardless of whether a linear or a circular polarization basis is used.

A HIGH FREQUENCY INVERSE SCATTERING MODEL TO RECOVER

THE SPECULAR POINT CURVATURE FROM POLARIMETRIC SCATTERING DATA

BY

BING-YUEN FOO

B.Sc. University of Manitoba

THESIS

May 21, 1982

Submitted in partial fulfillment of the requirements
for the degree of Master of Science in
Information Engineering in the Graduate College of the
University of Illinois at Chicago Circle, 1982

Chicago, Illinois

UNIVERSITY OF ILLINOIS AT CHICAGO CIRCLE

THE GRADUATE COLLEGE

May 21, 1982

I HEREBY RECOMMEND THAT THE THESIS PREPARED UNDER MY SUPERVISION BY Bing-Yuen Foo

ENTITLED A High Frequency Inverse Scattering Model to Recover the Specular Point Curvature from Polarimetric Scattering Data

BE ACCEPTED IN PARTIAL FULFILLMENT OF THE REQUIREMENTS FOR THE DEGREE OF Master of Science (Electrical Engineering)

Dr. Wolfgang-M. Boerner Wolfgang-M. Boerner

In Charge of Thesis

Recommendation concurred in

Dr. Wolfgang-M. Boerner Wolfgang-M. Boerner

Dr. Bruce H. McCormick Bruce H. McCormick

Dr. Wai-Kai Chen

Dr. Piergiorgio L. E. Uslenghi Piergiorgio Uslenghi

Dr. J. Richard Huynen (ext.) J. R. Huynen

Committee on Final Examination

Dr. Jonathan D. Young (ext.) (ACCEPTED BY CORRESPONDENCE)

Dr. Sujeet K. Chaudhuri (ext.) (ACCEPTED BY CORRESPONDENCE)

D517

ABSTRACT

Based on the time-domain first order correction to the physical optics current approximation, a relationship between the phase factors of the polarimetric scattering matrix elements and the principal curvatures at the specular point of a scatterer is established.

The above phase-curvature relationship is tested by applying it to theoretical as well as experimental backscattering data obtained for a prolate spheroidal scatterer. The results of these tests not only determine the acceptability of the phase-curvature relationship, they also point out the range of kb values over which the first order correction to the physical optics currents is valid, and which serves as a compromise range between the high frequency condition required by the curvature recovery model and the drawback to lower frequencies required to prevent critical magnification of measurement errors.

Another curvature recovery equation is derived by transforming the linear polarization basis to the circular polarization basis. The curvature recovery model is proven to satisfy the image reconstruction identities of invariant transformation. A scattering ratio is defined and its behavior is investigated at high frequencies. Its plots on the complex plane provides a simple way to help judge the accuracy of polarimetric scattering measurement, regardless of whether a linear or a circular polarization basis is used.

ACKNOWLEDGMENTS

I am deeply indebted to my adviser, Dr. Wolfgang-Martin Boerner, who introduced to me the topic of Electromagnetic Inverse Scattering, continually exposed me to different research fields, and guided the research and the completion of this thesis. His enthusiasm, his dynamic attitude and dedication to research, which I admire, impress me profoundly.

I am also indebted and grateful to Dr. Sujeet Kumar Chaudhuri, who enlightened me with much patience during his stay in Chicago in 1981. Not only did he derive the phase-curvature relationship described in this thesis, but he also kindly provided the theoretical data for numerical verification. Without the full direction and help of Dr. Boerner and Dr. Chaudhuri, the completion of this thesis would not have been possible.

I would like to express my deep gratitude to Dr. Jonathan D. Young, of the Electro-Science Laboratory at the Ohio State University, Columbus, for providing the smoothened scattering data, without which many insights of the numerical investigation would not have been obtained. I also thank him for allowing me to view the complete procedure of obtaining the measurement data during a recent visit of the EMID-CL-UIC research staff to the Electro-Science Laboratory on March 25 and 26, and for his patient explanations, illuminating discussions and instructions for the appropriate use of the data.

I am extremely grateful to Mr. Benedict Chuk-Min Ho, who patiently helped me comprehend the theory of Electromagnetic Inverse Scattering. The many invaluable discussions, suggestions and continual assistance must be acknowledged.

This work was supported, in parts, by the National Science and Engineering Research Council of Canada under Operating Grants A7240 and A3804, the U.S. Office of Naval Research under Grant N00014-80-C-0773, the Naval Air Systems Command Research Program under N00019-80-C-0620, and the U.S. Army Research Office under D-AAG-28-80K-0027. I am very thankful for all the financial support I received during my studies and the preparation of this thesis.

I would like to thank M.K who has been giving me constant encouragement and incentive.

Special thanks are due to Mr. Chau-Wing Yang for his fruitful discussions and great assistance in the preparation of this thesis.

Special thanks are also due to Miss Kathleen Sluis and Miss Sue Bourgart for arranging to let me use the facilities in their office during the typing of the manuscript.

Last but not least, I would like to acknowledge my colleagues in the Electromagnetic Imaging Division, namely, Mr. C.Y. Chan, Mr. S. Saatchi, Mr. M. Davidovitz, Mr. J. Nespor, Mr. B. Beker, Mr. A. Manson, Mr. V. Mirmira and Mr. D. Kruchten, for their encouragement and stimulating discussions.

TABLE OF CONTENTS

LIST OF SYMBOLS

α	polarization angle defined in Figure 3.1
β	angle defined in the general form of [T]
∇	the del operator
λ	wavelength
λ_s	eigenvalue in (4.36)
$\mathcal{L}$	an operator defined in section 2.2
ϕ_d	relative phase of like polarized elements, $\phi_{22} - \phi_{11}$ in the linear polarization scattering matrix
ϕ	aspect angle defined in Figure 3.2
ϕ_1, ϕ_2, ϕ_3, ϕ_4	phase angles defined in the general form of [T]
ϕ_{AA}	phase of S_{AA}
ϕ_{BB}	phase of S_{BB}
ϕ_{11}, ϕ_{22}, ϕ_{12}	phases of the elements of the scattering matrix
τ	retarded time
θ	phase of $A_F(k)$
$\tilde{R}$	ratio of like polarized elements, S_{22}/S_{11} in the linear polarization scattering matrix
R	magnitude of $\tilde{R}$
ε_o	patch radius
σ_{max}	optimum radar cross-section
$\hat{a}_1$, $\hat{a}_2$	arbitrary orthonormal vectors
a	semi-minor axis of prolate spheroid
$\hat{a}_{Hi}$	unit vector in the direction of the incident magnetic field
$\hat{a}_{Hr}$	unit vector in the direction of receiver polarization
$\hat{a}_n$, $\hat{n}$	normal vector to surface of scatterer

$\hat{a}_R$	unit vector of $\vec{R}$
$A(t)$, $A_F(k)$	silhouette area of scatterer and its Fourier Transform
(A,B), $(\hat{A},\hat{B})$	linear polarization basis with orthonormal vectors A, B
$\vec{A}_p$	vector potential due to surface current
$\hat{a}_u$	unit vector in the u-direction at specular point
$\hat{a}'_u$	unit vector in the u-direction at integration point
$\hat{a}_v$	unit vector in the v-direction at specular point
$\hat{a}'_v$	unit vector in the v-direction at integration point
b	semi-minor axis of prolate spheroid
C	semi-major axis of prolate spheroid
[C], [C(RL)]	circular polarization scattering matrix with basis (R,L)
C_{RR}, C_{LL}, C_{RL}	elements of [C(RL)]
c	free space velocity of electromagnetic wave
De	denominator defined in section 3.2.1
D	the scattering ratio defined in section 4.2
e	relative phase error
$\underline{E}^i$	incident electric field polarization vector
E^i_H, E^i_V	components of $\underline{E}^i$ in the horizontal and vertical directions
E^i_L, E^i_R	components of $\underline{E}^i$ in the left circular and right circular directions
$\underline{E}^s$	scattered electric field polarization vector
E^s_L, E^s_R	components of $\underline{E}^s$ in the left circular and right circular directions
E, F, G	the coefficients of the first fundamental form of a surface

$\underline{h}$	polarization vector
(H,V), $(\hat{H},\hat{V})$	linear polarization basis with unit vectors in the horizontal and vertical directions
$\vec{H}$	total magnetic field
$\vec{H}_i$	incident magnetic field
$\vec{H}_s$	scattered magnetic field
$\vec{H}_{s(po)}$	physical optics scattered magnetic field impulse response
$\vec{H}_{s(po1)}$	first order correction to physical optics far-field impulse response
H_{ui}	component of $\vec{H}_i$ in the u-direction
H_{vi}	component of $\vec{H}_i$ in the v-direction
$\hat{i}$, $\hat{j}$, $\hat{k}$	unit Cartesian vectors
Im	imaginary part of
$\vec{J}$	surface current density
$\vec{J}_{po}$	physical optics current
$\vec{J}_{po1}$	first order correction to physical optics current
$\vec{J}_{\varepsilon}$	correction current term
J_u	scalar current component in the u-direction
J_v	scalar current component in the v-direction
$\vec{k}$	vector k(frequency) space
k	wave number
K_u	principal curvature in the u-direction
K_v	principal curvature in the v-direction
K	Gaussian curvature
L, M, N	coefficients of the second fundamental form of a surface
$(\hat{R},\hat{L})$	circular polarization basis in the right-circular and left-circular directions
[P]	power scattering matrix

$\vec{r}$	position vector to observation point
$\vec{r}'$	position vector to integration point
r_o	radar range
$\vec{R}$	$\vec{r} - \vec{r}'$
R	magnitude of $\vec{R}$
Re	real part of
$\vec{r}(u,v)$	curvilinear mapping of surface
S	surface of integration
S_ε	integration patch
[S],[S(A,B)],[S(AB)]	scattering matrix with general polarization basis (A,B)
S_{11}, S_{22}	like polarized elements of scattering matrix [S]
S_{12}, S_{21}	cross-polarized elements of scattering matrix [S]
S_{AA}, S_{BB}, S_{AB}	elements of scattering matrix with polarization basis (A,B)
[T], [T(RL;HV)]	unitary matrix which transforms linear polarization with basis (H,V) to circular polarization with basis (R,L)
Tr	trace of a square matrix
t	time
u, v	curvilinear coordinates of surface
x, y, z	Cartesian coordinates of surface

LIST OF FIGURES

FIGURE PAGE

CHAPTER I

INTRODUCTION AND LITERATURE REVIEW

1.1 Introduction

When a conducting object is illuminated by electromagnetic radiation, *in general*, radiation is scattered in all directions by the object. The problem of direct scattering is that of determining the scattered field in all directions when the properties of the incident field as well as those of the object are known. The problem of far-field inverse scattering is defined as that of extracting the geometrical properties and/or *reconstructing* the shape of the scatterer under interrogation, given the incident field within the neighborhood of the scatterer and the scattered far field. This problem is fundamental to problems such as radar target classification, discrimination and identification in remote sensing and surveillance (Boerner, 1978, 1980).

It has been demonstrated that an electromagnetic scatterer acts as a sensitive polarization transformer, depending on its profile. Thus, depolarization effects must be taken into account in this problem of vector nature. Sinclair (1948) introduced the *scattering matrix* of a radar target for complete depolarization characterization. The question then arises as to what geometrical properties of the surface profile of the target may be extracted from the scattering matrix of the target. A study of differential geometry reveals that for a *smooth*, *convex* shape, there exists a pair of lines of principal curvatures orthogonal to and intersecting with each other at any specular point on the scatterer's surface. Since the principal

curvatures at a point totally determine any other normal curvatures at the same point, these two principal curvatures serve as a complete curvature characterization at the specular point of the scatterer. It will be shown in this thesis that if the polarization of the incident magnetic field is in one of the directions of the principal curvatures at the specular point of interest, then the cross-polarized backscattered returns vanish. This kind of null polarizations generates the idea that the principal curvatures are possibly related to the non-zero co-polarized backscattered returns, and it also generated many recent studies in radar polarimetry. This specific degeneracy of target depolarization phenomenology provides the initial motivation for writing this thesis.

1.2 Literature Review

Inverse techniques cover a vast amount of literature and they have been developed in many otherwise diverse fields of physical sciences where the characteristics of a medium are estimated from experimental data, obtained from measurements made usually at a distance from the medium, utilizing the laws that relate these characteristics to the experimental data in a given situation. The inverse problem of electromagnetic scattering has not been solved in the general case. Stringent requirements are often needed to be kept on the shapes of the scatterer to be recovered and on the operating frequency range. Moreover, the existing solutions generally demand an exhaustive amount of input information of as many aspects and frequencies as possible. There are many approaches for obtaining

approximate solution to the electromagnetic inverse scattering problem. The following only highlights the ramp response approach and other specific approaches which have been proven successful and potentially promising for future research, and which are directly relevant to this thesis. An excellent and quite complete review of electromagnetic inverse problems is given in Boerner [21].

Kennaugh, Cosgriff and Moffatt have introduced the use of the impulse response in electromagnetic scattering problems [10,12]. Using the physical optics approximation, it was shown that the impulse response of a smooth conducting object is directly proportional to the second derivative of the cross-sectional area of the scatterer. This remarkable high frequency inverse scattering identity is known as the Kennaugh-Cosgriff formula [10]. The area profile can thus be recovered from the ramp response, since the ramp response is then directly proportional to the cross-sectional area rather than its derivative (Kennaugh and Moffatt, 1965). Young [22] used the ramp response synthesized from complex scattering data at ten harmonically related frequencies in the target's low resonance regime to estimate the area function, from which a "likely image" of the target was generated at three orthogonal look angles using his approximate limiting surface technique. The images obtained are decent, but in general they are not uniquely specified since more than one shape satisfies any three look-angle area function set.

A more systematic approach was carried out by Das and Boerner, who showed that the reconstruction of a smooth conducting target, convex in shape, can be considered as a two-step process: (i) an electromagnetic step of obtaining suitable radar measurables from which one can make an estimation of a geometrical function of the conducting scatterer; and

(ii)a geometrical step of reconstructing the shape and size of the object from the knowledge of the geometrical function estimated in the first step. With the Radon transform concept, they showed that the inverse three-dimensional Radon transform of the cross-sectional area of a scatterer is simply the target's characteristic function, which is a complete specification of shape. The area function can, as in the previous approach, be estimated by the ramp response method (Boerner, 1980). Thus, the electromagnetic inverse scattering problem can be formulated as the classical Radon problem. Moreover, they also indicated that the classical Radon problem is intimately related to the problem of reconstruction from projections which has long been investigated and applied in diverse fields, particularly in Computer-Assisted Tomography. Thus, the many reconstruction techniques and algorithms well developed in other fields can be applied in radar target imaging as well.

A solution for the inverse scattering problem using the space-time Integral equation was reported by Bennett et al [23]. The technique developed was iterative and restricted to the class of rotationally symmetric conducting targets. In this approach, the inverse problem is formulated as an inversion of the space-time integral equation. The shapes reconstructed are excellent for this simple class of shapes, but no extension to more general shapes has been made recently.

An important aspect of electromagnetic inverse scattering is to incorporate the problem with utilization of polarization. A

monostatic inverse scattering model based on polarization utilization was developed by Chaudhuri and Boerner [2,17,24]. In brief, approximation was made of high frequency scattered fields and an equivalent ellipsoidal model was developed. The utilization of the space-time integral equation and Minkowski's theory lead to a system of equations for the recovery of the surface profile. The numerical technique is iterative, and when the curvature difference at the specular point approaches to zero, the recovery of that particular point is not possible; the system of the recovery equations also becomes ill-conditioned even if the curvature difference is small.

Based on the first order polarization correction to physical optics [8], Ho graphically reconstructed the shape of a sphere-capped cylinder with polarization correction incorporated into the Radon transform approach [25,26]. The results show that the quality of images are significantly improved with polarization correction. It must be noted here that Ho took advantage of the plane symmetry of the sphere-capped cylinder, and reduced the Radon transform by one dimension. In this class of objects, the two-dimensional inverse transform of the area function normal to the equatorial plane gives the width perpendicular to the plane. The width over this plane of symmetry is actually a complete specification of the shape. Since in the two-dimensional case, the Radon transform becomes the projection, thus the filtered back projection algorithm was directly borrowed from the theory of reconstruction from projections (Shepp and Logan, 1974).

In this thesis, a high frequency inverse scattering model is

developed for the recovery of the specular point curvature from polarimetric scattering data. Not only does the model show that the specular geometry can be directly extracted from polarimetric data, but it also contributes in viewing the electromagnetic inverse scattering problem as one of reconstruction from curvatures in differential geometry. In the introduction of the next chapter, the main objective of this thesis will be clearly specified.

CHAPTER II

THE SPACE-TIME INTEGRAL EQUATION AND FIRST ORDER CORRECTION TO PHYSICAL OPTICS

2.1 Introduction

In recent years, due to advances made in radar technology, it has become possible to measure the complete relative phase scattering matrix of an object reliably [1,2,3]. Thus the utilization of these polarimetric scattering data in radar target identification or discrimination and in other inverse scattering applications has become of considerable interest in current theoretical and experimental research efforts [1-7]. The main objective of this thesis is to investigate the information content of the scattering matrix [S], on the shape, size, curvature, etc. of a scatterer, when it is given for the monostatic case and in the high frequency region (i.e. the wavelength of the interrogating signal is small compared to the object characteristic dimension).

The scattering matrix [S], which manifests total polarization information for a fixed frequency and a given aspect, is comprised of four measurable complex elements (four magnitudes and four phases). It will be shown here that the difference in suitable phase terms in this matrix, under the high frequency interrogation conditions, can lead to the recovery of the difference in principal curvatures at the specular point, from a given general [S] matrix. This procedure avoids unitary transformations used in the pursuit of cross-polarization nulls required in certain radar target identification techniques [3-5]. The underlying concept used to achieve the above results is based on Bennett's first order far-field polarization correction [8,9]

to the Kennaugh-Cosgriff's physical optics formula for the electromagnetic backscattered field [10,11].

In this chapter, the space-time integral equation, and how it is used to obtain a first order correction to physical optics, is discussed so that later, in Chapter III, its possible extension to obtain higher order correction terms can be presented clearly. The relationship between the principal curvatures and the general [S] matrix is also developed in Chapter III. A discussion of numerical verification with theoretical as well as measured data is given in Chapter V.

2.2 The Space-Time Integral Equation

An electromagnetic wave incident on a perfectly conducting body induces currents on the surface of the scatterer, which in turn radiate and produce the scattered field. The current distribution produces a vector potential given by

$$\vec{A}_p(\vec{r},t) = \frac{1}{4\pi} \iint_S \frac{\vec{J}(\vec{r}\,',\tau)}{R}\, dS' \quad ,$$

where $\vec{J}(\vec{r},t)$ is the induced surface current density at time t, $\vec{r}$ is the position vector to the observation point, $\vec{r}\,'$ is that to an integration point, $R = |\vec{r} - \vec{r}\,'|$, $\tau = t - R/c$. The geometry is illustrated in Figure 2.1.

The total magnetic field $\vec{H}$ is equal to the sum of the incident field $\vec{H}_i$ and the scattered field $\vec{H}_s$ due to $\vec{J}$,

$$\vec{H}(\vec{r},t) = \vec{H}_i(\vec{r},t) + \vec{H}_s(\vec{r},t)$$

where $\vec{H}_s(\vec{r},t) = \nabla \times \vec{A}_p$

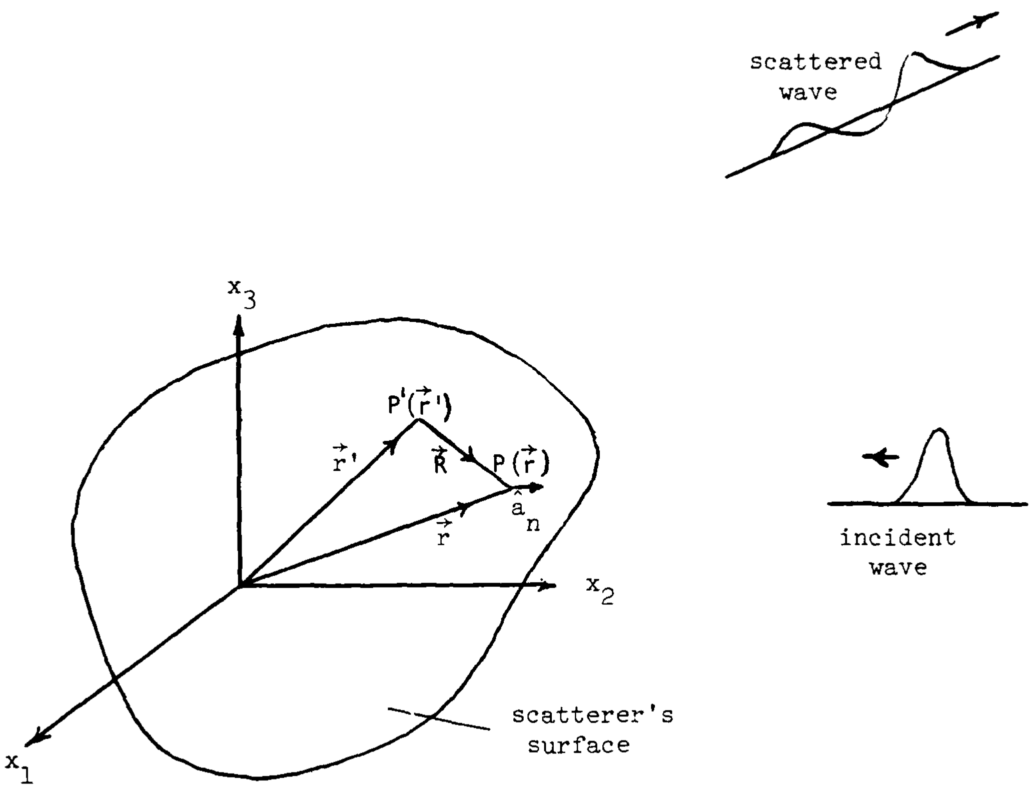

Figure 2.1 Geometry for the Derivation of the Space-Time Integral Equation

(Redrawn after Bennett, "Time Domain Solution Via Integral Equations--- Surfaces and Composite Bodies" July 1979)

$$= \frac{1}{4\pi} \iint_S \mathcal{L}\{\vec{J}(\vec{r}',\tau)\} \times \hat{a}_R \, dS' \quad [16]$$

The operator $\mathcal{L}$ is defined as $1/R^2 + (1/Rc)\partial/\partial\tau$, and $\hat{a}_R$ is the unit vector of $\vec{R}$. An expression for $\vec{J}$ can be obtained by shrinking the observation point to a point on the scatterer's surface under a limiting procedure. For the case of a perfectly conducting scatterer, the H-field boundary condition ($\vec{J} = \hat{a}_n \times \vec{H}$), with $\hat{a}_n$ being the unit outward normal vector to the surface, can then be invoked to yield a vector integral equation as shown in Bennett [23]

$$\vec{J}(\vec{r},t) = 2\hat{a}_n \times \vec{H}_i(\vec{r},t) + \frac{1}{2\pi} \iint_S \hat{a}_n \times \{\mathcal{L}\vec{J}(\vec{r}',\tau) \times \hat{a}_R\} \, dS' \quad (2.1)$$

The first term on the right-hand side of (2.1) is identified as the physical optics approximation and is also the source term, whereas the second integral represents the contribution of retarded currents at points on the scatterer's surface other than the observation point $P(\vec{r})$ i.e.

$$\vec{J}(\vec{r},t) = \vec{J}_{po}(\vec{r},t) + \vec{J}_{\varepsilon}(\vec{r},t),$$

with $\vec{J}_{\varepsilon}(\vec{r},t) = \frac{1}{2\pi} \iint_S \hat{a}_n \times \{\mathcal{L}\vec{J}(\vec{r}',\tau) \times \hat{a}_R\} \, dS'$ (2.2)

being the correction to the physical optics current $\vec{J}_{po}$. For the far scattered magnetic field ($\vec{H}_s$), with $R \to r$, it can be shown that [8]

$$r_o\vec{H}_s(\vec{r},t) = \frac{1}{4\pi} \iint_S [\frac{\partial}{\partial\tau}\vec{J}(\vec{r}',\tau)] \times \hat{a}_r \, dS' \quad (2.3)$$

where r_o is the radar range. Using (2.3), the physical optics approximation for the far scattered impulse response field was derived [8,23] and is equivalent to the Kennaugh-Cosgriff formula [10-12] which can be written as

$$r_o \vec{H}_{s(po)}(\vec{r},t) = \frac{1}{2\pi} \frac{d^2}{dt^2} A(t)\, \hat{a}_{H_i} \tag{2.4}$$

where $\hat{a}_{H_i}$ is the unit vector in the direction of $\vec{H}_i$, and $A(t)$ is the silhouette area of the scatterer as delineated by the incident impulsive plane wavefront moving at half the free space velocity, c. Discussion here is restricted to the illuminated side of a smooth, conducting, convex object.

Since the impulse response given in (2.4) depends solely on the area function, it manifests no depolarization effects. Depolarization effects were taken care of by Bennett et al [8,9] in their first order correction to physical optics approximation.

2.3 A First Order Correction to Physical Optics Using the Space-Time Integral Equation [8]

To obtain an analytic expression for the first order correction to the physical optics far field, the correction to the induced surface current needs to be considered first. The integral in (2.2) cannot be handled analytically without the knowledge of the geometry of the scatterer. Yet the integration can be carried out over a patch, S_ε, around the specular point, assuming the patch being so small that it is virtually flat. The contributions of retarded currents outside the patch and effects such as creeping waves are ignored to avoid the total surface integration. Under this "leading edge" simplification, the first order correction obtained is valid and accurate towards the high frequency end of the phasor frequency response.

The expansion of the vector triple cross-product in (2.2) yields the first order correction current

$$\vec{J}_{pol}(\vec{r},t) = \frac{1}{2\pi}\iint_{S_\varepsilon}[\mathcal{L}J_u(\vec{r}\,',\tau)][(\hat{a}_n \cdot \hat{a}_R)\hat{a}_u' - (\hat{a}_n \cdot \hat{a}_u')\hat{a}_R]\, dS'$$

$$+ \frac{1}{2\pi}\iint_{S_\varepsilon}[\mathcal{L}J_v(\vec{r}\,',\tau)][(\hat{a}_n \cdot \hat{a}_R)\hat{a}_v' - (\hat{a}_n \cdot \hat{a}_v')\hat{a}_R]\, dS'$$

where the primed quantities are associated with the integration point $P'(\vec{r}\,')$ and $\hat{a}_u$, $\hat{a}_v$ are the unit vectors tangent to the principal curves at the point of interest. The geometry information embedded in $\hat{a}_n \cdot \hat{a}_R$ can be extracted by expressing $\hat{a}_R = (\vec{r} - \vec{r}\,')/R$ in a Taylor series expansion as follows:

$$\vec{r}\,' - \vec{r} = \vec{r}_u \Delta u + \vec{r}_v \Delta v$$

$$+ \frac{1}{2!}[\vec{r}_{uu}(\Delta u)^2 + 2\vec{r}_{uv}(\Delta u)(\Delta v) + \vec{r}_{vv}(\Delta v)^2]$$

$$+ \frac{1}{3!}[\vec{r}_{uuu}(\Delta u)^3 + 3\vec{r}_{uuv}(\Delta u)^2(\Delta v) + 3\vec{r}_{uvv}(\Delta u)(\Delta v)^2 + \vec{r}_{vvv}(\Delta v)^3]$$

$$+ \ldots,$$

where $\vec{r}_u = \frac{\partial \vec{r}}{\partial u}$, etc. The above series describes any neighboring point $(\Delta u, \Delta v)$ in the vicinity of $\vec{r}$ in terms of the derivatives of $\vec{r}$ at the specular point. The geometry of the small patch is thus extrapolated in terms of the properties of the surface at the specular point.

The scalar product of $\hat{a}_n$ and $\hat{a}_R$ expressed by a series truncated at second order (i.e. terms $(\Delta u)^2$ and $(\Delta v)^2$, etc.) introduces (E, F, G) and (L, M, N), the coefficients of the first and second fundamental forms of the surface $\vec{r}(u,v)$ [13,14]. To simplify the algebra, the principal curves are chosen as the parametric curves to represent the curvilinear mapping $\vec{r}(u,v)$ for the surface of the patch, thus

forcing F and M to zero [8,13,14]. The principal curvatures along $\hat{a}_u$ and $\hat{a}_v$ at the specular point are obtained as [13]

$$K_u = \frac{L}{E}$$

$$K_v = \frac{N}{G} ,$$

respectively. Finally, $\mathcal{L}J_u(\vec{r}',\tau)$ and $\mathcal{L}J_v(\vec{r}',\tau)$ can be approximated as $J_u(\vec{r},t)/R^2$ and $J_v(\vec{r},t)/R^2$, respectively, by assuming that the currents are spatially constant on a small, flat, circular patch of radius ε_o. With the procedure outlined above the analytic expression arrived at in [8] is

$$\vec{J}_\varepsilon(\vec{r},t) = [\hat{a}_u J_u(\vec{r},t) - \hat{a}_v J_v(\vec{r},t)] \frac{K_u - K_v}{4} \varepsilon_o \tag{2.5}$$

The corresponding first order far-field impulse response correction was obtained by assuming physical optics currents for J_u and J_v in the above equation and then substituting it into (2.3). A crucial assumption made in [8] is that the patch radius ε_o increases linearly with time t, spreading from the specular point at the leading edge. The final expression for the first order correction to the scattered far field is

$$r_o \vec{H}_{s(pol)}(\vec{r},t) = \frac{K_u - K_v}{4\pi} \cdot [\hat{a}_u H_{ui} - \hat{a}_v H_{vi}] \frac{dA}{dt} , \tag{2.6}$$

where H_{ui} and H_{vi} are the components of $\vec{H}_i$ in the directions of $\hat{a}_u$ and $\hat{a}_v$, respectively.

It is clear that the first order correction exhibits depolarization effects, which are proportional to the difference in the principal curvatures at the specular point. Moreover, the

first order correction takes the functional form of the first derivative of the silhouette area function A(t), whereas the physical optics far field, which exhibits no depolarization effects, takes the functional form of the second derivative of A(t). The practical aspects of using this first order correction in geometry extraction (curvature difference at the specular point in this case) are analyzed in the next chapter.

CHAPTER III

CURVATURE RECOVERY FROM HIGH FREQUENCY [S] MATRIX ELEMENTS

3.1 Derivation of the Phase-Curvature Relationship

The polarimetric scattering data measured with a monostatic radar system are given by

$$[S] = \begin{bmatrix} S_{11} & S_{12} \\ S_{21} & S_{22} \end{bmatrix} = \begin{bmatrix} |S_{11}|e^{j\phi_{11}} & |S_{12}|e^{j\phi_{12}} \\ |S_{21}|e^{j\phi_{21}} & |S_{22}|e^{j\phi_{22}} \end{bmatrix}$$

The general polarization geometry with respect to the principal directions at the specular point is shown in Figure 3.1. The elements S_{11} and S_{22} represent the backscattered signals when the transmitted and the received polarizations are identical, i.e. $\hat{a}_1$ and $\hat{a}_2$, respectively. On the other hand, S_{12} and S_{21} represent the cases when the transmitted and the received polarizations are orthogonal to each other (transmit-$\hat{a}_1$, receive-$\hat{a}_2 \rightarrow S_{21}$, etc.). In order to relate the measurable [S] matrix to the theory presented in Chapter II, the total physical optics scattered far field (i.e. the physical optics and first order correction) is transformed from the time (t) domain to the frequency (k, the wave number) domain by using Fourier transformation. In the time domain, combining (2.4) and (2.6), the total high frequency scattered far field is

$$r_o \vec{H}_s(\vec{r},t) = \frac{1}{2\pi} \frac{d^2}{dt^2} A(t)\, \hat{a}_{H_i} + \frac{K_u - K_v}{4\pi} \cdot \frac{d}{dt} A(t)$$
$$\cdot \left[(\hat{a}_{H_i} \cdot \hat{a}_u)\, \hat{a}_u - (\hat{a}_{H_i} \cdot \hat{a}_v)\, \hat{a}_v \right] \qquad (3.1)$$

The Fourier transform of (3.1), with the initial condition

$$A_F(0) = \{F.T.[A(t)]\}_{k=0} = 0,$$

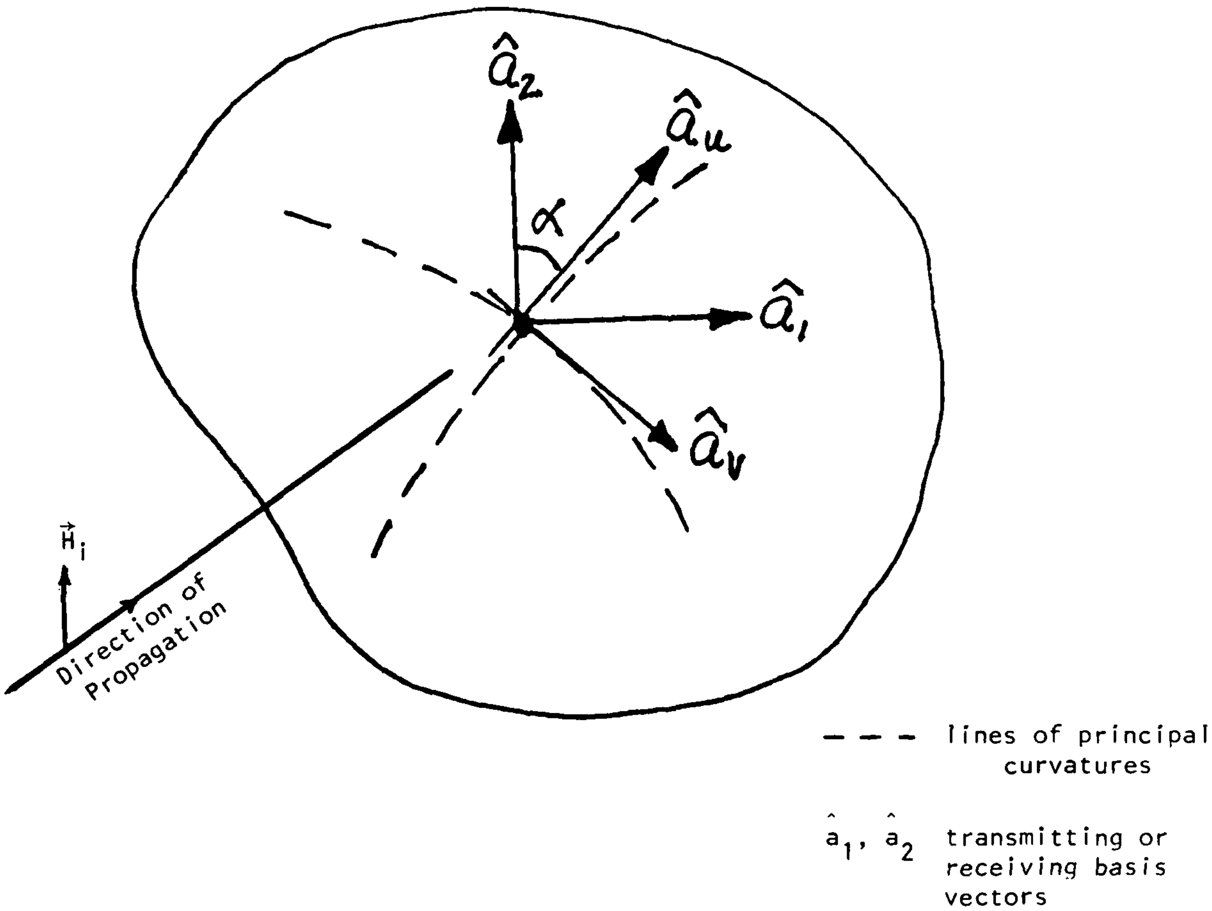

Figure 3.1 Specular Point Coordinate Systems

yields

$$r_o\vec{H}_s(\vec{r},k) = \frac{1}{2\pi}(jk)^2 A_F(k)\,\hat{a}_{H_i}$$

$$+ (jk)A_F(k)\,\frac{K_u - K_v}{4\pi}\,[(\hat{a}_{H_i}\cdot\hat{a}_u)\hat{a}_u - (\hat{a}_{H_i}\cdot\hat{a}_v)\hat{a}_v] \quad (3.2)$$

where $A_F(k) = \text{F.T.}[A(t)]$.

From the geometry in Figure 3.1, it is seen that

$$\hat{a}_1 = \sin\alpha\,\hat{a}_u + \cos\alpha\,\hat{a}_v \quad \text{and}$$
$$\hat{a}_2 = \cos\alpha\,\hat{a}_u - \sin\alpha\,\hat{a}_v \quad (3.3)$$

For measuring S_{11} the transmitter polarization becomes $\hat{a}_{H_i} = \hat{a}_1$, and the receiver polarization becomes $\hat{a}_{Hr} = \hat{a}_1$. Thus, using (3.2), one has

$$\begin{aligned} S_{11} &= \hat{a}_{Hr}\cdot(r_o\vec{H}_s) \\ &= \frac{1}{2\pi}(jk)^2 A_F(k)\,(\hat{a}_1\cdot\hat{a}_1) \\ &\quad + (jk)A_F(k)\,\frac{K_u - K_v}{4\pi}\,[(\hat{a}_1\cdot\hat{a}_u)(\hat{a}_1\cdot\hat{a}_u) \\ &\qquad - (\hat{a}_1\cdot\hat{a}_v)(\hat{a}_1\cdot\hat{a}_v)] \end{aligned} \quad (3.4)$$

Similarly, for S_{22}, $\hat{a}_{H_i} = \hat{a}_2$, $\hat{a}_{Hr} = \hat{a}_2$; for S_{21}, $\hat{a}_{H_i} = \hat{a}_1$, $\hat{a}_{Hr} = \hat{a}_2$; and for S_{12}, $\hat{a}_{H_i} = \hat{a}_2$, $\hat{a}_{Hr} = \hat{a}_1$. Now using (3.2), (3.3) and (3.4), one gets (ignoring scale factors)

$$S_{11} = \frac{1}{2\pi}(jk)^2 A_F(k) - (jk)A_F(k)\,\frac{K_u - K_v}{4\pi}\cos 2\alpha \quad (3.5)$$

$$S_{22} = \frac{1}{2\pi}(jk)^2 A_F(k) + (jk)A_F(k)\,\frac{K_u - K_v}{4\pi}\cos 2\alpha \quad (3.6)$$

$$S_{21} = (jk)A_F(k)\,\frac{K_u - K_v}{4\pi}\sin 2\alpha \quad (3.7)$$

$$S_{21} = S_{12} \quad \text{(reciprocity satisfied)}$$

Using (3.5) and (3.6), it can be shown that

$$\begin{aligned} \frac{K_u - K_v}{2} &= -j \frac{k}{\cos 2\alpha} \frac{S_{11} - S_{22}}{S_{11} + S_{22}} \\ &= -j \frac{k}{\cos 2\alpha} \frac{1 - \tilde{R}}{1 + \tilde{R}} \end{aligned} \tag{3.8}$$

where $\tilde{R} = Re^{j\phi_d}$

$$= \frac{S_{22}}{S_{11}}$$

$$= \frac{|S_{22}|}{|S_{11}|} e^{j(\phi_{22} - \phi_{11})}$$

It is clear that in order for the equality in (3.8) to hold true and therefore represent a physical case in which $(K_u - K_v)$ is a real number, one needs

$$\text{Re} \frac{1 - \tilde{R}}{1 + \tilde{R}} = 0, \text{ implying } 1 - R^2 = 0 \tag{3.9}$$

where Re stands for real part.

Thus for (3.8) to represent a physical situation, the condition required is

$$R = \frac{|S_{22}|}{|S_{11}|} = 1, \text{ implying } |S_{22}| = |S_{11}|$$

From electromagnetic scattering theory, it is known that the above condition is attained at relatively high frequencies (i.e. physical optics to geometrical optics region). It is interesting to note that algebraic manipulation of (3.8) independently points out that

it is a high frequency formula which is, of course, true since the physical optics approximations for the scattered fields are being used.

With the condition (3.9), now (3.8) can be written as

$$\frac{K_u - K_v}{2} = -\frac{k}{\cos 2\alpha}\tan(\phi_d/2) \qquad (3.10)$$

Where $\phi_d = \phi_{22} - \phi_{11}$.

In the rest of the text, the above expression will be referred to as the "phase-curvature" relationship.

For the inverse scattering applications α is an unknown quantity (Figure 3.1). Thus, before (3.10) can be used to recover the curvature difference at the specular point, α needs to be determined. For this purpose, consider

$$\frac{S_{21}}{S_{11}} = \frac{\frac{K_u - K_v}{2}\sin 2\alpha}{(jk) - \frac{K_u - K_v}{2}\cos 2\alpha}$$

from (3.5) and (3.7). Using (3.10), one obtains

$$\frac{S_{21}}{S_{11}} = -\frac{(\tan 2\alpha)\,(\tan(\phi_d/2))}{\tan(\phi_d/2) + j}$$

$$\alpha = \frac{1}{2}\tan^{-1}\left\{\frac{-S_{21}}{S_{11}}(1 + j\cot(\phi_d/2))\right\} \qquad (3.11)$$

Once again for α to be a real angle (and therefore representing the given physical situation) one needs

$$\frac{S_{21}}{S_{11}} = D_o\,(1 - j\cot(\phi_d/2))$$

where D_0 is a real number.

Using (3.11), without applying any unitary transformation, the cross-polarized nulls of a given scattering matrix are known.

Two special cases of (3.10) are when $\alpha = 0$, or $\pi/2$ (i.e. the incident linear polarization coincides with one of the directions of the principal curvatures at the specular point). For these special cases, there is no depolarization of the energy in the backscattered direction ($S_{21} = S_{12} = 0$). The corresponding [S] matrix is referred to as the cross-pol. null scattering matrix. The phase-curvature relationship becomes

$$\frac{K_u - K_v}{2} = \mp k \tan \frac{\phi_{22} - \phi_{11}}{2} \tag{3.12}$$

In chapter V, the validity of (3.12) will be numerically tested with both theoretical and experimental scattering matrix data.

3.2 Numerical Analysis

In this section, a numerical analysis of applying the phase-curvature relationship on the polarimetric scattering matrix of a prolate spheroidal scatterer is presented. The 2:1 prolate spheroid was used as a test case because of its well-defined finite curvature difference at any point on the surface and also because the theoretical as well as experimental data over a large range of frequencies were readily available for this object. For the time being, since both theoretical and experimental data are available only for the special cases in which the incident polarization coincides with one of the directions of the principal curvatures at the specular points (i.e. points on the equator of the prolate

spheroid (Figure 3.2)), equation (3.12) rather than the more general phase-curvature relationship (3.10) is directly tested. In these cases, the incident polarizations are along the vertical and horizontal directions. To verify the theory of curvature recovery, it is essential to check

(i) whether the right-hand side of (3.12) will approach the actual value of $(K_u - K_v)/2$ for a given equatorial specular point as k increases;

(ii) whether k Re $\{ (1 - \tilde{R})/(1 + \tilde{R}) \}$ will tend to zero despite that k increases;

(iii) whether the imaginary part of $k \{ (1 - \tilde{R})/(1 + \tilde{R}) \}$ will settle to the constant value of $(K_u - K_v)/2$;

A more interesting and compact presentation of results is to plot the right-hand side of (3.8) on a complex plane (i.e. the imaginary part versus the real part of $\{ k (1 - \tilde{R})/(1 + \tilde{R}) \}$. It is predicted that this scattering chart will be a spiral which, as frequency increases, will converge to (or hover around) a point on the imaginary axis. The distance of this point on the imaginary axis from the origin will be equal to the required value of $(K_u - K_v)/2$ for the specular point of interest. It is expected that this complex plane plot will be particularly useful when the input data are not very accurate and are noisy (measurement data). In the above tests, the exact value of the curvature difference $K_u - K_v$ has been calculated by using Minkowski's support function for ellipsoidal surfaces [17]. Another way is through the use of differential geometry (Appendix I). The value of k is normalized with respect

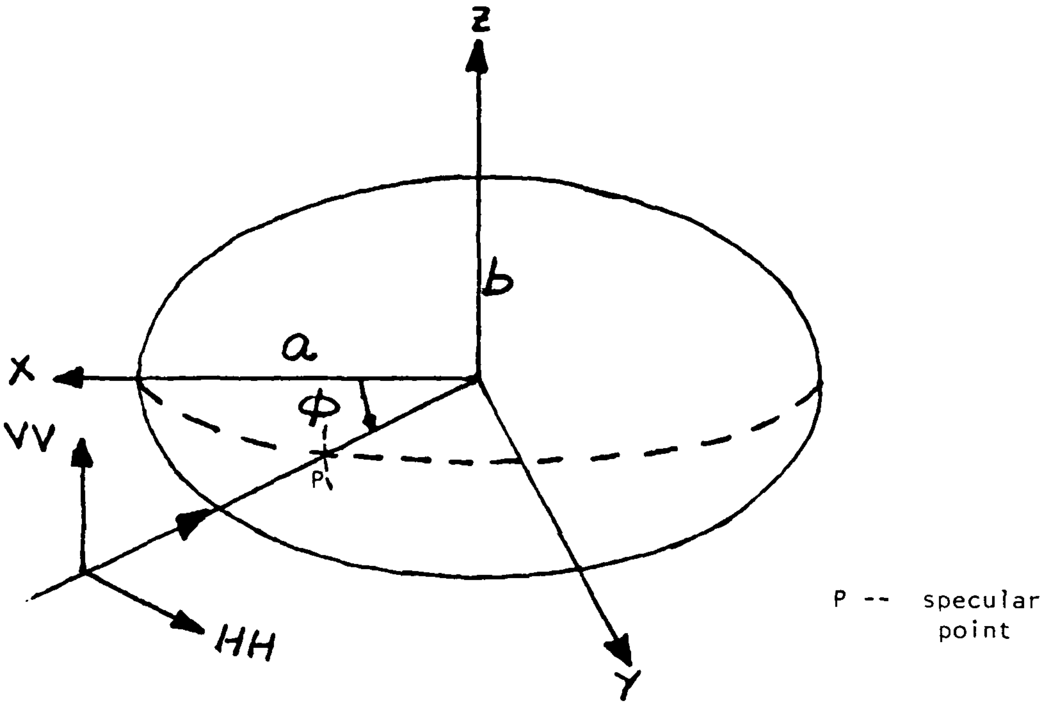

Figure 3.2 Incidence for Equatorial Specular Point

to the length of the semi-minor axis of the prolate spheroid.

It is useful to consider the following types of measurement errors for the interpretation of the numerical results and the explanation of the deviation from theoretical prediction given in chapter V.

3.2.1 Relative Phase Error between TE and TM Incidences

If the target is not illuminated simultaneously with TE (vertical) and TM (horizontal) polarizations, then even an offset of one millimeter between the separate positions of the same antenna along the direction of incidence will cause phase distortion of about ten degrees to the phase difference $(\phi_{vv} - \phi_{hh})$ at a frequency of 4 GHz. If, however, the target is slightly displaced in the direction of propagation with the TE and TM measurements simultaneously made, then both ϕ_{vv} and ϕ_{hh} are distorted to the same extent. Thus the relative phase difference and the subsequent calculations are not affected at all.

To investigate how the scattering chart is affected assuming that a relative phase error of e radians does occur, the complex ratio $(1 - \tilde{R})/(1 + \tilde{R})$ can be broken down into its real and imaginary parts, with ϕ_d replaced by $(\phi_d + e)$.

$$\mathrm{Re}\ \frac{1 - \tilde{R}}{1 + \tilde{R}} = \frac{1 - R^2}{De}$$

$$\mathrm{Im}\ \frac{1 - \tilde{R}}{1 + \tilde{R}} = \frac{-2R \sin(\phi_d + e)}{De}$$

where $De = 1 + R^2 + 2R \cos(\phi_d + e)$. Note that a spheroidal wave function expansion could be used for error estimation.

It is obvious that the real part is much more resistant to

changes caused by the error e than the imaginary part. Thus the spiral will become a helix elongating mainly along the imaginary axis and away from the exact value of $(K_u - K_v)/2$. In Chapter V, the relative phase error will be simulated within the set of theoretical data.

3.2.2 Rotation of Target with respect to Incidence Direction

If the target is rotated with respect to the direction of incidence (i.e. the incident polarizations are not along the directions of principal curvatures), then it is the general phase-curvature relationship (3.10) which should be tested instead. Hence, a multiplicative factor of cos 2α (Figure 3.1) will account for the sole effect of rotation error. The scattering chart will retain its spiral shape however.

3.2.3 Canting

If the target is slightly canted with the z-axis still being horizontal, then obviously the effect will be that which resulted from changing the aspect angle ϕ (Figure 3.2).

3.3 Discussion of Second Order Corrections to the Physical Optics Approximation

The first order correction to the physical optics approximation due to Bennett et al [8] has been shown to be proportional to the difference in principal curvatures and to have the functional form of the first derivative of the silhouette area of the target. It might be expected that more geometry of the specular point can be identified by extending the first order correction. For a general case in which $(K_u - K_v)$ is not zero, geometrical parameters, such as

derivatives or mixed derivatives of principal curvatures, torsion of the principal curves, etc., can appear in the second order correction term. Another motivation in the pursuit of the second order correction is the possible relaxing of the high frequency restriction required for the validity of the first order correction term. In order to elaborate on this conjecture, note that, since $\frac{d^2A}{dt^2}$ of the physical optics term corresponds to $(jk)^2 A_F(k)$ in the frequency domain, and $\frac{dA}{dt}$ of the first order correction term corresponds to $(jk)A_F(k)$, there might be a trend that higher order corrections become more dominant (important) for lower frequencies within the high frequency realm of physical optics.

One approach to the problem of extension is to take into account the higher order derivatives of $\vec{r}(u,v)$ that were truncated in the first order correction. The first order term has been obtained by retaining the second order derivatives of $\vec{r}$ with respect to u and v. To obtain the second order correction term, the integrand in (2.2) for $\vec{J}_\varepsilon$ has been expanded with inclusion of the higher order surface derivatives of $\vec{r}$. After some algebraic manipulations, the integrand was written as a sum of several terms like $\hat{a}_u$, $\hat{a}_v$, $\vec{r}_{uu}$, $\vec{r}_{vv}$, ... (up to the third order derivatives) multiplied by the powers of Δu and/or Δv. This is expected since these vectors introduce the higher order depolarization concepts. In contrast, the first order correction term is in the directions of $\hat{a}_u$ and $\hat{a}_v$ explicitly.

The vectors such as $\vec{r}_{uu}$, $\vec{r}_{uv}$, etc. can be resolved in $\hat{a}_u$, $\hat{a}_v$ and $\hat{a}_n$ directions by introducing the Christoffel symbols through the use of the Gauss and Weingarten equations in differential geometry

[12,13]. These Christoffel symbols depend on the basic geometric parameters of the surface, namely, (E, F, G) and (L, M, N). All terms in the $\hat{a}_n$ direction can be neglected on the basis of physical considerations that the induced surface current cannot have a component in the normal direction to the surface. The appearance of the $\hat{a}_n$ term is due to the truncation of the Taylor series. The totality of all terms in the series should, in theory, nullify the current component in the $\hat{a}_n$ direction. Since the depolarization derivative vectors, and hence the Christoffel symbols, are all evaluated at the specular point, they can be taken outside the surface integral in (2.2), which then is written as a sum of integrals of the type

$$\iint_{S_\varepsilon} \frac{(\Delta u)^2}{R^3}\, dS' , \qquad \iint_{S_\varepsilon} \frac{(\Delta v)^4}{R^4}\, dS' , \ \ldots \text{ etc.}$$

For direct scattering problems the integration may yield complicated analytic solutions despite the fact that S_ε is known. For inverse scattering problems, where S_ε is unknown, the integration may be approximated by assuming a flat patch for S_ε. Since the Taylor series dictated a small patch, leading edge effects and thus the high frequency restrictions must be adhered to. An approximate expression for $\vec{J}_\varepsilon$ can thus be obtained by choosing a circular patch of very small radius ε_o as the most simple case. However, the expression thus obtained has been found to have a factor of ε_o^3 in contrast to ε_o in the first order correction. The relatively small value of ε_o^3 compared with ε_o renders the expression for the second order correction current thus obtained insignificant. The

far-field correction term corresponding to this second order current term then has very little significance in comparision to the physical optics or the first order term, and therefore is of little consequence to most practical situations.

Nevertheless, it is suggested that one may assume some simple known curved patch (instead of a flat patch), and take into account the whole vicinity of the specular point rather than only the point itself, in further pursuit of specular geometry through the backscattered leading edge returns.

CHAPTER IV

THE HF CURVATURE RECOVERY MODEL AND THE TRANSFORMATION INVARIANTS OF THE SCATTERING MATRIX

4.1 Relation to the Transformation Invariants of [S]

The scattering matrix [S(A,B)] with respect to an orthogonal basis (A,B) can be transformed to [S'(A',B')] with respect to another orthogonal basis (A',B') through a unitary transformation [18,19, 20]. The transformation is invariant and satisfies [3,38]

$$\text{Span}\ \{[S(A,B)]\} = \text{Span}\ \{[S'(A',B')]\} = \text{invariant} \tag{4.1}$$

and
$$\text{Det}\ \{[S(A,B)]\} = \text{Det}\ \{[S'(A',B')]\} = \text{invariant} \tag{4.2}$$

where Det stands for the determinant of the scattering matrix and the span is defined in the following.

Applying equations (3.5 - 3.7) for a basis (A,B) with polarization angle α (Figure 3.1),

$$\begin{aligned}
\text{Span}\ \{[S(A,B)]\} &= |S_{AA}|^2 + |S_{BB}|^2 + 2|S_{AB}|^2 \\
&= (\frac{1}{2\pi})^2 k^2 |A_F(k)|^2 |jk - \frac{K_u - K_v}{2}\cos 2\alpha|^2 \\
&+ (\frac{1}{2\pi})^2 k^2 |A_F(k)|^2 |jk + \frac{K_u - K_v}{2}\cos 2\alpha|^2 \\
&+ 2(\frac{1}{2\pi})^2 k^2 |A_F(k)|^2 [\frac{K_u - K_v}{2}\sin 2\alpha]^2 \\
&= 2(\frac{1}{2\pi})^2 k^2 |A_F(k)|^2 \{k^2 + [\frac{K_u - K_v}{2}]^2\}\ ,
\end{aligned} \tag{4.3}$$

which is independent of α.

For a given frequency (high enough so that the theory is valid) and a given aspect, the right-hand side of equation (4.3) is indeed invariant.

Similarly,

$$\mathrm{Det}\ \{[S(A,B)]\} = S_{AA}S_{BB} - S_{AB}{}^2$$

$$= (\frac{1}{2\pi})^2 (jk)^2 A_F^2(k)\{(jk)^2 - [\frac{K_u - K_v}{2}]^2 (\cos^2\alpha$$

$$- \sin^2\alpha)^2\} - (\frac{1}{2\pi})^2 (jk)^2 A_F^2(k) [\frac{K_u - K_v}{2}]^2 \sin^2 2\alpha$$

$$= (\frac{1}{2\pi})^2 k^2 A_F^2(k)\{k^2 + [\frac{K_u - K_v}{2}]^2\} \qquad (4.4)$$

which is also invariant and independent of α.

Hence equations (4.3) and (4.4) are the high frequency versions of the invariance equations (4.1) and (4.2).

4.2 The HF Scattering Ratio

It is interesting to define D (referred to as "the HF scattering ratio" in this thesis) as the ratio of Det {[S(A,B)]} to Span {[S(A,B)]},

$$D \equiv \frac{S_{AA}S_{BB} - S_{AB}{}^2}{|S_{AA}|^2 + |S_{BB}|^2 + 2|S_{AB}|^2}$$

$$= \frac{A_F{}^2(k)}{2|A_F(k)|^2}$$

$$= 0.5\ e^{j2\theta} \qquad (4.5)$$

where θ = Arg $A_F(k)$ = the phase of $A_F(k)$ (4.6)

For the case in which incidence polarization is along one of the directions of principal curvatures, $|S_{AB}|$ equals zero. Let S_{AA} be $|S_{AA}|e^{j\phi_{AA}}$ and so on, thus

$$D = \frac{|S_{AA}||S_{BB}|\ e^{j(\phi_{AA} + \phi_{BB})}}{|S_{AA}|^2 + |S_{BB}|^2}$$

Thus $\theta = \text{Arg } A_F(k) = \dfrac{\phi_{AA} + \phi_{BB}}{2}$ (4.7)

and $\dfrac{|S_{AA}|\ |S_{BB}|}{|S_{AA}|^2 + |S_{BB}|^2} = \dfrac{1}{2}$, which requires that $|S_{AA}| = |S_{BB}|$. This condition is consistent with high frequency electromagnetic scattering.

Returning again to the general case in which $|S_{AB}| \neq 0$,

$$S_{AA}S_{BB} - S_{AB}^{\ 2} = |S_{AA}||S_{BB}|e^{j(\phi_{AA} + \phi_{BB})} - |S_{AB}|^2 e^{j2\phi_{AB}}$$

$$= (|S_{AA}||S_{BB}|\cos\ (\phi_{AA} + \phi_{BB}) - |S_{AB}|^2\cos\ 2\phi_{AB})$$

$$+j(|S_{AA}||S_{BB}|\sin\ (\phi_{AA} + \phi_{BB}) - |S_{AB}|^2\sin\ 2\phi_{AB})$$

Considering amplitude only,

$$\frac{\{\ |S_{AA}|^2|S_{BB}|^2 - 2|S_{AA}||S_{BB}||S_{AB}|^2\ \cos\ (\phi_{AA}+\phi_{BB}-2\phi_{AB}) + |S_{AB}|^4\ \}^{\frac{1}{2}}}{|S_{AA}|^2 + |S_{BB}|^2 + 2|S_{AB}|^2}$$

$$= \frac{1}{2}$$

The above equation is an identity, if

(i) $|S_{AA}| = |S_{BB}|$ (4.8)

(ii) $\phi_{AA} + \phi_{BB} - 2\phi_{AB} = \pi$ (4.9)

simultaneously hold.

Again, (4.8) is consistent with high frequency scattering.

It should be noted that when (jk) is neglected compared to

$(jk)^2$ in (3.5) and (3.6) for high frequencies, both (4.8) and particularly (4.9) result. Hence, in general,

$$|D| = 0.5 \tag{4.10}$$

is not a trivial result merely from (4.8) as in the previous special case, but rather a consequence of the first order correction to physical optics.

4.3 Interpretation of the HF Phase Sum $(\phi_{AA} + \phi_{BB})$

From the above analysis, with only the phase being considered, it is found that

$$\tan 2\theta = \tan 2(\text{Arg } A_F(k))$$

$$= \frac{|S_{AA}||S_{BB}| \sin (\phi_{AA} + \phi_{BB}) - |S_{AB}|^2 \sin 2\phi_{AB}}{|S_{AA}||S_{BB}| \cos (\phi_{AA} + \phi_{BB}) - |S_{AB}|^2 \cos 2\phi_{AB}}$$

Assuming (4.8) and neglecting $|S_{AB}|$ compared to $|S_{AA}|$, the above equation becomes (4.7), which is now also valid for the general case. Its validity enables the phase sum $(\phi_{AA} + \phi_{BB})$ to be interpreted as twice the argument of the Fourier transform of the silhouette area of the target within the high frequency range.

4.4 Numerical Analysis

If the real and imaginary parts of D, the scattering ratio, are plotted on a complex plane, a circle of radius 0.5 will be expected for high frequency polarimetric data input. Since phase changes rapidly with frequency, a circle rather than a cluster of points of phases about 2 Arg $A_F(k)$ will appear. This, and a direct

plot of $|D|$ versus k will be shown in Chapter V. One significance of these plots is to check the accuracy of experimental polarimetric data of high frequencies by observing the deviation from the perimeter of the circle of radius 0.5.

4.5 Transformation to Circular Polarization Basis Vectors

The orthonormal vectors along the horizontal and vertical directions are usually chosen as the polarization bases (denoted by $(\hat{H},\hat{V})$) for both the transmitting and the receiving systems. However, a circular polarization basis pair may also be used [36,40], particularly in radar meteorology, in which circular polarization has a particular appropriateness on account of the direct correspondence between the mean orientation angle and the relative phase of received circular polarization components[29]. Circular polarization has also been utilized in the backscatter measurements of dielectric spheroids [32,33]. One way to investigate the form which the phase-curvature relationship may take in circular polarization basis is to transform [S(HV)] with respect to the linear basis $(\hat{H},\hat{V})$ to [C(RL)] with respect to a circular polarization basis $(\hat{R},\hat{L})$ [31,6,27]. Such transformation of [S] depends on the specification of the transformation of $(\hat{H},\hat{V})$ to $(\hat{R},\hat{L})$ by a matrix [T(RL;HV)]:

$$\begin{bmatrix} \hat{R} \\ \hat{L} \end{bmatrix} = [T(RL;HV)] \begin{bmatrix} \hat{H} \\ \hat{V} \end{bmatrix} \tag{4.11}$$

where $\hat{L}$ and $\hat{R}$ denote the left-circular and right-circular polarization vectors, respectively. The left-circular and right-circular senses are defined in Figure 4.1. In general, the transformation of the linear basis $(\hat{H},\hat{V})$ to any other orthonormal basis $(\hat{A},\hat{B})$ (not necessarily circular polarization basis) through [T] must satisfy the normalization requirements

$$\hat{H} \cdot \hat{H}^{*} = 1$$
$$\hat{V} \cdot \hat{V}^{*} = 1$$

$$\hat{A} \cdot \hat{A}^{*} = 1$$
$$\hat{B} \cdot \hat{B}^{*} = 1$$

and the orthogonality requirement

$$\hat{H} \cdot \hat{V}^{*} = 0$$
$$\hat{A} \cdot \hat{B}^{*} = 0$$

These requirements can be shown to be mathematically equivalent to

$$[T]^{*T} = [T]^{-1}$$

which satisfies the definition of a unitary matrix. Hence [T] is a unitary matrix, and its most general form can be written as [30]

$$[T] = \begin{bmatrix} e^{j\phi_1} \cos \beta & e^{j\phi_2} \sin \beta \\ -e^{j\phi_3} \sin \beta & e^{j\phi_4} \cos \beta \end{bmatrix}$$

with $\phi_2 - \phi_1 = \phi_4 - \phi_3$. The most general basis $(\hat{A},\hat{B})$ is an elliptic one. When all phases are set to zero, [T] is just an ordinary rotational matrix which rotates $(\hat{H},\hat{V})$ to another linear basis by an angle β. An example is given by the invariant transformation described by equations (4.3) and (4.4), which shows from the curvature recovery model that rotational transformation alone renders the invariants independent of the polarization angle (Figure 3.1). A more general case can be given

by, for instance, setting

$$\beta = \pi/4$$

$$\phi_1 = \phi_4 = 0$$

$$\phi_2 = -\phi_3 = \pi/2$$

The corresponding [T] then becomes

$$[T] = \frac{1}{\sqrt{2}} \begin{bmatrix} 1 & j \\ j & 1 \end{bmatrix} , \tag{4.12}$$

and the corresponding $(\hat{A},\hat{B})$ reduces to a circular polarization basis

$$\begin{bmatrix} \hat{R} \\ \hat{L} \end{bmatrix} = \frac{1}{\sqrt{2}} \begin{bmatrix} 1 & j \\ j & 1 \end{bmatrix} \begin{bmatrix} \hat{H} \\ \hat{V} \end{bmatrix}$$

By limiting the transformation from $(\hat{H},\hat{V})$ to circular polarization basis only, any polarization vector can then be expressed in terms of either basis. For instance, the incident electric field polarization vector $\underline{E}^i$ can be written as

$$\underline{E}^i = [\ E_H^i \quad E_V^i\ ] \begin{bmatrix} \hat{H} \\ \hat{V} \end{bmatrix}$$

$$= [\ E_R^i \quad E_L^i\ ] \begin{bmatrix} \hat{R} \\ \hat{L} \end{bmatrix}$$

where the linear phasor components E_H^i, E_V^i can be related to the

circular phasor components E_R^i, E_L^i as follows

$$\begin{bmatrix} E_R^i \\ E_L^i \end{bmatrix} = [T(RL;HV)]^* \begin{bmatrix} E_H^i \\ E_V^i \end{bmatrix} \qquad (4.13)$$

where the symbols * and $[\ \ ]^T$ denote conjugation and transposition, respectively. In (4.13), the incident polarization vector can be regarded as being transformed in changing the polarization basis as specified by the unitary matrix [T] given by (4.11). The scattered polarization vector $\underline{E}^s$ can similarly be transformed. $\underline{E}^s$ and $\underline{E}^i$ can both be specified in terms of the circular polarization basis. Yet, it is preferable to use distinct systems of unit vectors to specify the incident and scattered fields, so that right-hand elliptical polarization may have the same sense with regard to the coordinate system for incident radiation as it does with regard to the coordinate system for scattered radiation [30,7] (Figure 4.1). If (4.11) is prescribed for the incident system, the desired similarity of sense for the two coordinate systems can be accomplished by writing

$$\begin{bmatrix} \hat{R} \\ \hat{L} \end{bmatrix}^s = [T(RL;HV)]^* \begin{bmatrix} \hat{H} \\ \hat{V} \end{bmatrix} \qquad (4.14)$$

for the scattered system. Because of the conjugation now introduced, the relative phases in [T] are negated, and thus the sense of rotation is reversed. Also, it follows that

$$\begin{bmatrix} \hat{R} \\ \hat{L} \end{bmatrix}^s = \begin{bmatrix} \hat{R} \\ \hat{L} \end{bmatrix}^* .$$

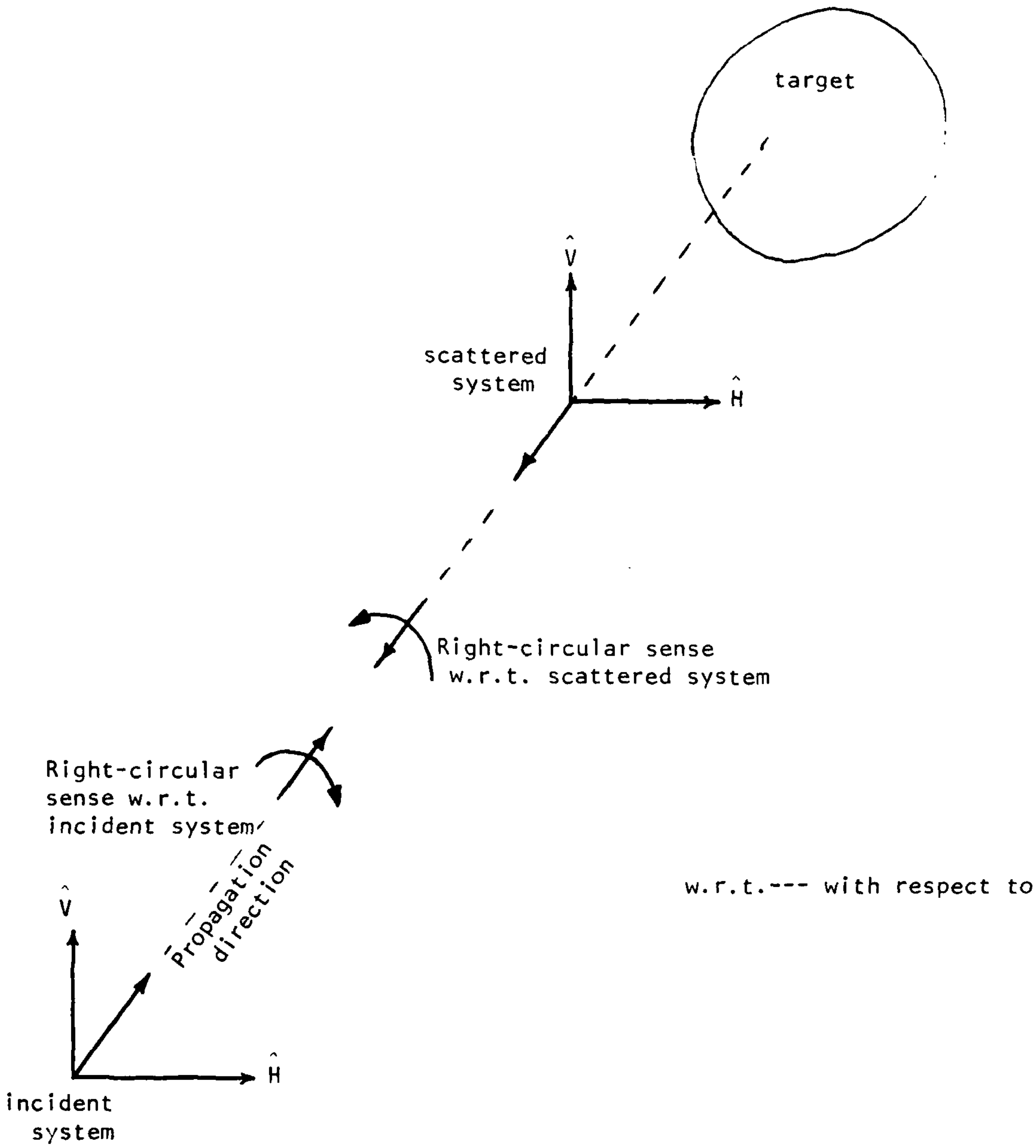

Figure 4.1 Incident and Scattered Coordinate Systems

On adopting this choice for the circular polarization basis of the scattered field, (4.15) follows from (4.14), with the double conjugation being ignored,

$$\begin{bmatrix} E_R^s \\ E_L^s \end{bmatrix} = [T(RL;HV)] \begin{bmatrix} E_H^s \\ E_V^s \end{bmatrix} \tag{4.15}$$

in the same way (4.13) follows from (4.11).

In terms of the linear basis $(\hat{H},\hat{V})$, the scattering matrix $[S(HV)]$ fully describes the scattered depolarized field, with the incident field given, by

$$\begin{bmatrix} E_H^s \\ E_V^s \end{bmatrix} = [S(HV)] \begin{bmatrix} E_H^i \\ E_V^i \end{bmatrix} \quad . \tag{4.16}$$

Similarly, in terms of the circular basis $(\hat{R},\hat{L})$, it follows that

$$\begin{bmatrix} E_R^s \\ E_L^s \end{bmatrix} = [C(RL)] \begin{bmatrix} E_R^i \\ E_L^i \end{bmatrix} \quad . \tag{4.17}$$

Using the definition of the unitary matrix, it follows from (4.16), (4.17), (4.13) and (4.15) that

$$[C(RL)] = [T(RL;HV)]\,[S(HV)]\,[T(RL:HV)]^T \tag{4.18}$$

which transforms [S] to [C] through [T] defined in (4.11), and which is of the form of congruence transformation.

4.6 Curvature Recovery from the Circular Polarization [C]

If the unitary matrix in (4.12) is adopted, then (4.18) becomes

$$[C(RL)] = \begin{bmatrix} \frac{S_{HH} - S_{VV}}{2} + j\, S_{HV} & j\, \frac{S_{HH} + S_{VV}}{2} \\ j\, \frac{S_{HH} + S_{VV}}{2} & \frac{S_{VV} - S_{HH}}{2} + j\, S_{HV} \end{bmatrix} \qquad (4.19)$$

provided that $S_{HV} = S_{VH}$, which is true for the monostatic reciprocal case (also $C_{RL} = C_{LR}$). If conjugation in (4.14) is used to preserve the similarity of sense in both the scattered and incident systems, then an examination of (4.18) reveals that reciprocity is satisfied, i.e. [C] is symmetric(if [S] is symmetric). A different choice of [T] may result in a different [C]. For instance,

$$\text{if} \qquad [T] = \frac{1}{\sqrt{2}} \begin{bmatrix} 1 & +j \\ 1 & -j \end{bmatrix} \qquad (4.12')$$

$$\text{then} \qquad [C] = \begin{bmatrix} \frac{S_{HH} - S_{VV}}{2} + j\, S_{HV} & \frac{S_{HH} + S_{VV}}{2} \\ \frac{S_{HH} + S_{VV}}{2} & \frac{S_{HH} - S_{VV}}{2} - j\, S_{HV} \end{bmatrix} \qquad (4.19')$$

Returning to the [C] in (4.19), in view of (3.5) to (3.7), the matrix elements can be written as

$$C_{RR} = - k\, A_F(k)\ \frac{K_u - K_v}{4\pi}\ [\sin 2\alpha + j \cos 2\alpha] \tag{4.20}$$

$$C_{LL} = - k\, A_F(k)\ \frac{K_u - K_v}{4\pi}\ [\sin 2\alpha - j \cos 2\alpha] \tag{4.21}$$

$$C_{LR} = C_{RL} = - j\, \frac{1}{2\pi}\, k^2\, A_F(k) \tag{4.22}$$

Hence,

$$\left\{\frac{K_u - K_v}{2}\right\}^2 = - k^2\ \frac{C_{LL}\, C_{RR}}{C_{LR}^2} \tag{4.23}$$

which is an equation of curvature recovery from the scattering matrix in circular polarization.

Expressing the ratio $C_{LL}\, C_{RR} / C_{LR}^2$ in terms of the linear polarization [S] elements,

$$\frac{C_{LL}\, C_{RR}}{C_{LR}^2} = \frac{(1 - \mathcal{R})^2 + 4\left(\frac{S_{HV}}{S_{HH}}\right)^2}{(1 + \mathcal{R})^2} \tag{4.24}$$

Combining (4.23) and (4.24),

$$\frac{K_u - K_v}{2} = \pm\, jk\, \left\{\frac{C_{LL}\, C_{RR}}{C_{LR}^2}\right\}^{\frac{1}{2}} \tag{4.25}$$

$$= \pm\, jk \sqrt{\frac{(1 - \mathcal{R})^2 + 4\left(\frac{S_{HV}}{S_{HH}}\right)^2}{(1 + \mathcal{R})^2}} \tag{4.26}$$

Comparing (4.26) to (3.8), it can be observed that the unknown

polarization angle α in (3.8) is being disguised in (4.26) and appears in the form of S_{HV}/S_{HH} which is incorporated into the square root. Thus one advantage of utilizing circular polarization over utilizing linear polarization for curvature recovery is that the polarization angle does not have to be determined, but still the entire scattering matrix has to be measured.

It can be seen that for the case in which $S_{HV} = 0$ ($\alpha = 0$ or 90 degrees), (4.26) reduces to (3.8) and then (3.12). As in the derivation of the phase-curvature relationship, the imaginary part of the square root of $C_{RR}\, C_{LL} \;/\; C_{RL}^{\;2}$ should give better curvature difference and the real part should vanish, as frequency is increasing.

It is to be noted that under suitable conditions, quantities such as the radar cross sections σ_{RL}, σ_{RR}, σ_{LL} and quantities derived from them (e.g. $(1 - \tilde{R})/(1 + \tilde{R})$) yield meaningful measurables in measurements of the backscatter of dielectric spheroids and hydrometeors [32,33,34]; in radar target discrimination techniques, the quantity $|C_{RR}||C_{LL}| - |C_{RL}|^2$ in [36], in view of (4.20) to (4.22), can be interpreted as $[-(1/2\pi)^2 k^4 |A_F(k)|^2]$, which reveals area information for a smooth, convex, conducting target at high frequencies.

4.7 Transformation Invariants of the Scattering Matrix

The transformation of [S] to [C] due to transforming the linear basis $(\hat{H},\hat{V})$ to the circular basis $(\hat{R},\hat{L})$ can be achieved by introducing the appropriate relative phase between the two orthonormal vectors of the (H,V) basis in addition to rotation. To investigate if the transformation is still invariant in changing linear to circular bases, the Det of both sides of (4.18) is taken :

$$\mathrm{Det}\ \{[C]\} = \mathrm{Det}\ \{[T]\}\ .\ \mathrm{Det}\ \{[S]\}\ .\ \mathrm{Det}\ \{[T]^T\}$$

$$= \mathrm{Det}\ \{[T]\}\ .\ \mathrm{Det}\ \{[S]\}\ .\ \mathrm{Det}\ \{[T]^{*\ -1}\}$$

$$= \{\frac{\mathrm{Det}\ \{[T]\}}{|\mathrm{Det}\ \{[T]\}|}\}^2\ .\ \mathrm{Det}\ \{[S]\}$$

$$= e^{j2\mathrm{Arg}(\mathrm{Det}\{[T]\})}\ .\ \mathrm{Det}\ \{[S]\} \qquad (4.27)$$

From the general form of [T] given on page 33,

$$\mathrm{Arg}(\mathrm{Det}\ \{[T]\}) = \phi_1 + \phi_4 = \phi_2 + \phi_3$$

Hence,

$$\mathrm{Det}\ \{[C]\} = e^{j2(\phi_1 + \phi_4)}\ .\ \mathrm{Det}\ \{[S]\} \qquad (4.28)$$

It can be easily proven that $|\mathrm{Det}\ \{[T]\}| = 1$ for the unitary matrix [T], but it is generally not true that the determinant of a unitary matrix is purely real. Thus, the determinant of [C] is strictly invariant iff Det {[T]} is purely real, i.e.

$$\mathrm{Det}\ \{[T]\} = \pm 1\ , \qquad (4.29)$$

otherwise the invariant differs only by a phase shift of $2(\phi_1 + \phi_4)$. For examples, the [T] given by (4.12) renders

$$C_{RR}\ C_{LL} - C_{RL}^{\ 2} = S_{HH}\ S_{VV} - S_{HV}^{\ 2} \qquad (4.30)$$

as is also evident from (4.19). The invariant value is the same as that in (4.4) derived from the curvature recovery model, since the rotational matrix possesses a real, unity determinant. On the other hand, the [T] in (4.12') will not preserve strict transformation invariance, as is also

evident from (4.19') (i.e. the determinants of [C] and [S] are equal in magnitude but of opposite sign).

To show from the curvature recovery model the invariance of Span {[C]}, equations (4.20)-(4.22) and (3.5)-(3.7) can be used to give

$$\begin{aligned}\text{Span } \{[C]\} &= |C_{RR}|^2 + |C_{LL}|^2 + 2|C_{RL}|^2 \\ &= |S_{AA}|^2 + |S_{BB}|^2 + 2|S_{AB}|^2 \\ &= \text{Span } \{[S]\} \quad ,\end{aligned}$$

which equals the invariant value in (4.3).

It can be shown that the span is in general invariant, regardless of whether (4.29) holds or not. Denoting the trace of a square matrix (i.e. the sum of the diagonal elements) by Tr, it follows that

$$\begin{aligned}\text{Span } \{[C]\} &= \text{Tr } \{[C]^*[C]\} \\ &= \text{Tr } \{[[T][S][T]^T]^*[[T][S][T]^T]\} \quad \text{(from (4.18))} \\ &= \text{Tr } \{[[T]^*[S]^*[S][T]^T]\}\end{aligned}$$

$[S]^*[S]$ is identified as the power scattering matrix [P] of [S] [39,38], i.e.

$$[P] = [S]^*[S] \tag{4.31}$$

Let [P'] be the power scattering matrix of [C], i.e.

$$[P'] = [C]^*[C] \tag{4.32}$$

$$= [T]^*[S]^*[S][T]^T \tag{4.33}$$

Hence,

$$\text{Span } \{[C]\} = \text{Tr } \{[P']\}$$

$$= \sum_i P'_{ii}$$

$$= \sum_k \sum_l \{P_{kl} \; [\sum_i T^*_{ik} T_{il}]\}$$

Since the set of conditions

$$|T_{11}|^2 + |T_{21}|^2 = 1$$

$$|T_{12}|^2 + |T_{22}|^2 = 1$$

$$T_{11}T^*_{12} + T_{21}T^*_{22} = 0$$

is equivalent to the definition of a unitary matrix, hence (after some algebraic manipulation) it follows that

$$\text{Span } \{[C]\} = P_{11} + P_{22}$$

Thus,

$$\text{Span } \{[C]\} = \text{Tr } \{[P']\} = \text{Tr } \{[P]\} = \text{Span } \{[S]\} \qquad (4.34)$$

4.8 An Interpretation of the Scattering Ratio

The radar cross section σ_{rt} has been defined in [41] as follows :

$$\sigma_{rt} = |\underline{h}^r \cdot [S]\underline{h}^t|^2 \qquad (4.35)$$

where $\underline{h}^t$ is the transmitting polarization vector and $\underline{h}^r$ is the antenna height [20]. In this definition, $\underline{h}^t$ and $\underline{h}^r$ are normalized to unity. It has been shown in [20] that for radar systems that use identical transmitting and receiving antennas, the radar cross section is maximum if

$$[S]\underline{h} = \lambda_s \underline{h}^* \qquad (4.36)$$

where $\underline{h}$ denotes the antenna polarization which yields maximum power reception, and λ_s denotes the complex eigenvalue of (4.36). Moreover, the scattering matrix can be diagonalized by a change-of-basis unitary transformation, using a unitary matrix which consists of the eigenvectors of (4.36) 20,42 . The diagonalized form of [S] is

$$[S_d] = \begin{bmatrix} \lambda_{s1} & 0 \\ 0 & \lambda_{s2} \end{bmatrix}$$

where λ_{s1} and λ_{s2} are the eigenvalues, with $|\lambda_{s1}| > |\lambda_{s2}|$. The maximum radar cross section is given by [20]

$$\sigma_{max} = |\lambda_{s1}|^2 \tag{4.37}$$

The corresponding monostatic power scattering matrix is thus diagonalized too :

$$[P_d] = [S_d]^* [S_d] \quad \text{(from equation (4.31))}$$

$$= \begin{bmatrix} |\lambda_{s1}|^2 & 0 \\ 0 & |\lambda_{s2}|^2 \end{bmatrix}$$

By the invariance properties of [S],

$$\text{Span } \{[S]\} = \text{Span } \{[S_d]\}$$

$$= |\lambda_{s1}|^2 + |\lambda_{s2}|^2 \tag{4.38}$$

$$= \text{Tr } \{[P_d]\}$$

$$= \text{Tr } \{[P]\} \tag{4.39}$$

Assuming (4.29) for strict invariance,

$$\text{Det}\ \{[S]\} = \text{Det}\ \{[S_d]\}$$

$$= \lambda_{s1}\ \lambda_{s2} \tag{4.40}$$

Therefore,

$$D = \frac{\text{Det}\ \{[S]\}}{\text{Span}\ \{[S]\}}$$

$$= \frac{\lambda_{s1}\ \lambda_{s2}}{|\lambda_{s1}|^2 + |\lambda_{s2}|^2} \tag{4.41}$$

For high frequencies, it has been shown in this thesis that

$$D = 0.5\ e^{j2\text{Arg}\ A_F(k)} \tag{4.42}$$

Comparing (4.41) and (4.42) and assuming that frequency is increasingly high,

$$|\lambda_{s1}| \rightarrow |\lambda_{s2}| \tag{4.43}$$

and $$\text{Arg}\ \lambda_{s1} + \text{Arg}\ \lambda_{s2} \rightarrow 2\ \text{Arg}\ A_F(k) \tag{4.44}$$

Combining (4.37), (4.39), (4.41), (4.42) and (4.43),

$$\text{Tr}\ \{[P]\} \simeq 2\ \sigma_{max} \tag{4.45}$$

for high frequencies.

Accordingly, $|D|$ may be interpreted as the ratio of the maximum radar cross section to the trace of the power scattering matrix. The power scattering matrix has been defined by Graves in [39] and

represents the total power backscattered from the target for any transmitting polarization.

To conclude this chapter, it is to be noted that the invariant transformation can of course be extended to the more general elliptic case. The scattering ratio has tacitly been extended in its definition to the general elliptic polarization in Section 4.8. Equations (4.7) and (4.10) which describe the behavior of the scattering ratio are thus generalized.

CHAPTER V

NUMERICAL VERIFICATION

5.1 Data Description

Both theoretical and experimental data are available to verify the special case of the phase-curvature relationship (3.12), i.e. the case in which the incident polarization coincides with one of the directions of the principal curvatures at specular points on the equator of the prolate spheroid. The theoretical data was obtained by a time-domain synthesis of the impulse response technique [15]. The solutions generated by this technique were checked against other theoretical solutions [8,16] with excellent agreement [15]. The theoretical data were converted in the form of amplitudes and phases of the elements of the scattering matrix. The experimental data were measured at the Electro-Science Laboratory of the Ohio State University (ESL-OSU). The experiments were conducted [28] on a frequency-domain range yielding the backscattered returns S_{VV} and S_{HH} (S_{HV} and S_{VH} being zero in this case). The 'size' of the prolate spheroid used in the experiment was 6 inch : 12 inch, and the data were measured for two principal polarization cases in which $\alpha = 0$ (VV or TE) and $\alpha = \pi/2$ (HH or TM) for aspect angles from 0 (nose-on) to 90 degrees (broad-side on) in steps of 15 degrees (Figure 3.2). After measurement, the data were smoothed. Two of the smoothed frequency-domain data blocks, namely, the 2-4 GHz block and the 4-8 GHz block, were used in this thesis, covering a range of 3.19 to 12.76 in terms of the values of kb ($2\pi/\lambda$ .b). The error bounds

on the experimental data were specified to be $\pm$ 2 dB in magnitude and $\pm$ 10 degrees in phase data.

5.2 Direct Verification of the Phase-Curvature Relationship

5.2.1 Theoretical Data

A typical result obtained with the theoretical test data is presented in Figure 5.1. In Figure 5.1(a), the right-hand side of (3.12) is plotted against kb (in steps of 0.1 from 0.1 to 18). From this graph it is clear that as frequency increases, the phase-curvature relationship becomes more accurate. The aspect angle is 90 degrees (broadside incidence), and the corresponding curvature difference divided by two is 0.375, to which the right-hand side of (3.12) converges. In Figure 5.1(b), the real part of $(1 - \hat{R})/(1 + \hat{R})$ multiplied with k approaches zero. Although not presented in this thesis, the real part itself (without the factor k) converges to zero at a much faster rate, particularly at large values of k. In Figure 5.1(c), the imaginary part multiplied with k tends to the value 0.375. The scattering chart (imaginary part versus real part) is shown in Figure 5.1(d). As predicted, the plot is indeed a spiral which, as k is increased, converges to the point (0, -0.375) on the imaginary axis.

5.2.2 Experimental Data

An extensive amount of testing of the phase-curvature relationship has been conducted with the experimental input data. It was realized that because of the nature of the tangent function, a direct

test of (3.12) with input data which have a ± 10 degree error in phase measurement, is not very useful in a graphical presentation. Thus the complex plane plots of some typical measurement data are presented in Figures 5.2 to 5.4.

The plots in Figure 5.2(a)(i) to (iii) are the experimental versions of the theoretical plots in Figures 5.1(d), (b) and (c). Figures 5.2(a)(i) does indeed hover around the predicted point on the imaginary axis. This behavior is not so clearly visible in Figure 5.2(b)(i), where according to the theoretical predictions this plot should have given better results for the higher frequency range. This discrepancy is mainly attributed to the following factor : the phase error magnified through the tangent function gets even more magnified through the multiplication with large values of k. The plots shown in Figures 5.3(a) and (b) are for the nose-on incidence case ($\phi = 0$) for which there is no polarization dependence and $(K_u - K_v)/2$ vanishes. Figure 5.3(b) is of the 4-8 GHz block. The case presented in Figures 5.4(a) and (b) are for $\phi = 45$ degrees, which is representative of a typical aspect. Once again, the results for the 4-8 GHz block are not as good as the 2-4 GHz block.

It is to be noted that the relative phase error mentioned in Chapter IV becomes significant at high frequencies. Figure 5.5 shows the effects of an error of 0.5 millimeters between the TE and the TM antenna positions along the direction of propagation. The error is simulated within the theoretical data. The scattering chart of

Figure 5.1(d) now changes from a spiral to a helix elongating mainly along the imaginary axis and away from the exact value of $(K_u - K_v)/2$. If the error is negative, the helix elongates in the opposite direction. An observation of the scattering charts of the 4-8 GHz block reveals that the plots somewhat look like a helix rather than a spiral. Thus, the relative phase error partially explains that, for the 4-8 GHz data, the scattering chart deviates more from theoretical prediction than for the 2-4 GHz data. It is to be noted that in the 4-8 GHz block, there were many data points for which accurate results were found. In general, all the experimental tests and the theoretical data supported the approximate phase-curvature relationship well.

5.3 Verification of the Scattering Ratio D

5.3.1 Theoretical Data

A complex plot of D (imaginary part versus real part) with the theoretical data as input is depicted in Figure 5.6(a). For high frequencies, the phase of D, in theory, converges to a constant value of 2 Arg $A_F(k)$. However, a circle rather than a cluster of points of phases around 2 Arg $A_F(k)$ results. This is due to the fact that the phase fluctuates rapidly at frequencies not high enough. Even the range of frequencies covered by the set of theoretical data (kb up to 18) is not sufficiently high to show the convergence. As predicted, the radius of the circle is indeed 0.5. In Figure 5.6(b), only the amplitude of D is plotted versus kb. Clearly, the amplitude converges to 0.5 even at low values of k, in contrast to the behavior

of the phase of D.

5.3.2 Experimental Data

Figures 5.7 to 5.12 are the experimental versions of Figure 5.6. Figures 5.7 to 5.9 cover the frequency range from 2 to 4 GHz, with aspect angles being 90, 0 and 45 degrees respectively, whereas the rest cover the frequency range from 4 to 8 GHz. All the complex plots of D depict an envelope circle of radius 0.5. The nearer the data points to this envelope, the more accurate they are (for high values of kb).

It is interesting to observe that both Figure 5.12 and 5.4(b) show that the data block of 4-8 GHz of 45 degree aspect is least accurate among the experimental data blocks.

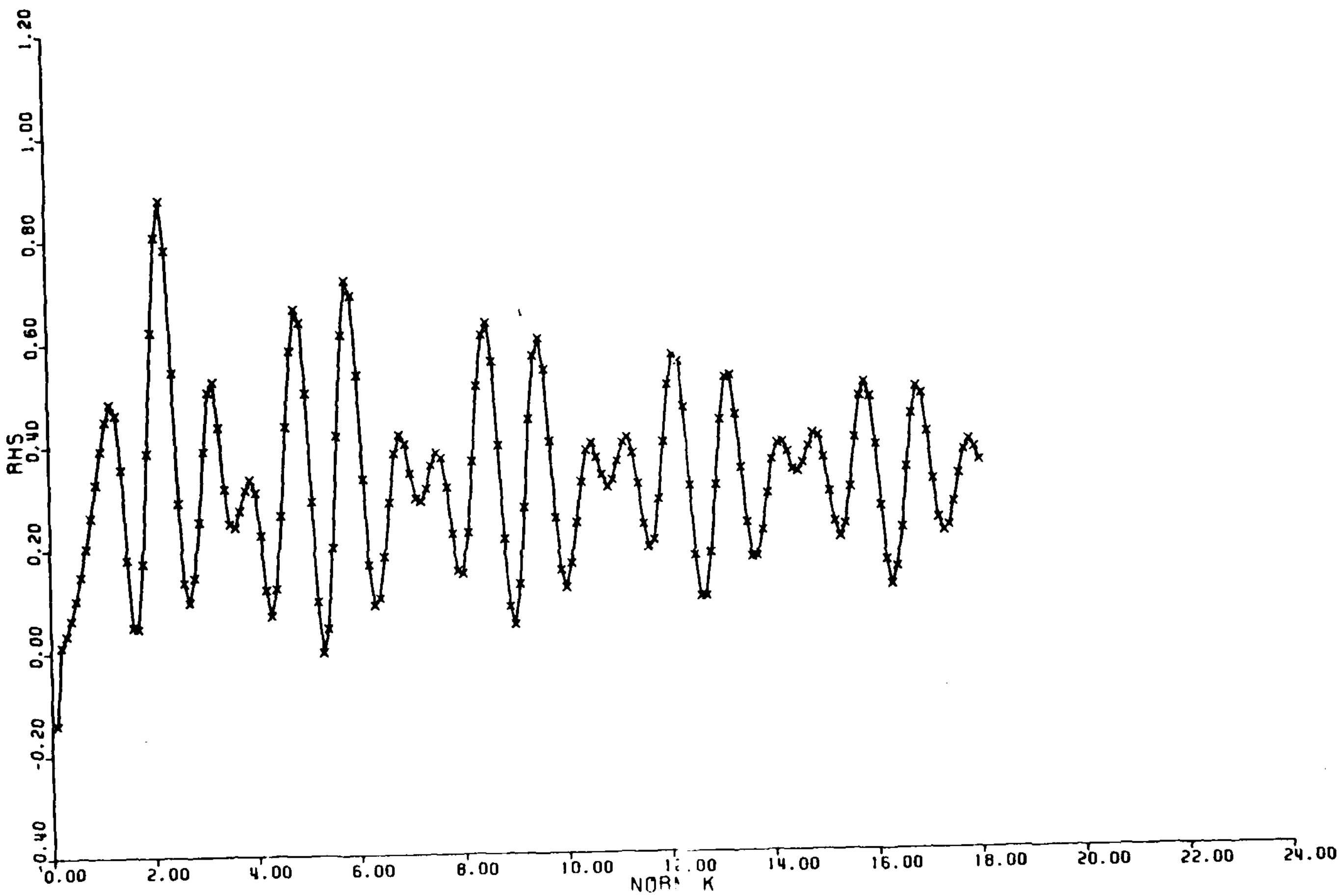

Figure 5.1(a) Right-hand Side of Eq.(3.12) versus k

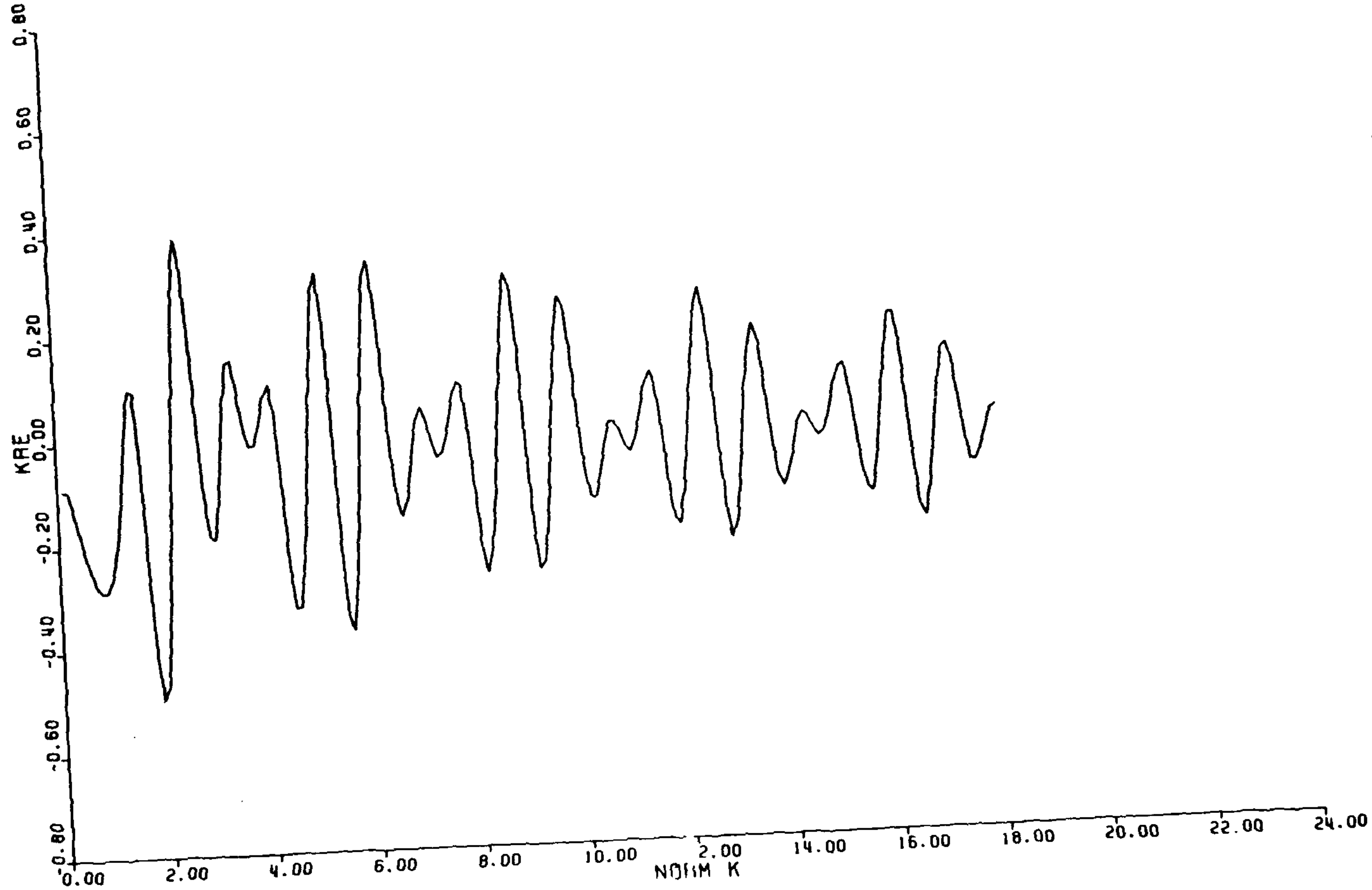

Figure 5.1(b) Convergence of k Re $\{(1 - \tilde{R})/(1 + \tilde{R})\}$

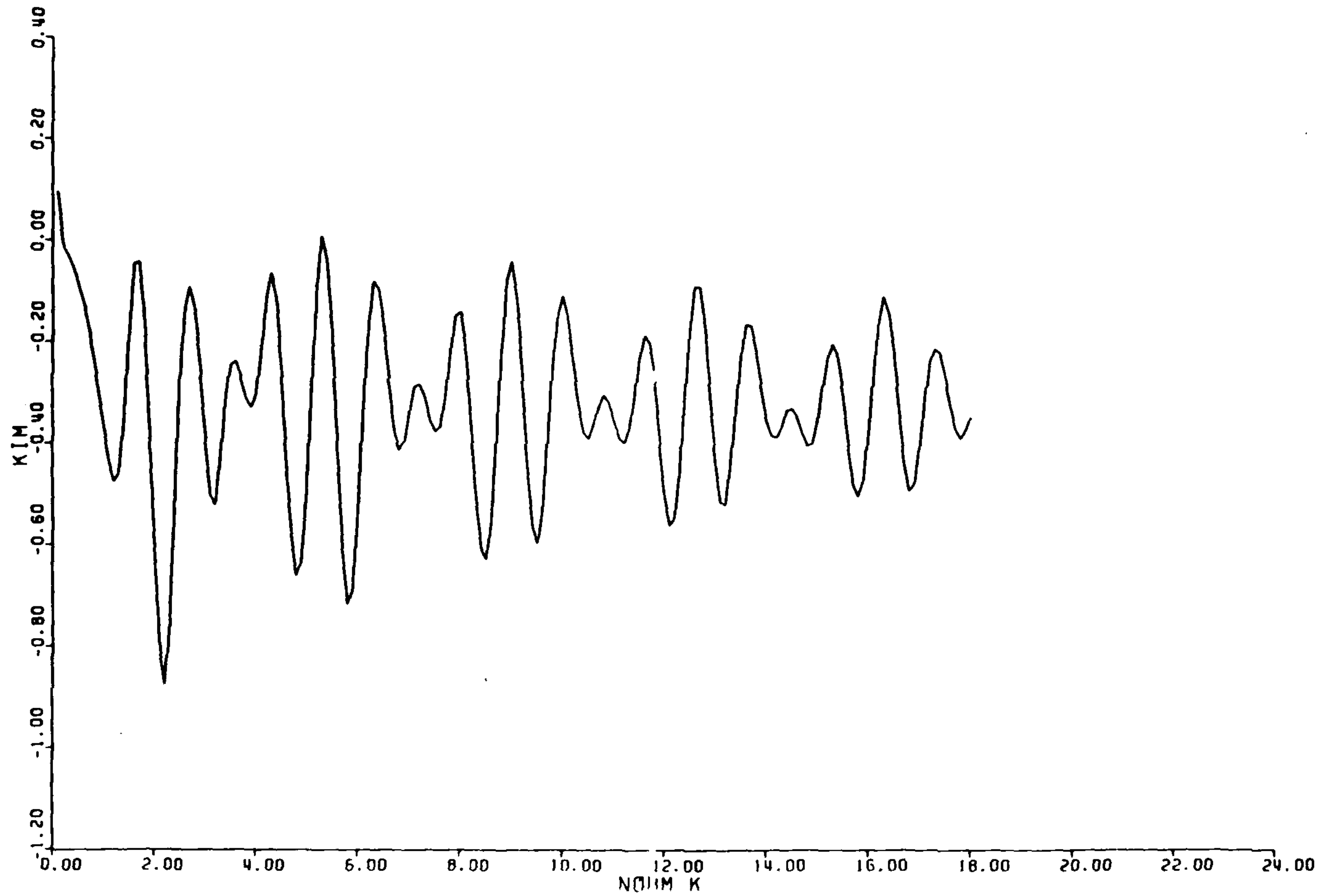

Figure 5.1(c) Curvature Recovery from k Im $\{(1 - \tilde{R})/(1 + \tilde{R})\}$

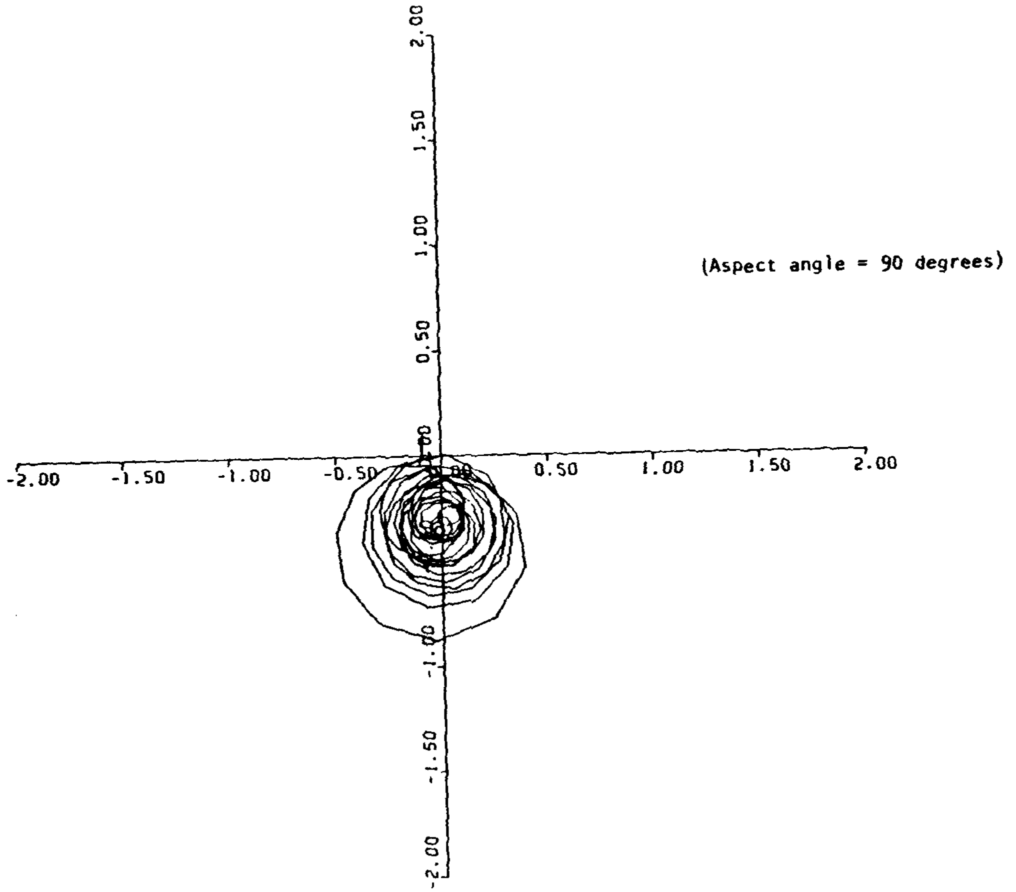

Figure 5.1(d) The Scattering Chart from Theoretical Data

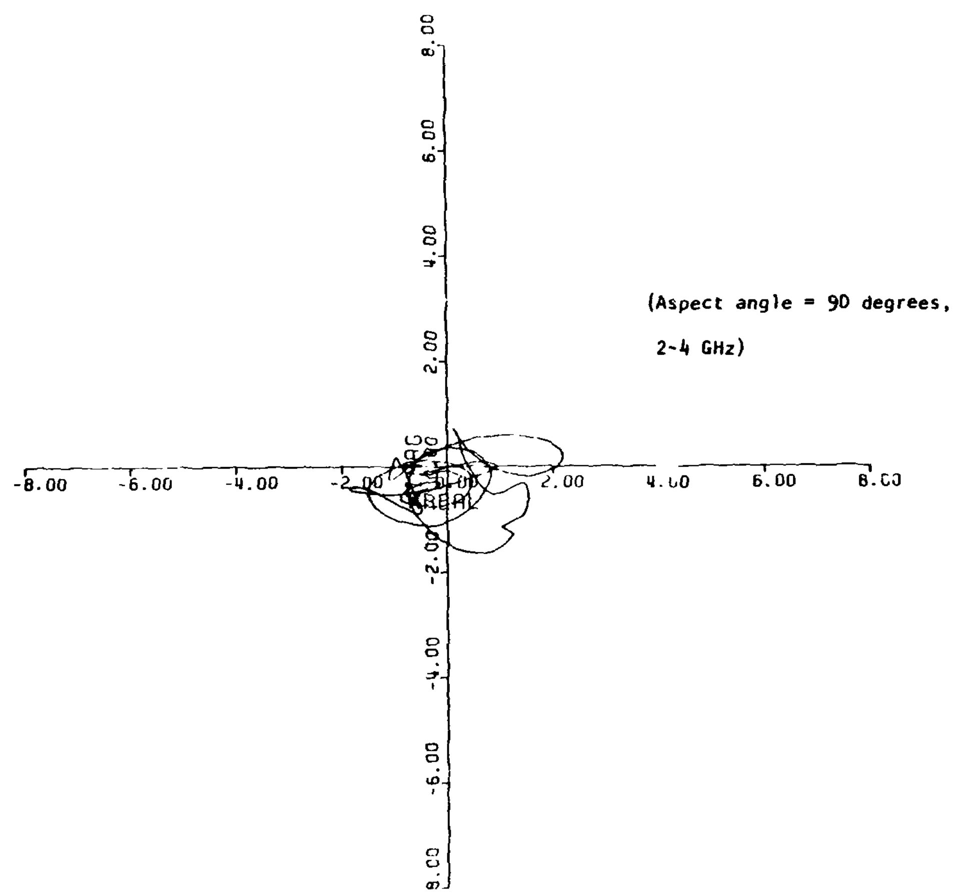

Figure 5.2(a)(i) The Scattering Chart from Experimental Data

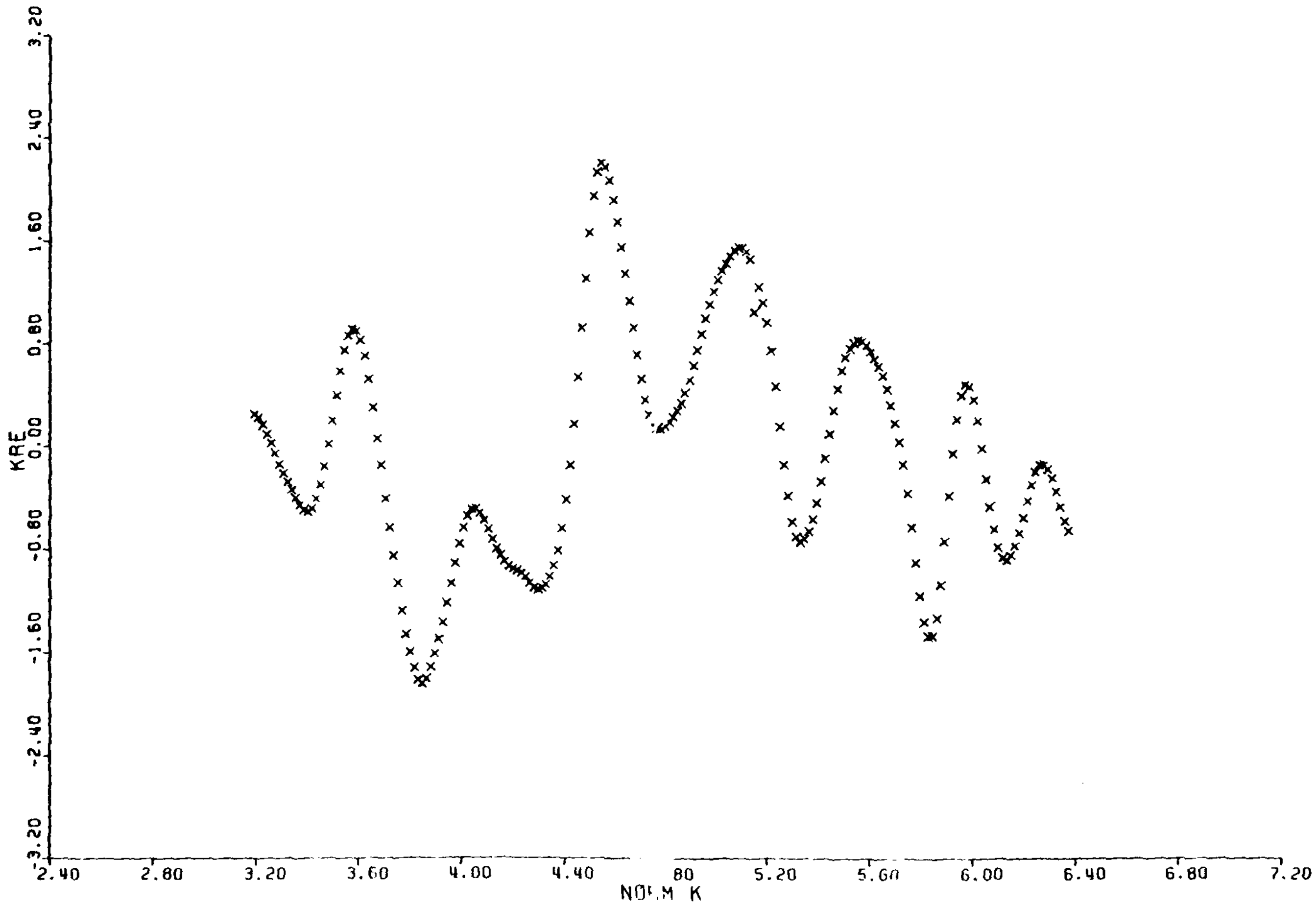

Figure 5.2(a)(ii) k Real Part versus k

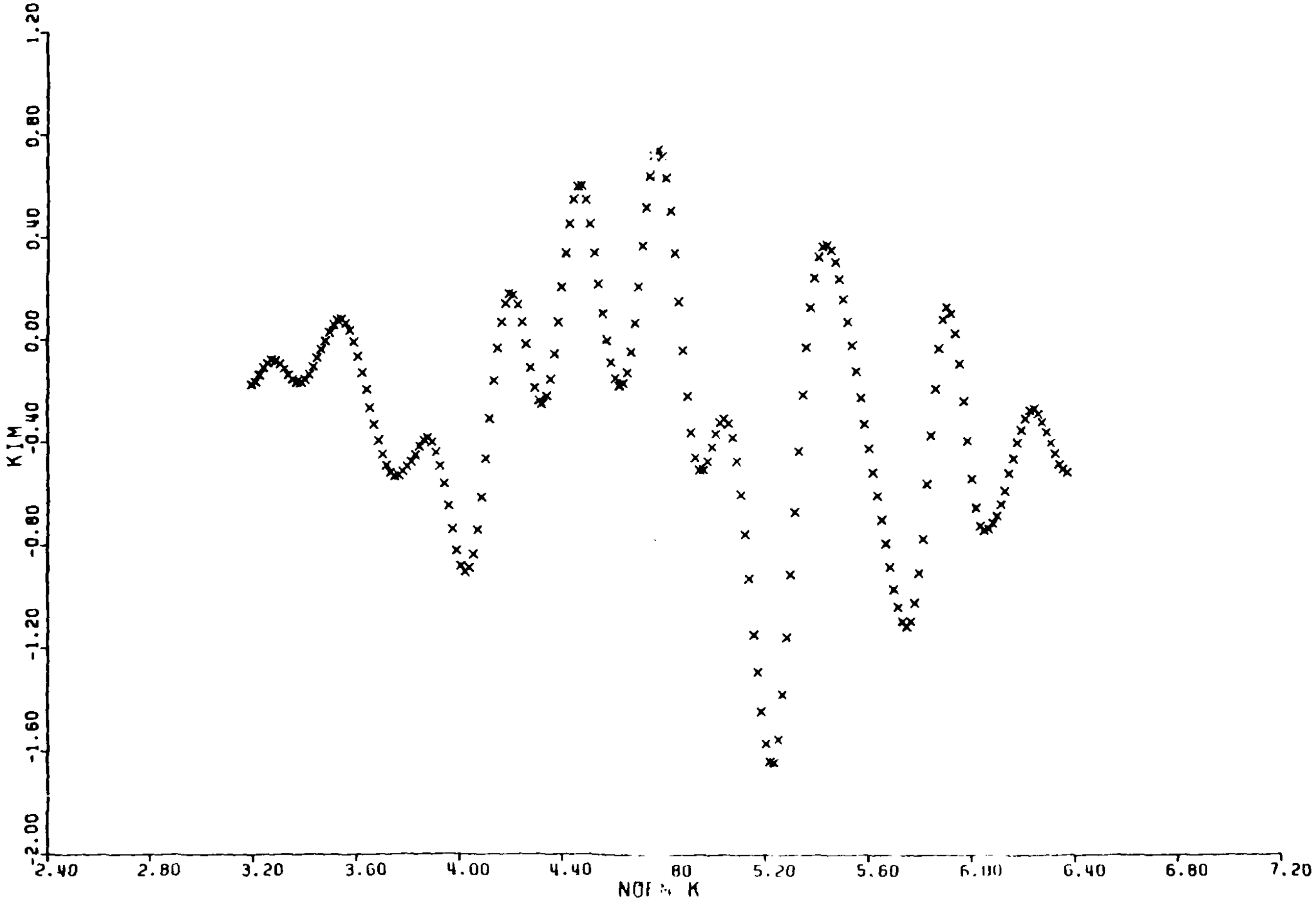

Figure 5.2(a)(iii) k Imaginary Part versus k

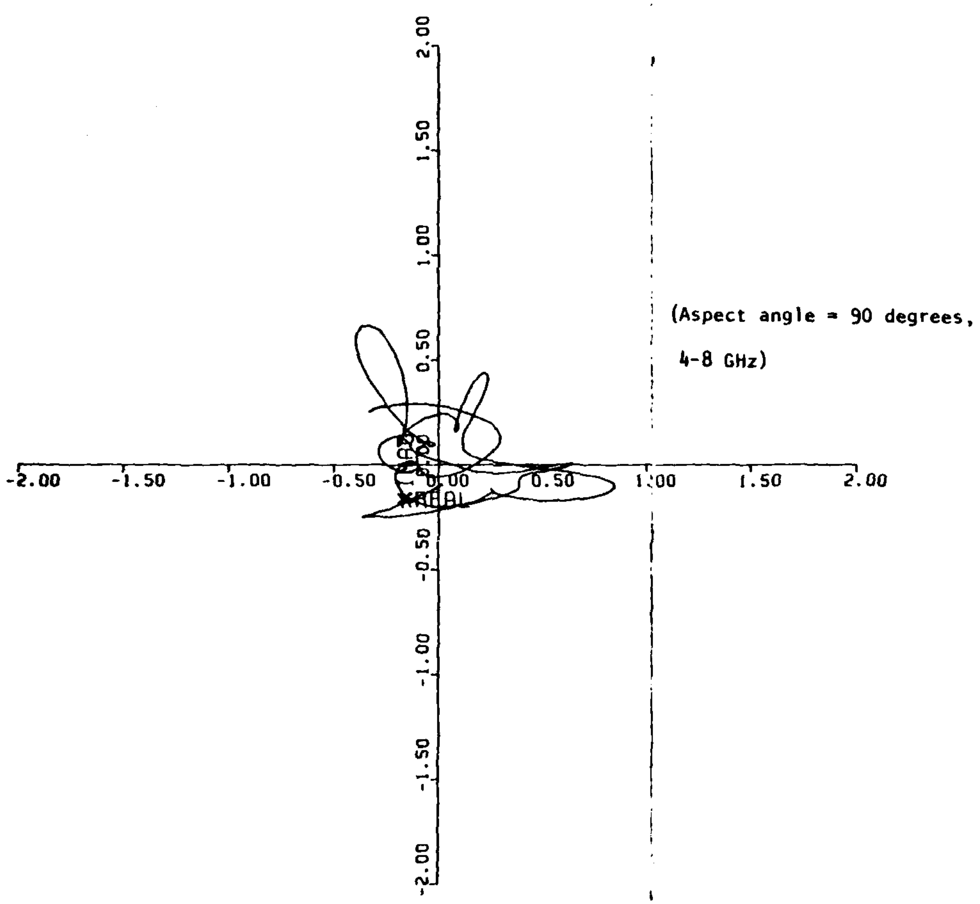

Figure 5.2(b)(i) The Scattering Chart from Experimental Data

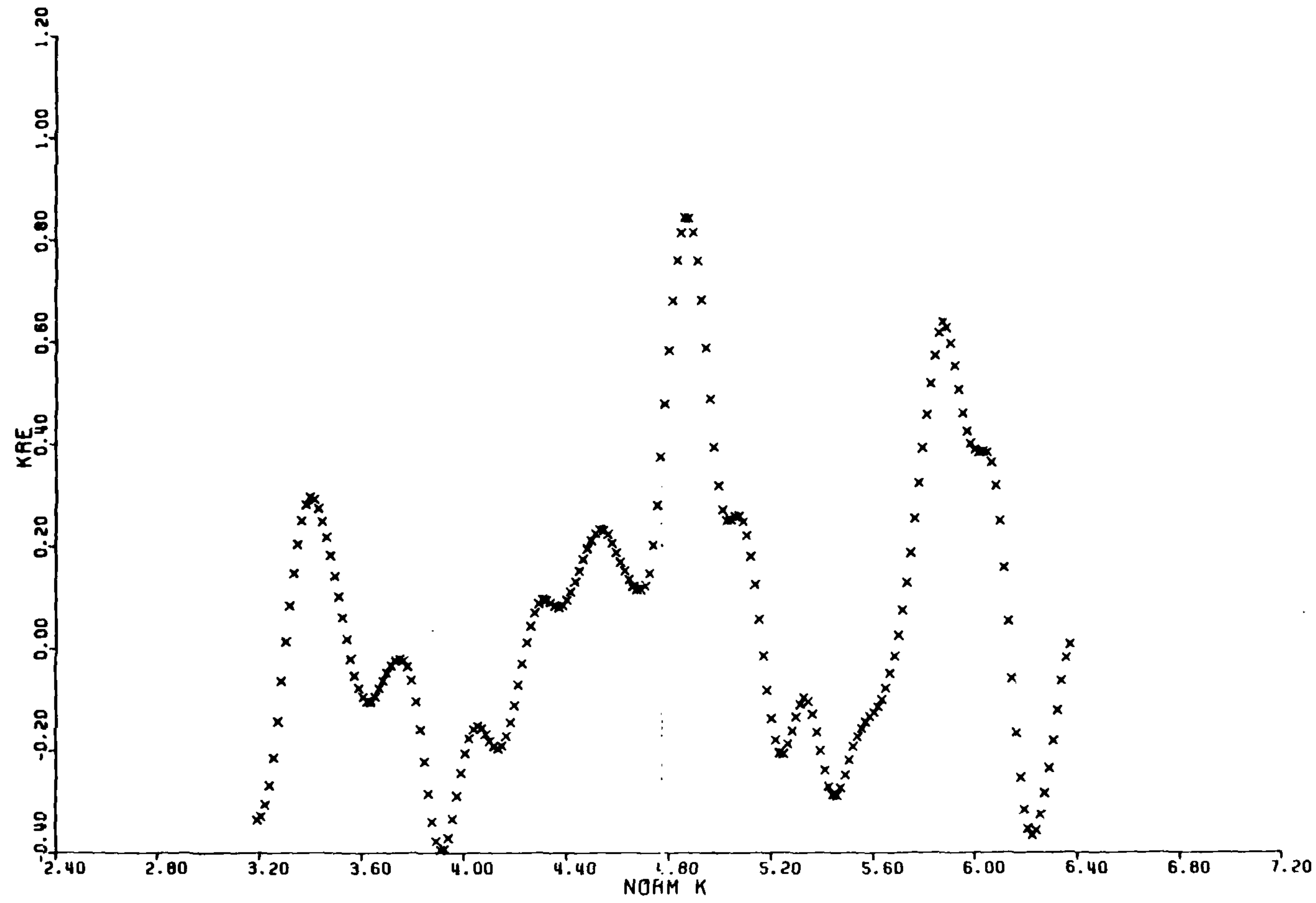

Figure 5.2(b)(ii) k Real Part versus k

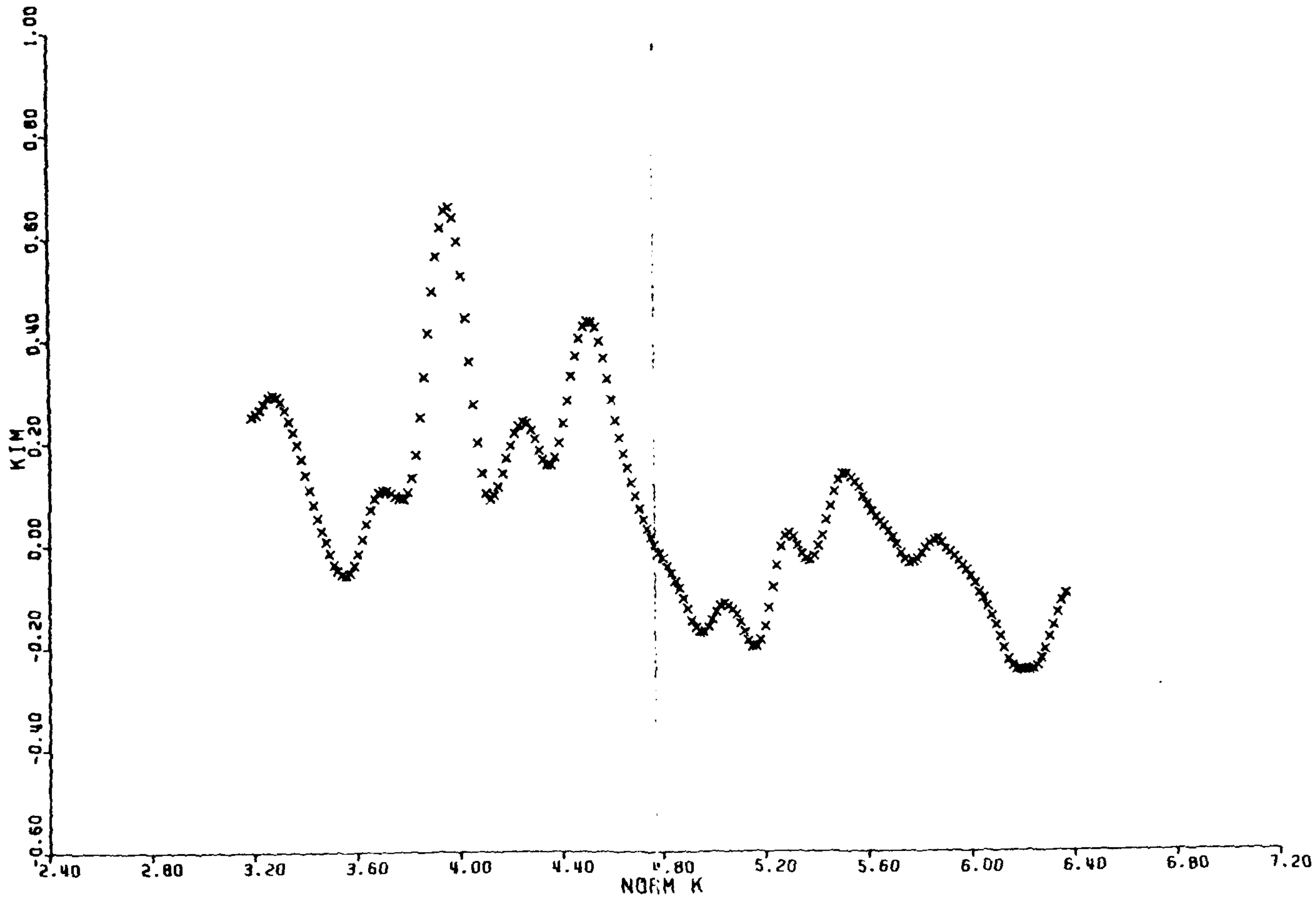

Figure 5.2(b)(iii) k Imaginary Part versus k

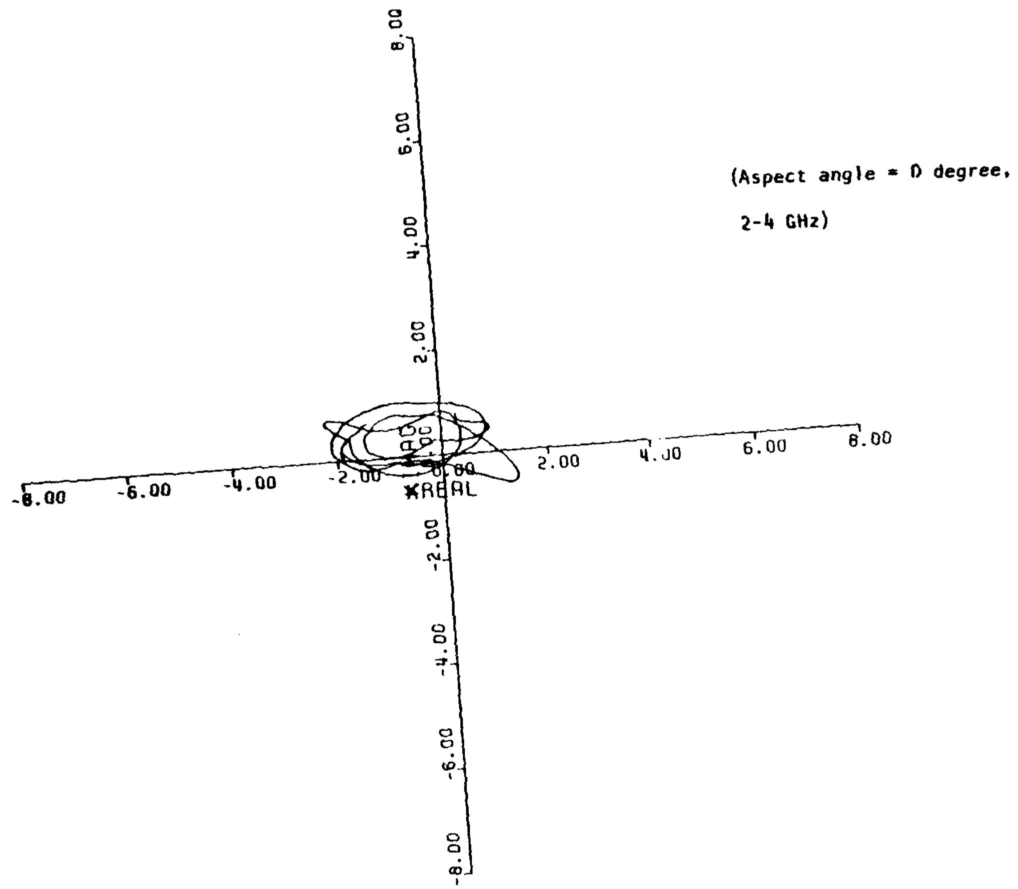

Figure 5.3(a)(i) The Scattering Chart from Experimental Data

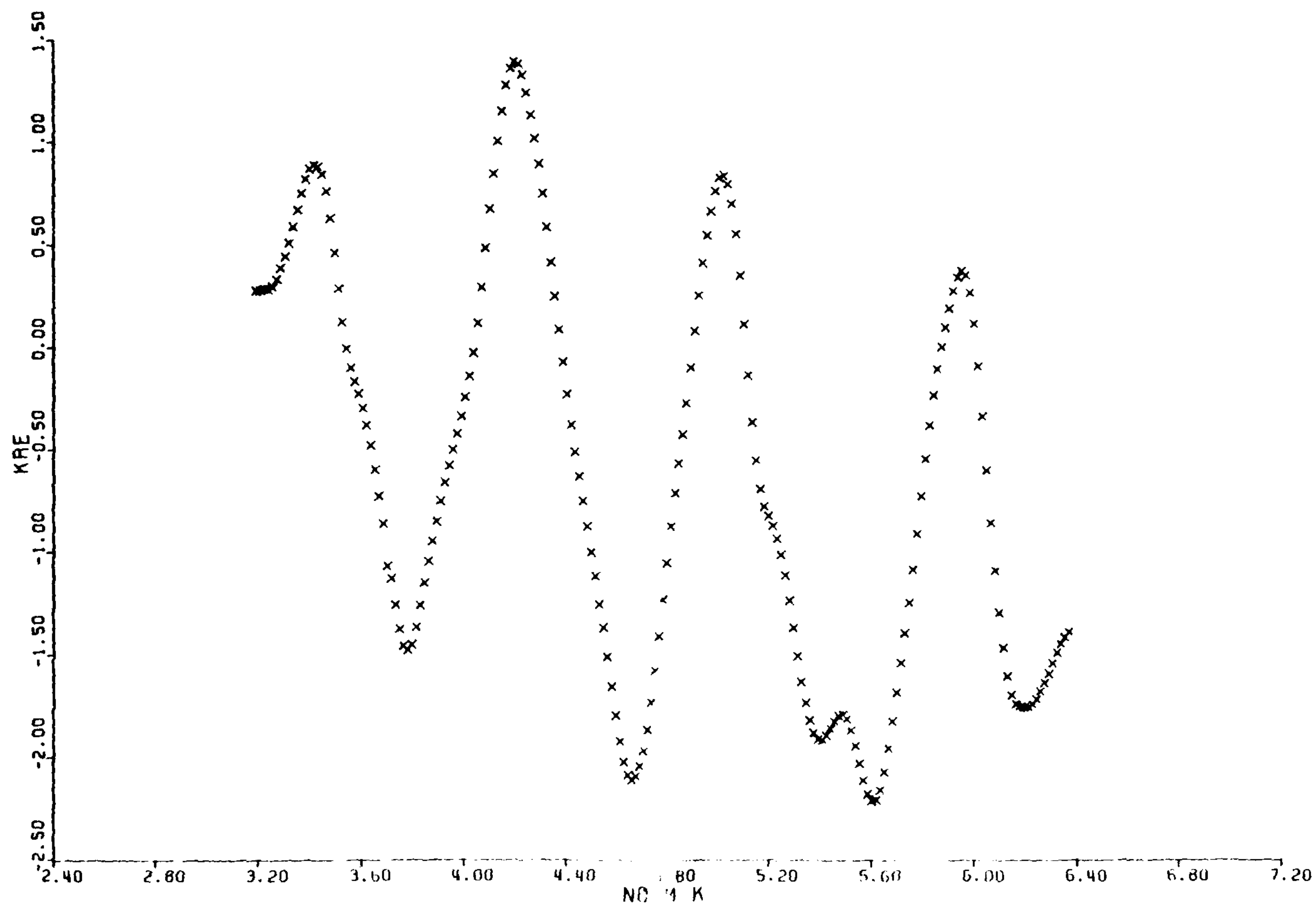

Figure 5.3(a)(ii) k Real Part versus k

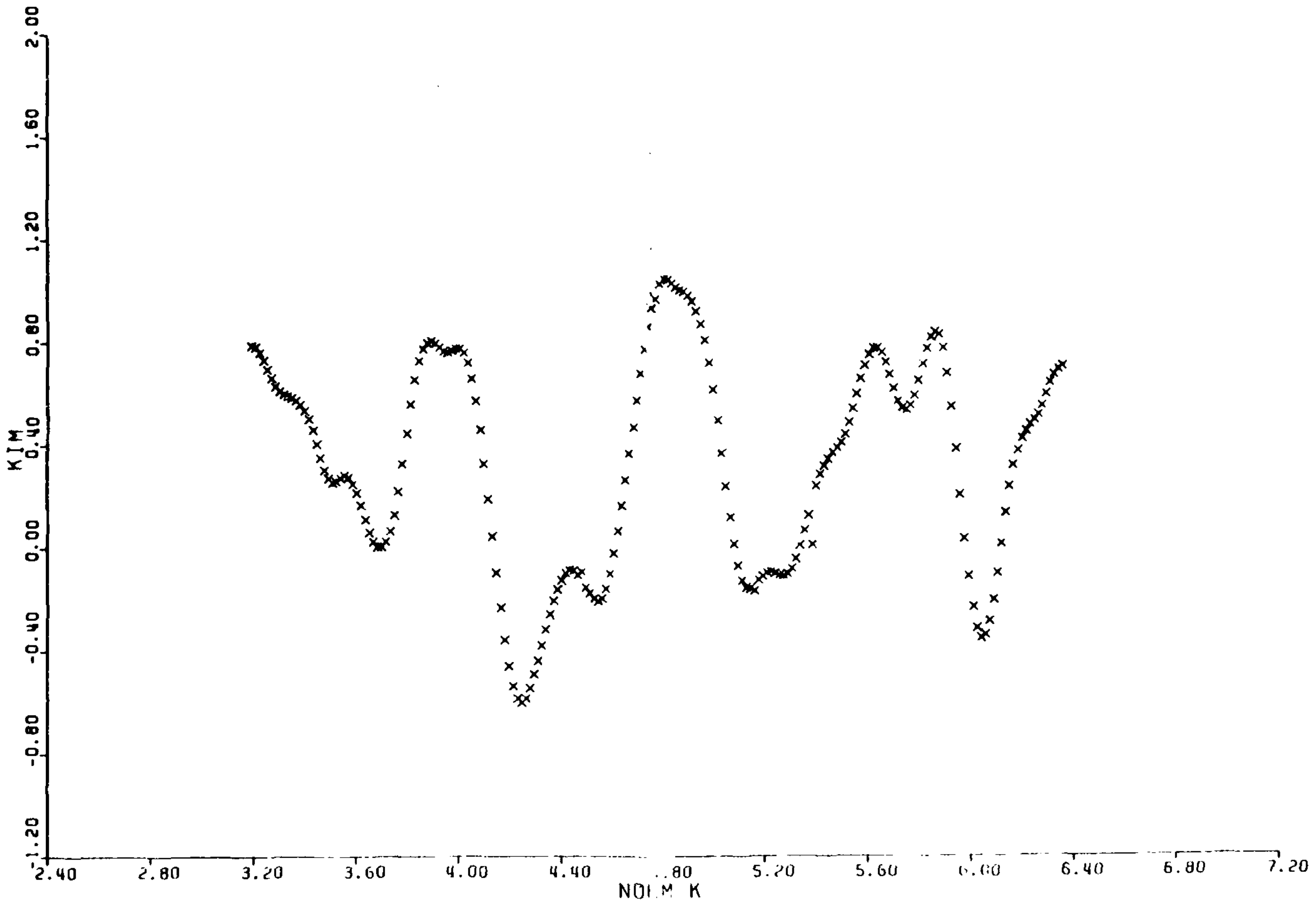

Figure 5.3(a)(iii) k Imaginary Part versus k

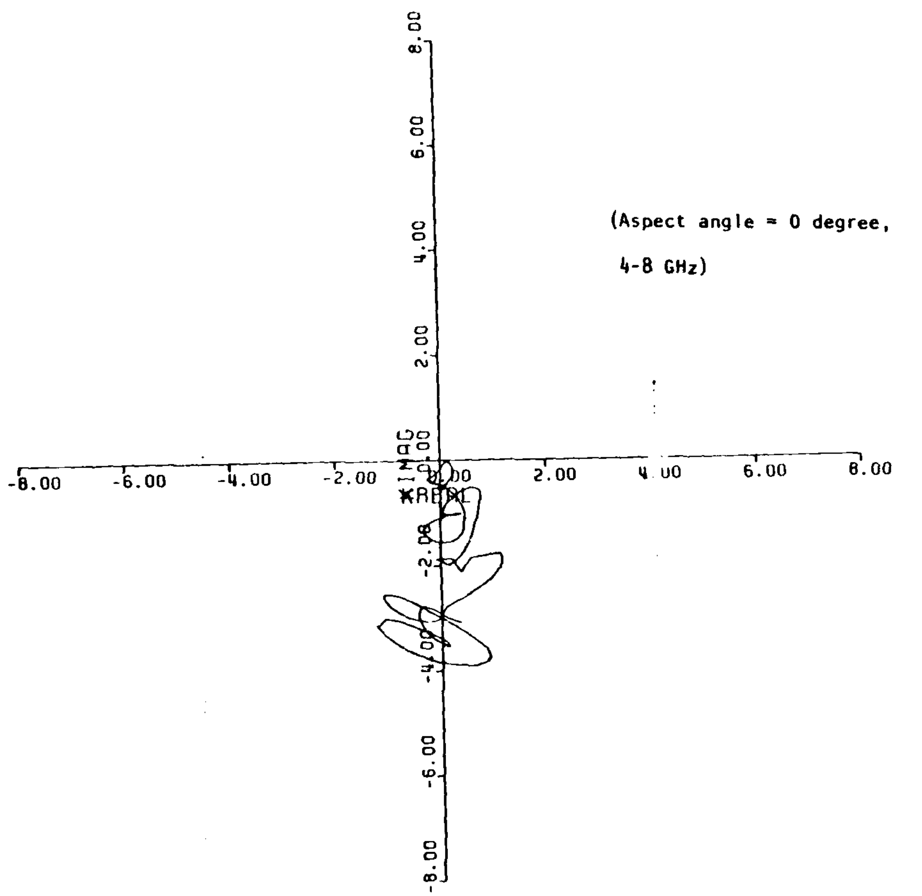

Figure 5.3(b)(i) Scattering Chart from Experimental Data

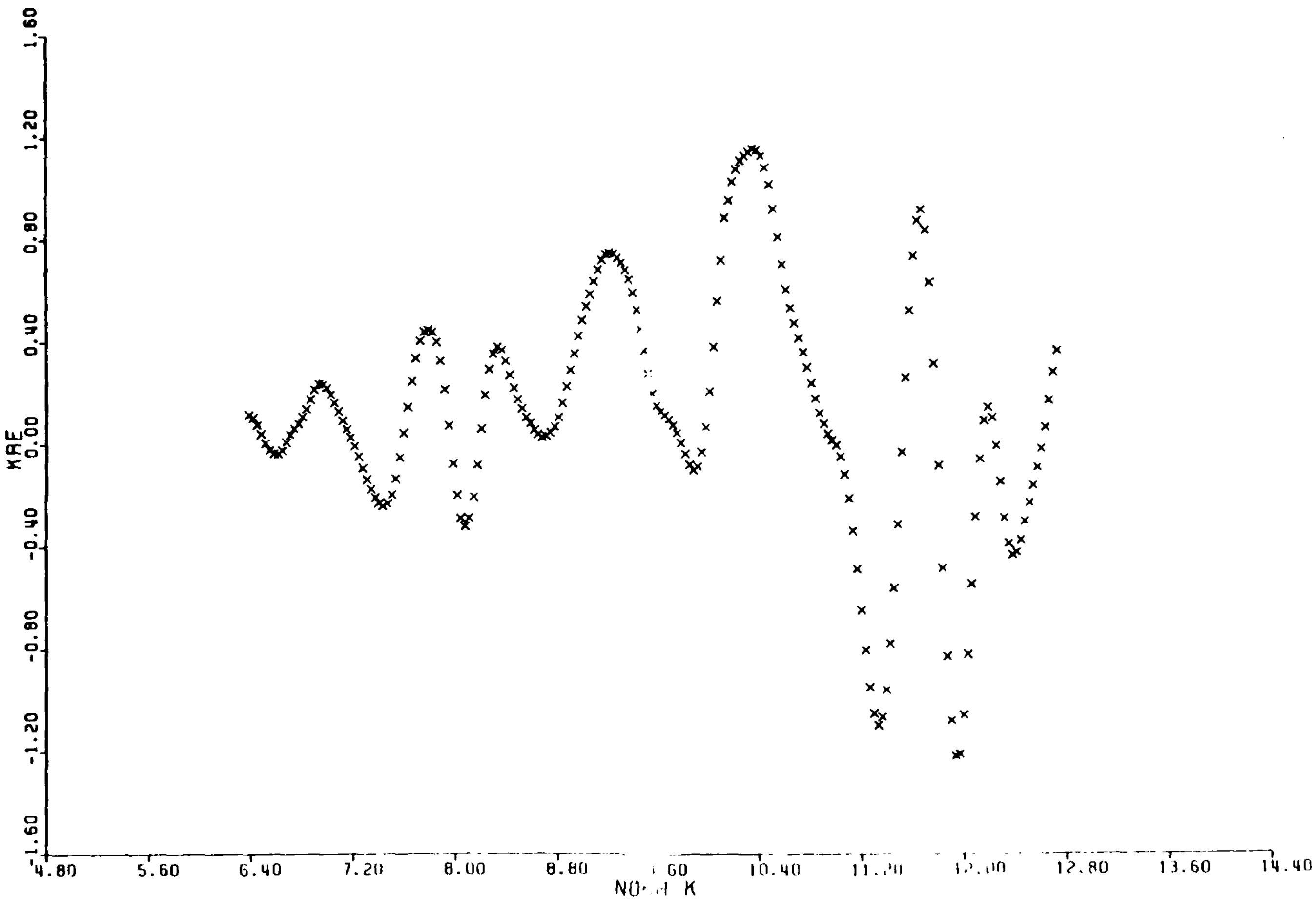

Figure 5.3(b)(ii) k Real Part versus k

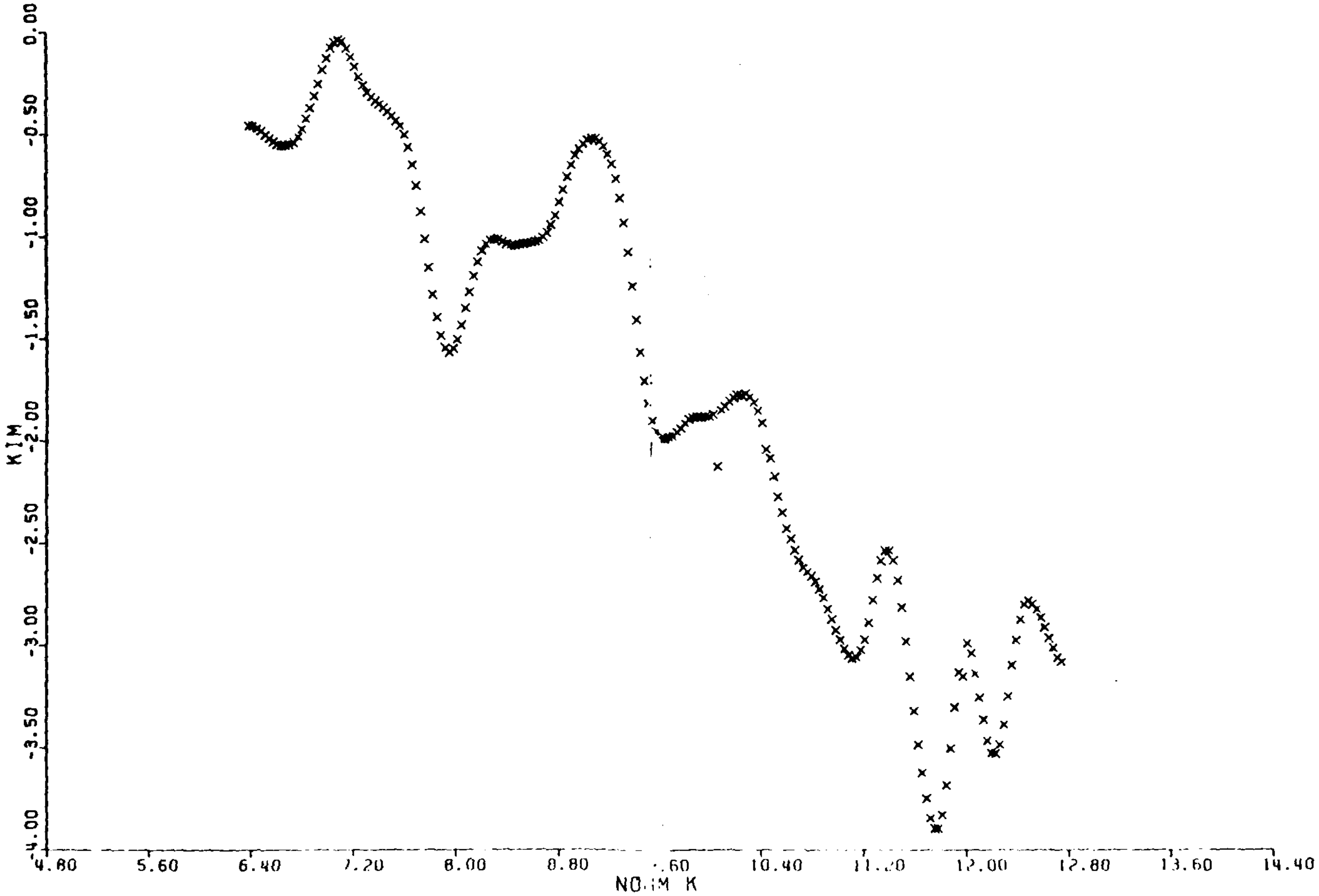

Figure 5.3(b)(iii) k Imaginary Part versus k

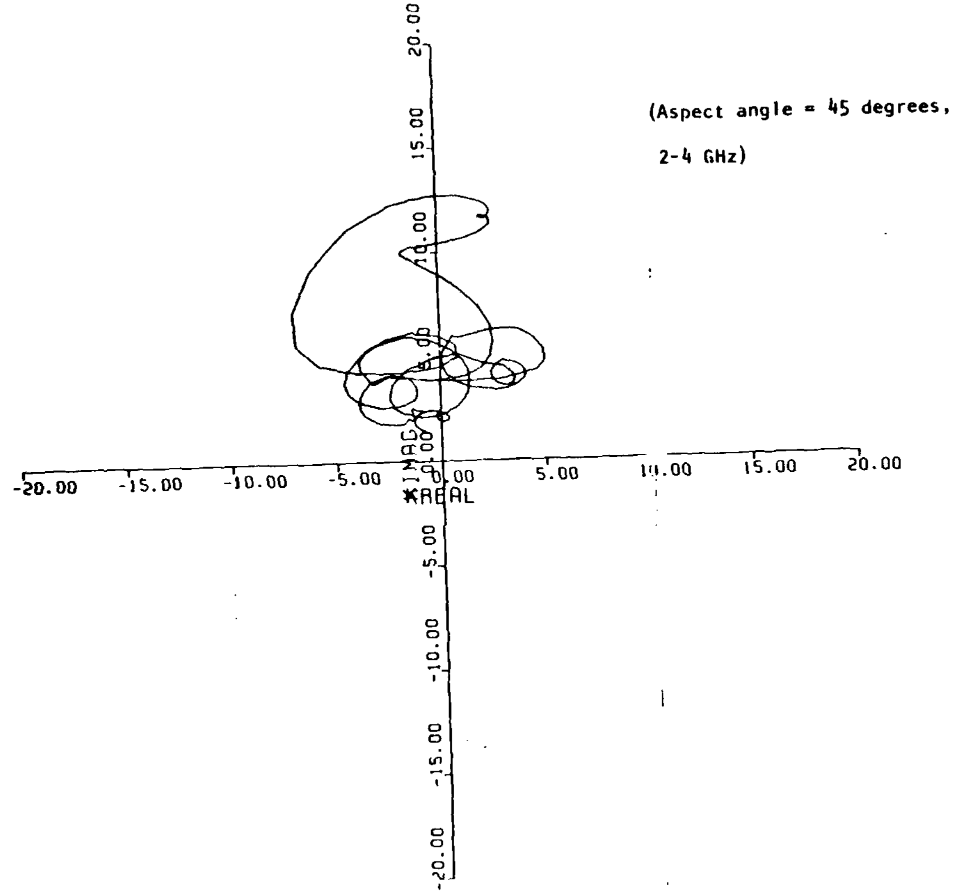

Figure 5.4(a)(i) The Scattering Chart from Experimental Data

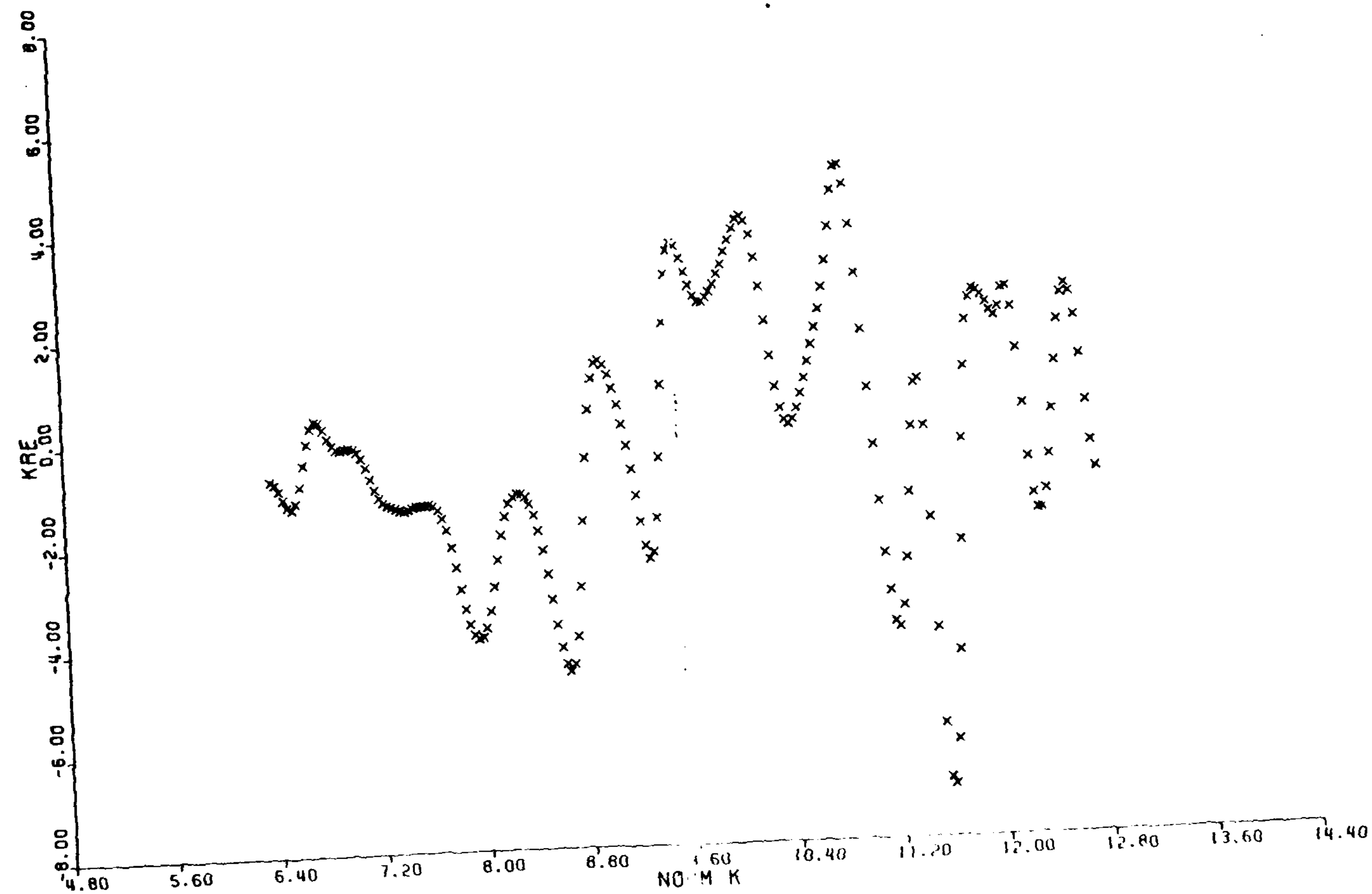

Figure 5.4(a)(ii) k Real Part versus k

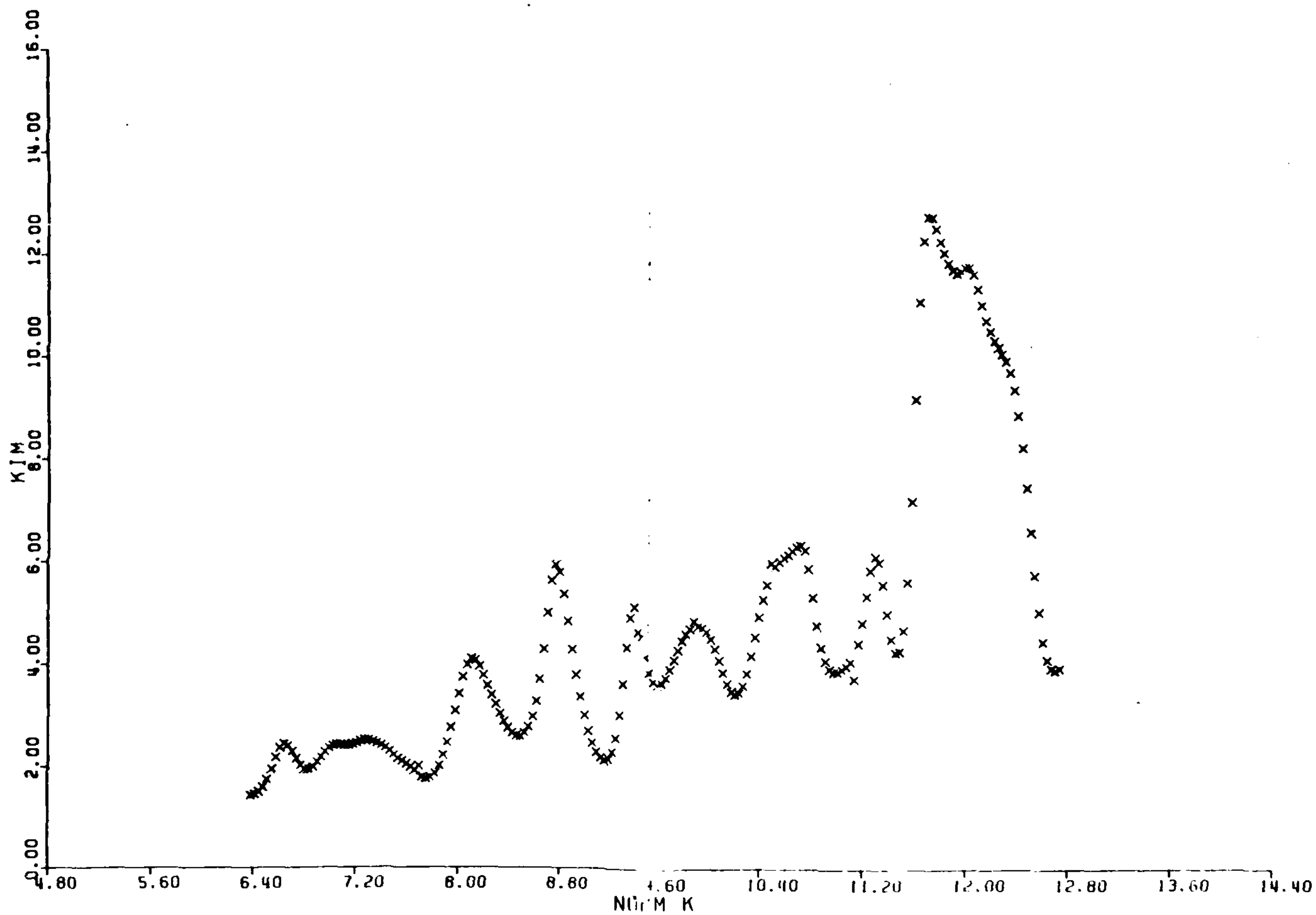

Figure 5.4(a)(iii) k Imaginary Part versus k

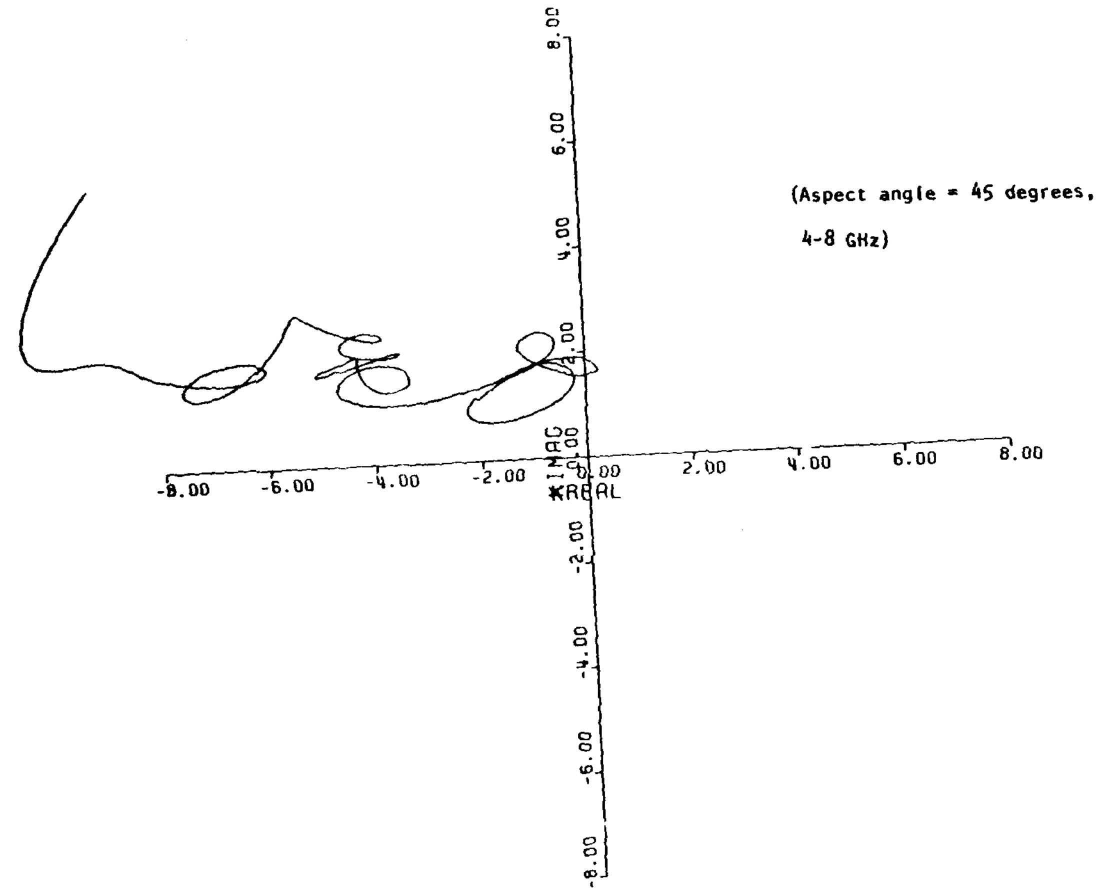

Figure 5.4(b)(i) The Scattering Chart from Experimental Data

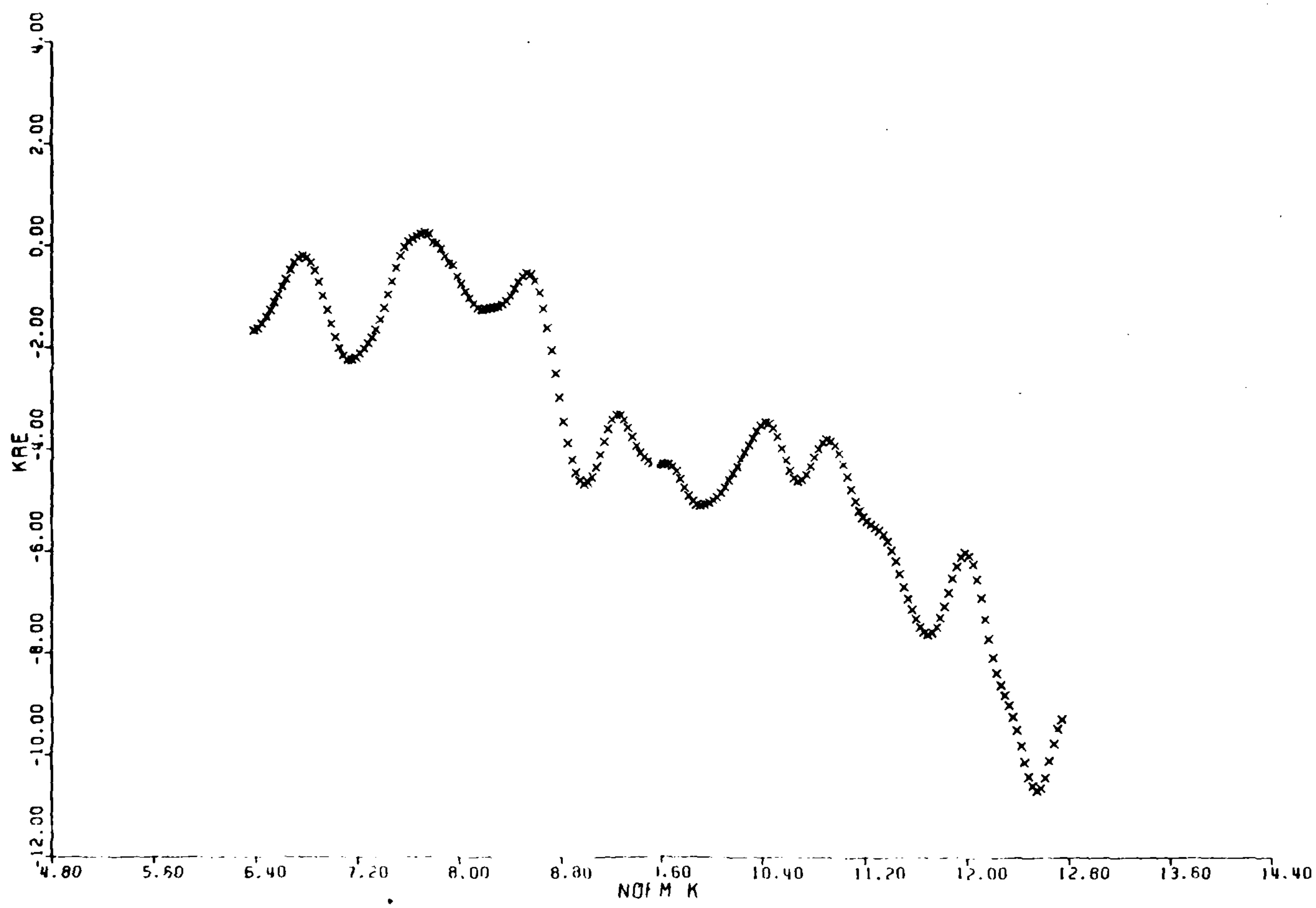

Figure 5.4(b)(ii) k Real Part versus k

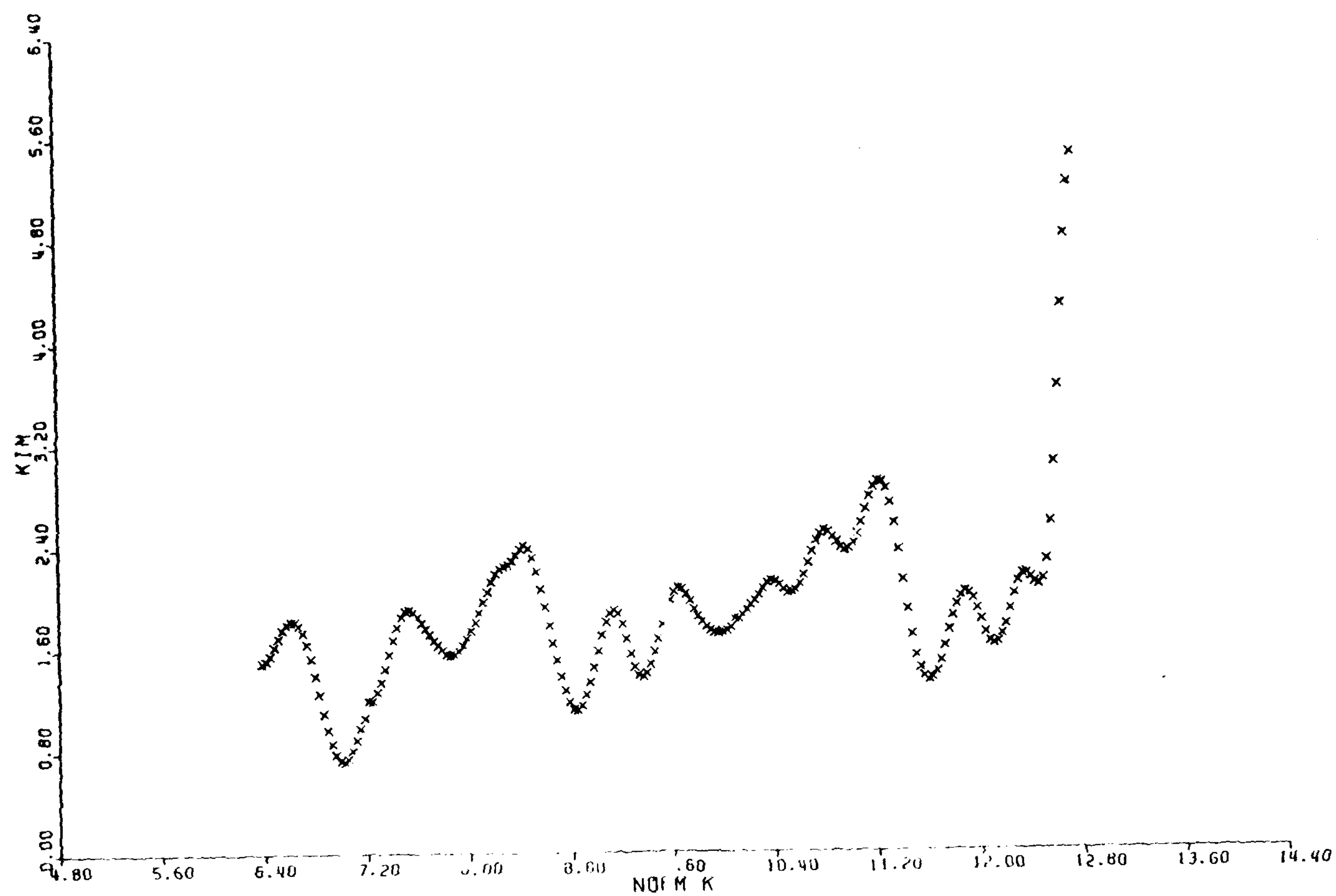

Figure 5.4(b)(iii) k Imaginary Part versus k

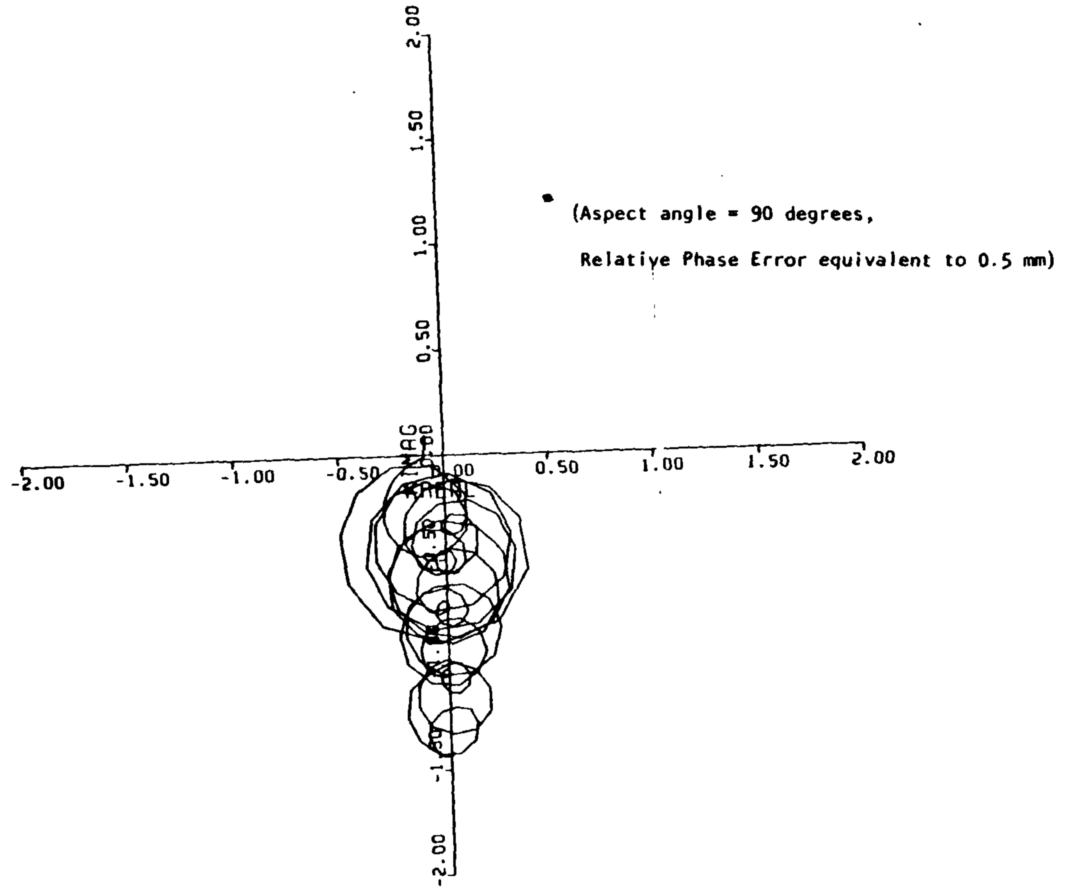

Figure 5.5(i) Effects of Relative Phase Error on the Scattering Chart from Theoretical Data

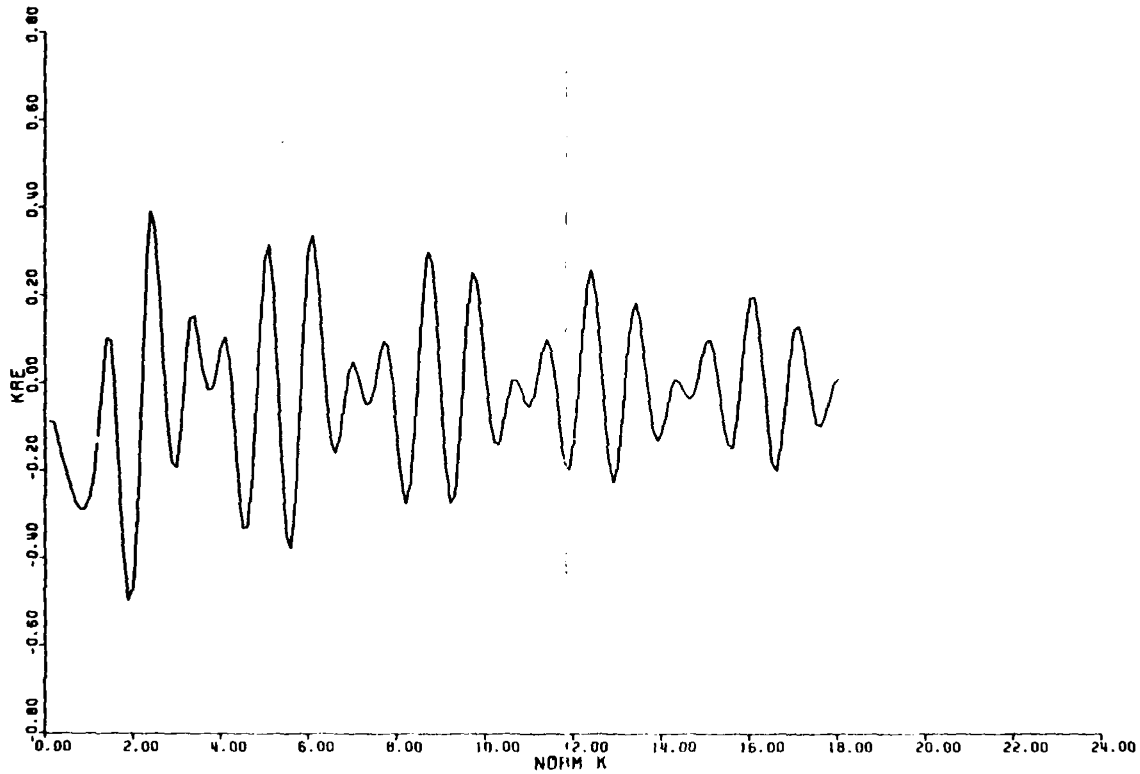

Figure 5.5(ii) Effects of Relative Phase Error on k times the REal Part

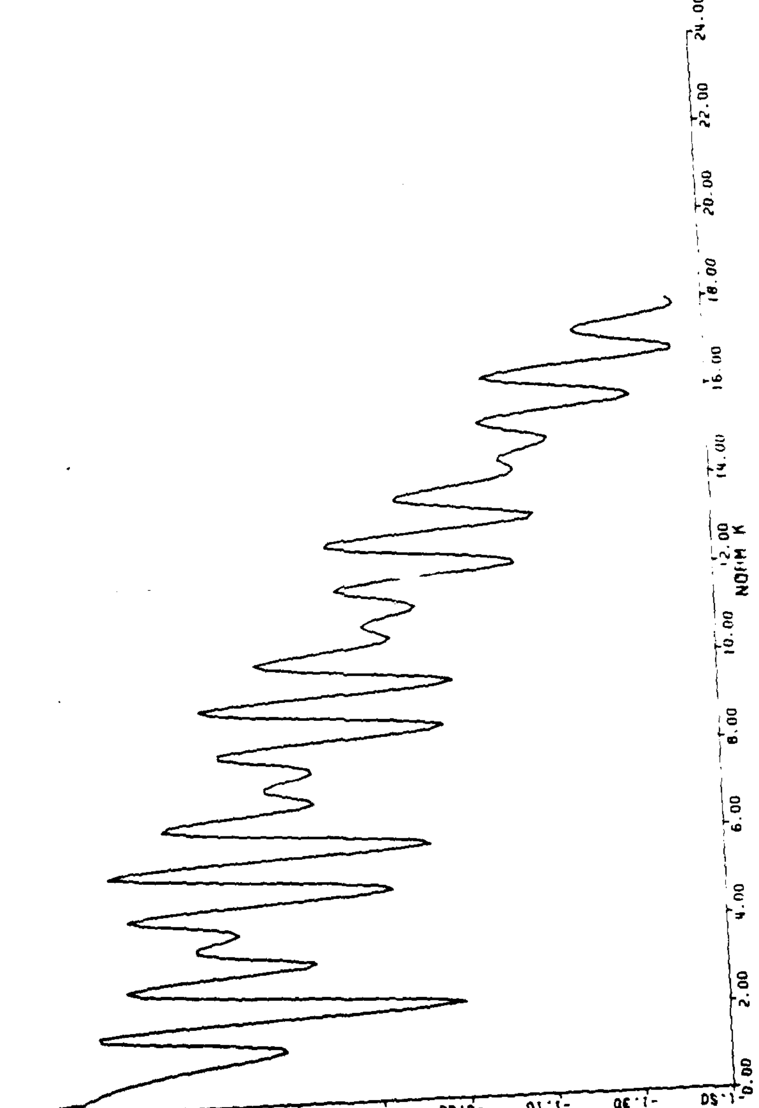

Figure 5.5(iii) Effects of Relative Phase Error on k times the Imaginary Part

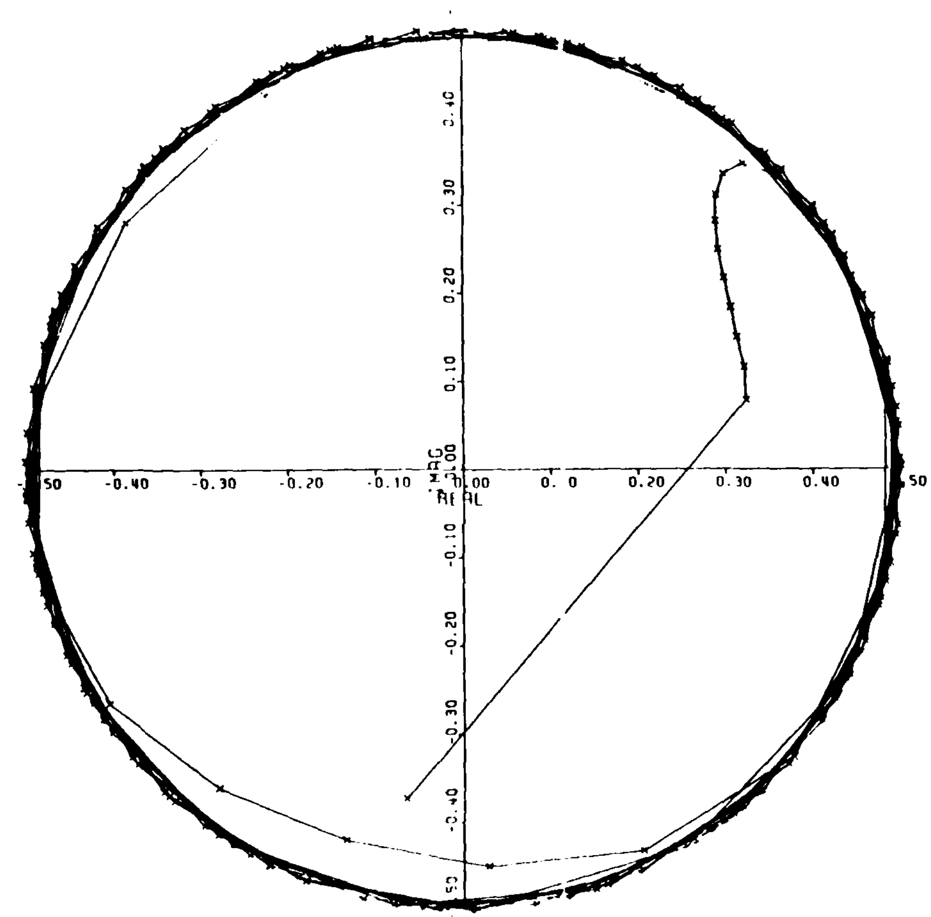

Figure 5.6(a) Complex Plot of D from Theoretical Data

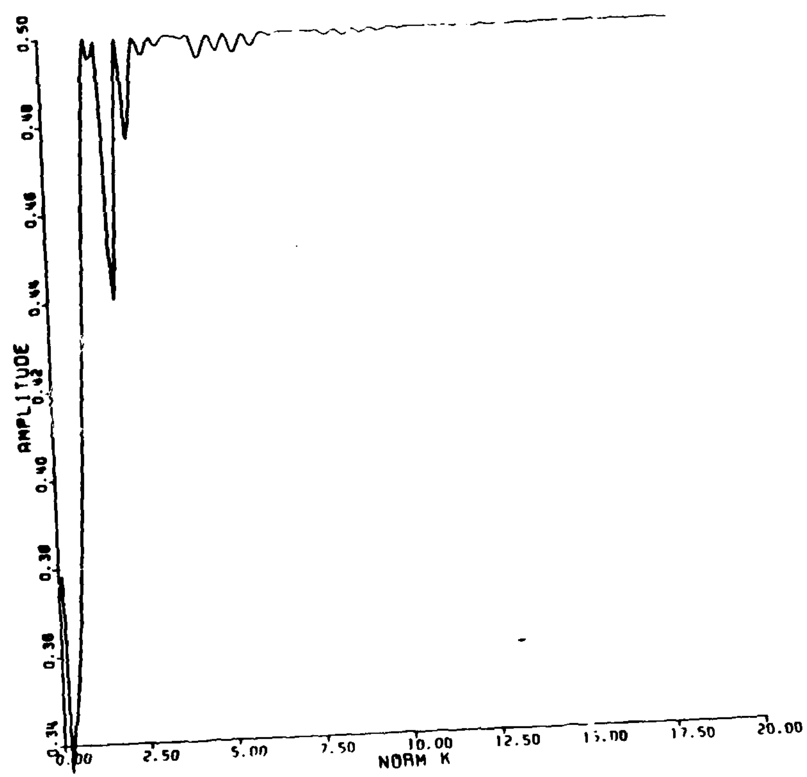

Figure 5.6(b) Amplitude Plot of D from Theoretical Data

AD-A115 805 ILLINOIS UNIV AT CHICAGO CIRCLE ELECTROMAGNETIC IMAGI--ETC F/G 20/14
A HIGH FREQUENCY INVERSE SCATTERING MODEL TO RECOVER THE SPECUL--ETC(U)
MAY 82 B FOO N00014-80-C-0708
UNCLASSIFIED EMID-CL-1982-05-21-01 NL

2 OF 2
AD A
115805

END
DATE
FILMED
07-82
DTIC

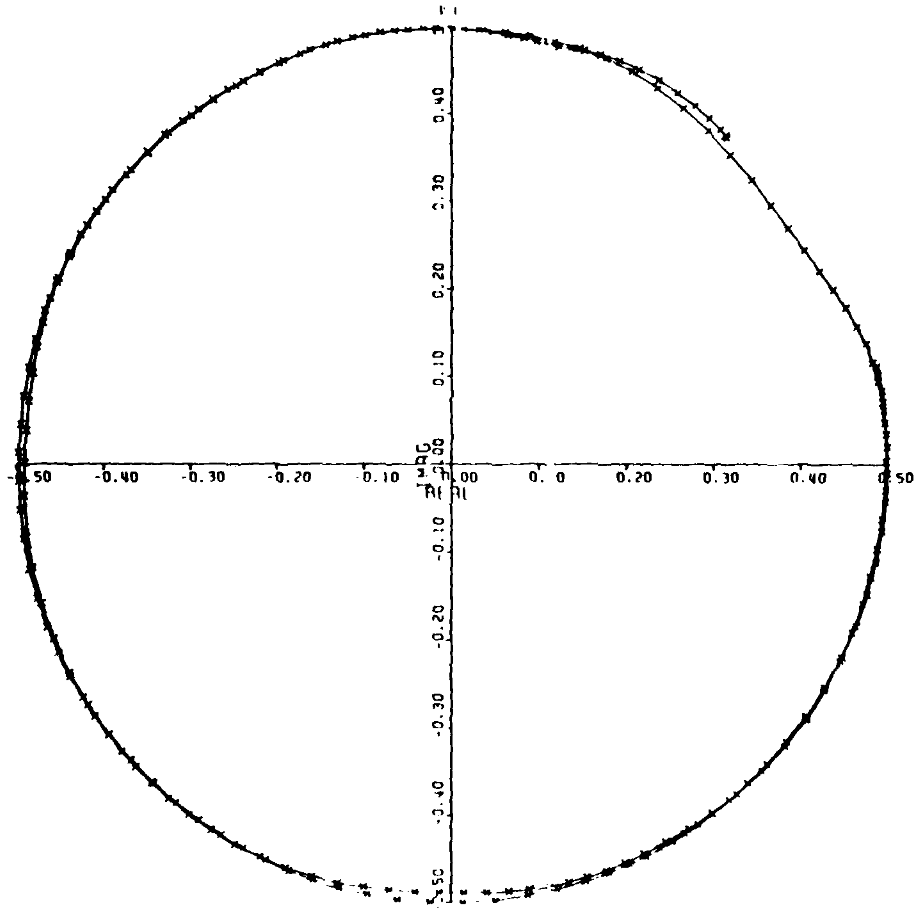

Figure 5.7(a) Experimental Version of Figure 5.6(a)
(Broadside Incidence, 2-4 GHz)

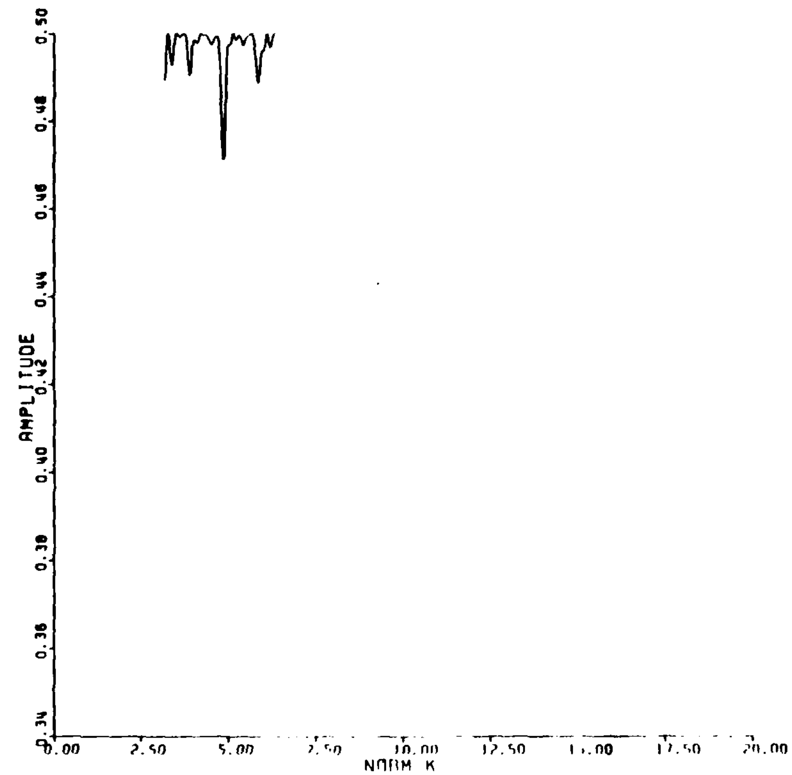

Figure 5.7(b) Experimental Version of Figure 5.6(b) (Broadside Incidence, 2-4 GHz)

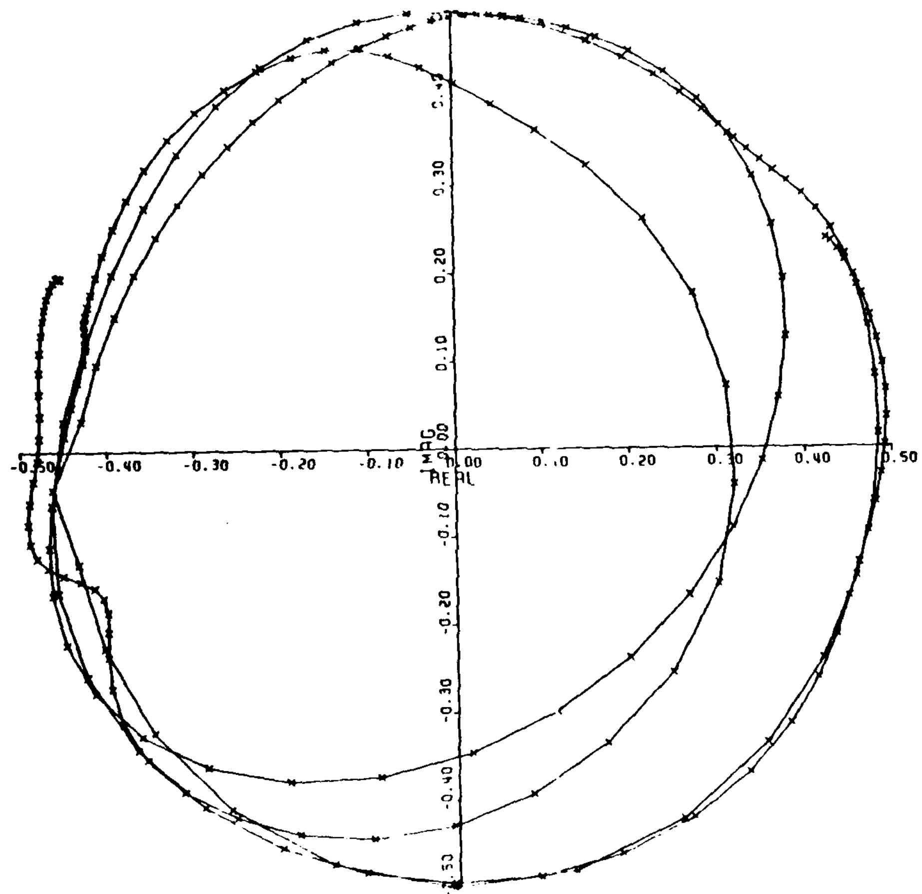

Figure 5.8(a) Experimental Version of Figure 5.6(a)
(Nose-on Incidence, 2-4 GHz)

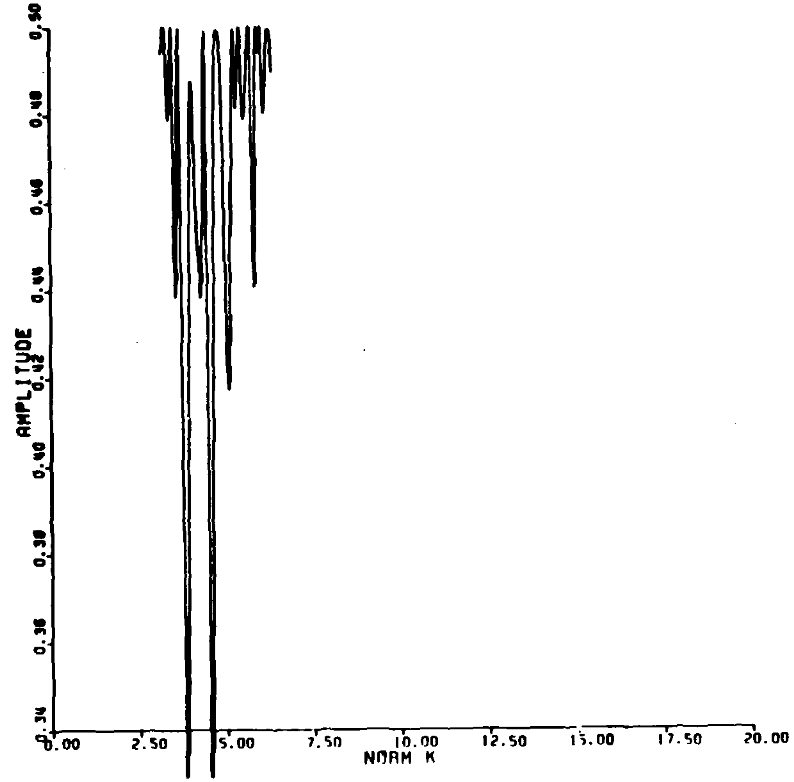

Figure 5.8(b) Experimental Version of Figure 5.6(b) (Nose-on Incidence 2-4 GHz)

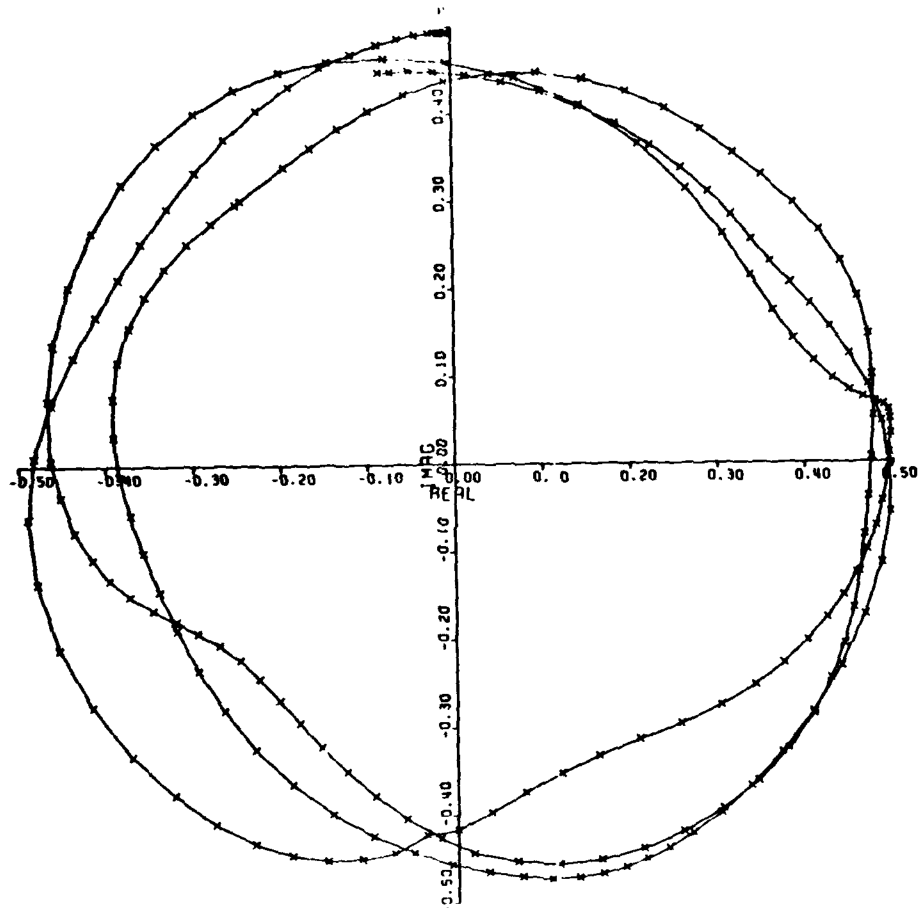

Figure 5.9(a) Experimental Version of Figure 5.6(a) (45 degree Incidence, 2-4 GHz)

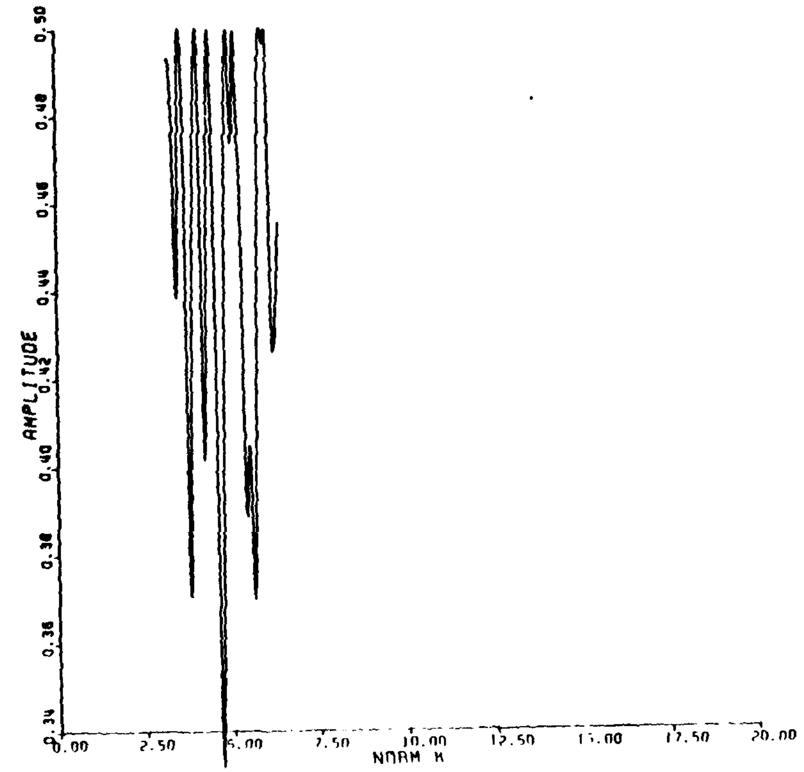

Figure 5.9(b) Experimental Version of Figure 5.6(b) (45 degree Incidence, 2.4 GHz)

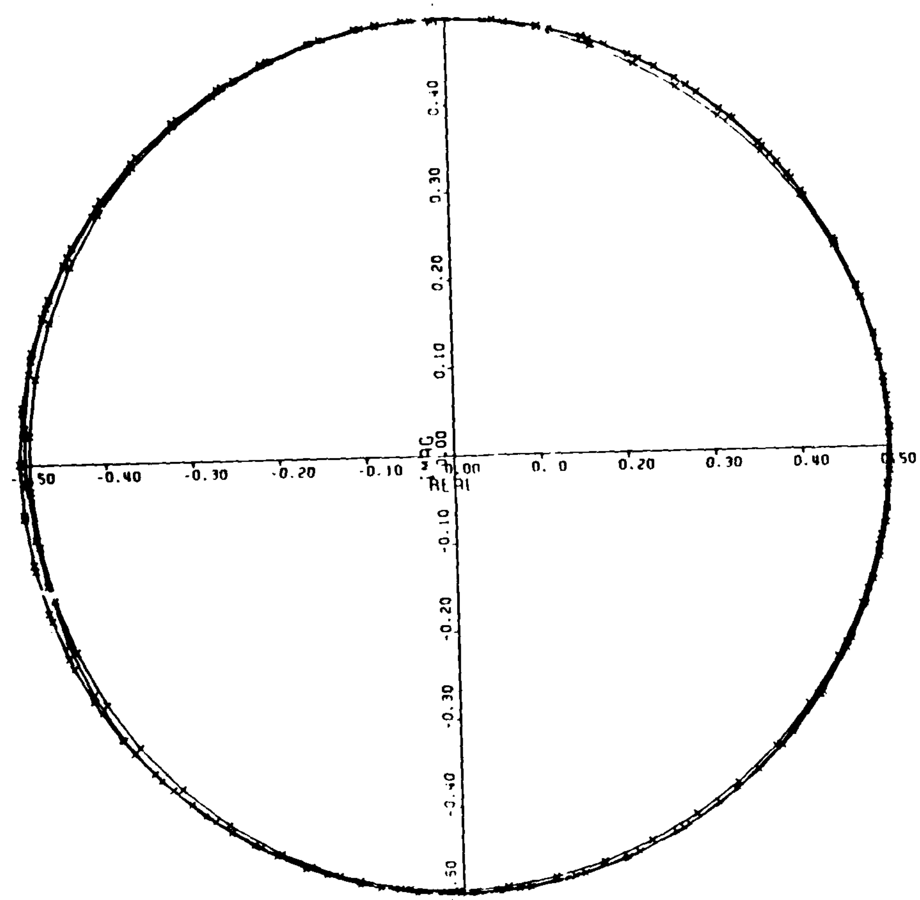

Figure 5.10(a) Experimental Version of Figure 5.6(a) (Broadside Incidence, 4-8 GHz)

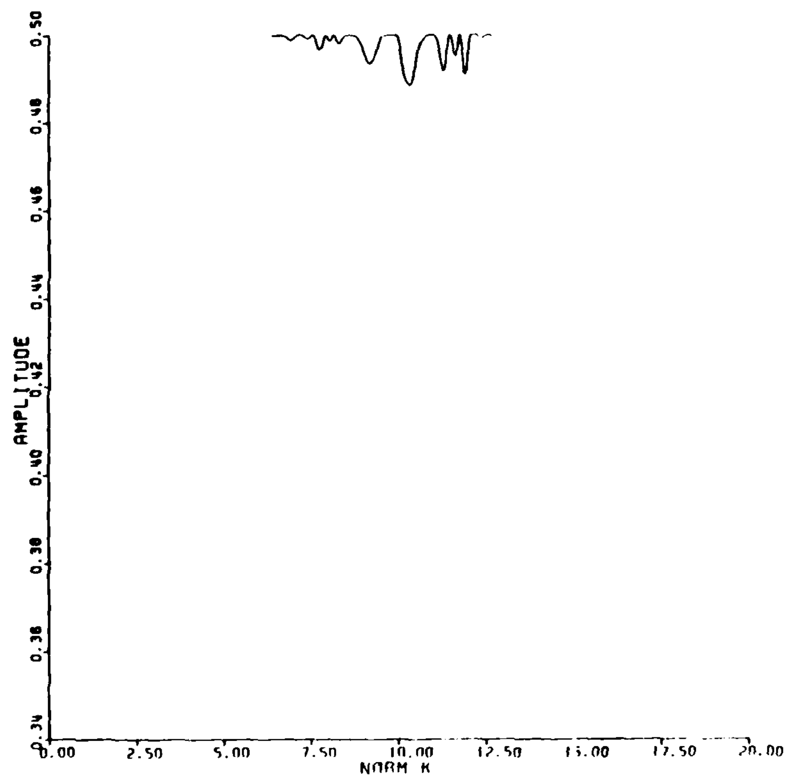

Figure 5.10(b) Experimental Version of Figure 5.6(b) (Broadside Incidence, 4-8 GHz)

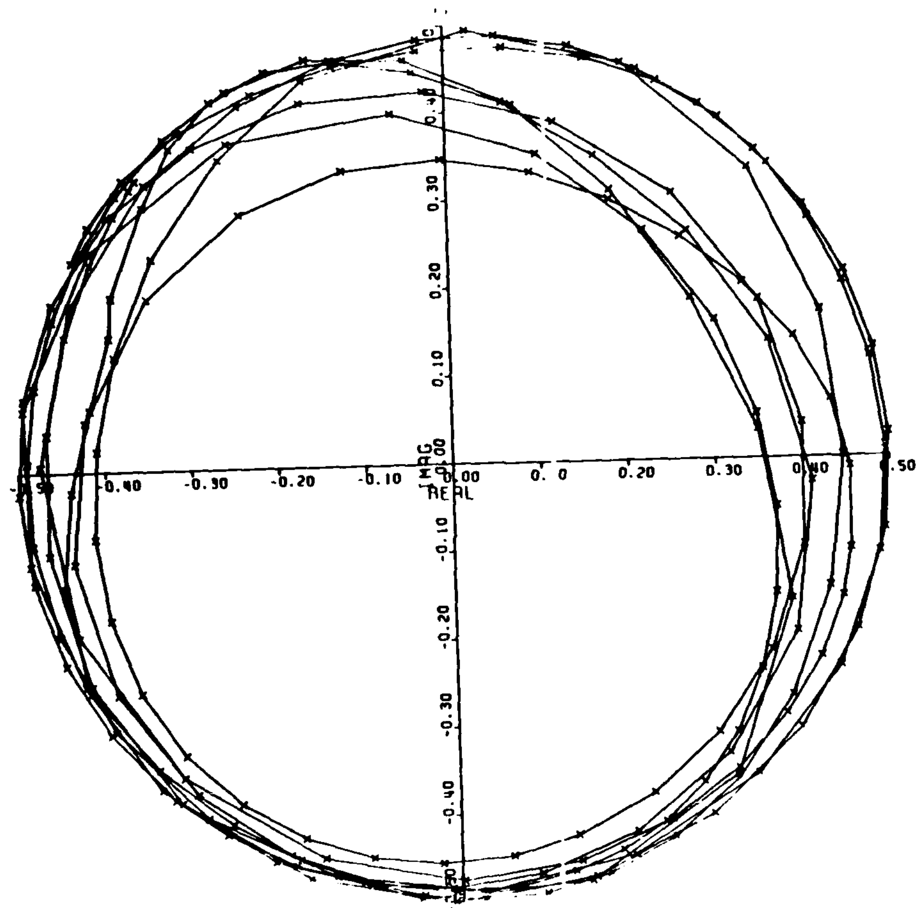

Figure 5.11(a) Experimental Version of Figure 5.6(a) (Close-on Incidence, 4-8 GHz)

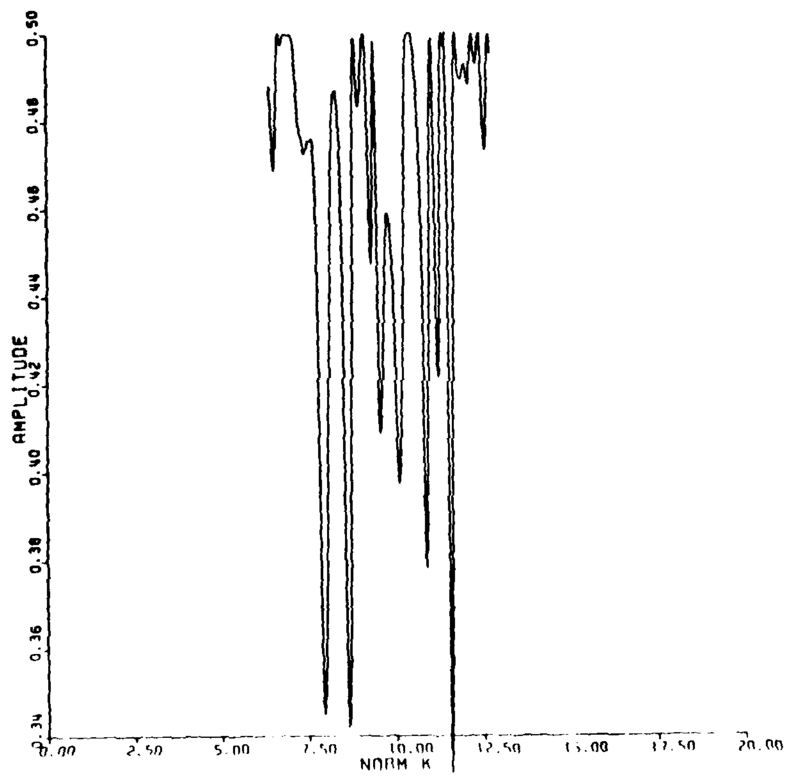

Figure 5.11(b) Experimental Version of Figure 5.6(b) (Close-on Incidence, 4-8 GHz)

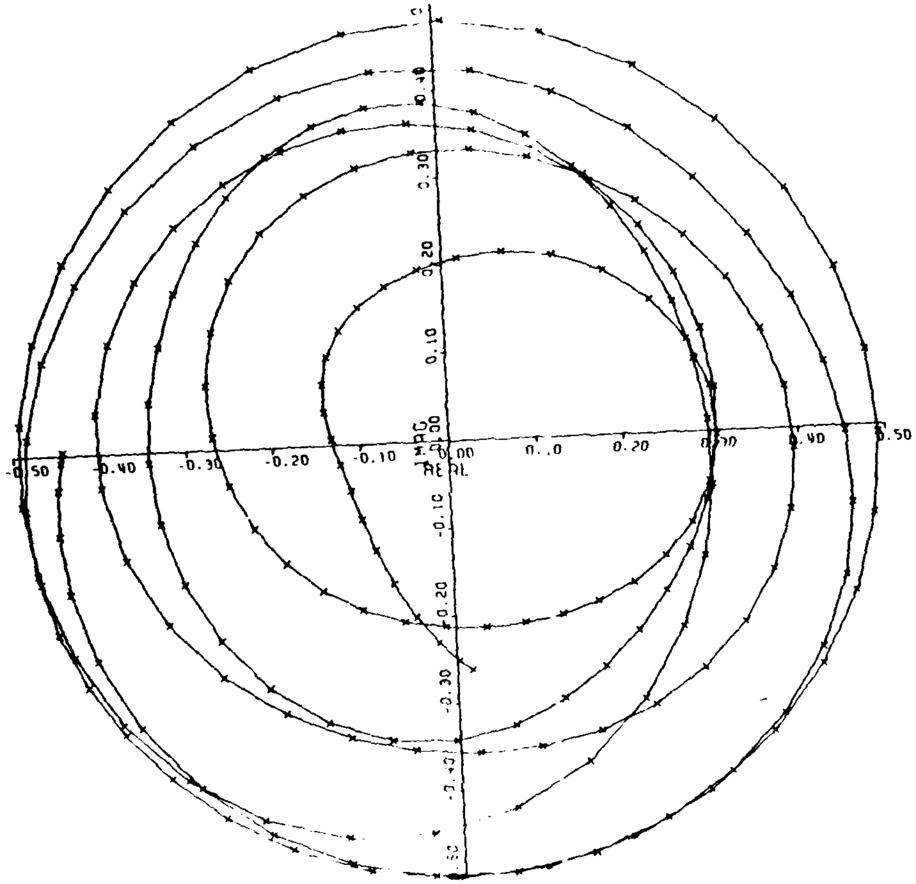

Figure 5.12(a) Experimental Version of Figure 5.6(a) (45 degree incidence, 4-8 GHz)

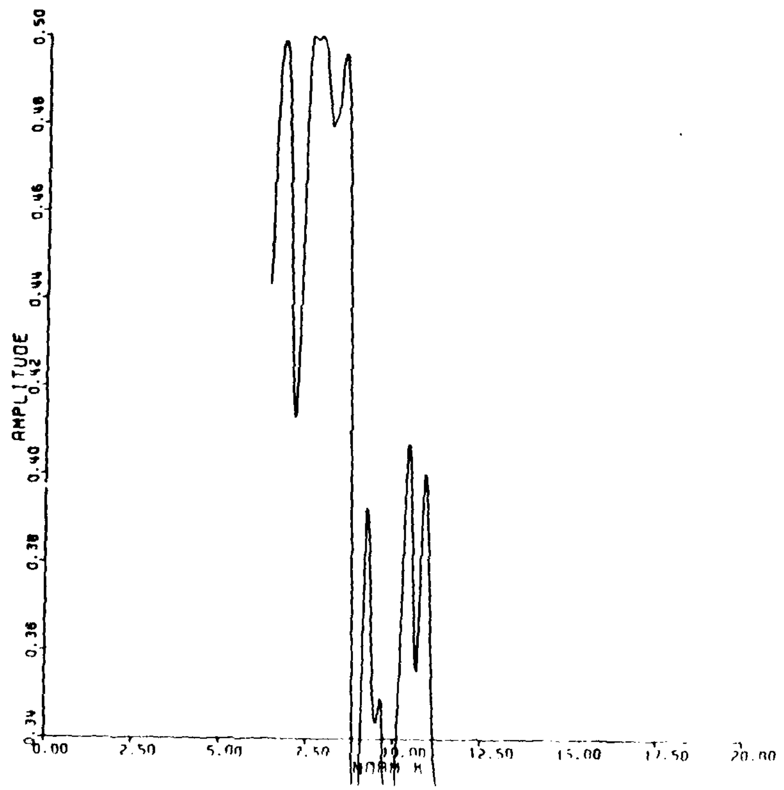

Figure 12(b) Experimental Version of Figure 5.6(b) (45 degree Incidence, 4-8 GHz)

CHAPTER VI

CONCLUSION

In the high frequency limits, the phase terms of the polarimetric scattering data have been used to determine the difference between the principal curvatures at the specular point. It is also known that the geometric optics backscattered cross-section is related to the geometric mean of the principal curvatures at the specular point (for smooth, convex objects at least [6]). Therefore, it should be possible to combine the above two concepts and determine the values of the individual principal curvature at the specular point. Further, by judicious use of differential geometry (e.g. Minkowski's formulation or Christoffel-Hurwitz formulation, etc.), these curvature values may yield the actual profile of the scatterer.

It must be pointed out here that the phase-curvature relationship concept does require a smooth, convex, well-behaved surface structure. If there are edge or other singular types of source contributions to the backscattered signal, curvature recovery with the method of this thesis will not be accurate. However, in the most recent development of radar target discrimination [5] the relative phase difference of the like polarized elements has been found to provide one of the most important classifiers for discriminating a smoothly (undulating) curved surface from a discontinuously rough surface with sharp edges.

It is found that there are several probable reasons why the 2-4 GHz experimental data give more accurate results than the 4-8 GHz data.

They are the tangent function in (3.10), the k factor and the relative phase error, which all become more significant at higher frequencies. Thus, the phase measurement needs to be very accurate and more accurate methods of obtaining the complete broadband polarimetric scattering data should be investigated.

It seems that not only is the 2-4 GHz range valid for the first order correction to physical optics for a 6"x12" prolate spheroid, but it is also a compromise range between the high frequency condition required by the curvature recovery model and the drawback to lower frequencies required to prevent critical magnification of measurement errors. At too high a frequency, the product of k and the tangent function will lead to erroneous results from measurement data.

Although the curvature recovery model is restricted to conducting scatterers, it may be possible to extend the model to dielectric scatterers, since the space-time integral equation, on which the model is based, has recently been extended and applied to dielectric bodies by Mieras and Bennett [37].

In concluding, both the amplitude difference and the phase difference of like-polarized elements of the scattering matrix in linear polarization tend to zero at high frequencies, yet the phase difference, however small, does contain curvature information of the scatterer. Regardless of the type of orthogonal polarization bases, the phase sum tends to a constant value which is twice the argument of the Fourier transform of the silhouette area of the target. The phase sum also tends to or equals the argument of the scattering ratio defined in this thesis. The magnitude of the

scattering ratio, whose definition is independent of whether linear, circular or general elliptic polarization is used, approaches 0.5 rapidly as frequency is increased. The magnitude of the ratio is interpreted as the ratio of the maximum radar cross section to the trace of the power scattering matrix. The complex plots of the scattering ratio provide a simple check on the accuracy of high frequency polarimetric measurements. Another curvature recovery equation has been derived in circular polarization basis vector notation. The curvature recovery model is proven to satisfy the image reconstruction identities of invariant transformation. Finally, the values of kb from 3.19 to 6.38 have been found to be most potentially suitable for curvature recovery of the 6"x12" prolate spheroid (and probably targets of similar size and shape), provided that polarimetric measurements can be improved to a better accuracy, and that further correction to physical optics approximation can be obtained.

APPENDIX I

DERIVATIONS OF EXPRESSIONS FOR PRINCIPAL CURVATURES FOR PROLATE SPHEROIDS

Let the semi-major axis of the prolate spheroid be C, and the semi-minor axes be a and b, such that $C > a = b$.

Let $\vec{r}(u,v)$ be a curvilinear mapping to represent the surface of the prolate spheroid. A set of parametric equations are

$$x = a \sin u \cos v$$

$$y = b \sin u \cos v$$

$$z = C \cos u$$

In vector form,

$$\vec{r} = (a \sin u \cos v)\ \hat{i} + (b \sin u \sin v)\ \hat{j} + (C \cos u)\ k$$

$$\frac{\partial \vec{r}}{\partial u} = (a \cos u \cos v,\ b \cos u \sin v,\ -C \sin u)$$

$$\frac{\partial \vec{r}}{\partial v} = (-a \sin u \sin v,\ b \sin u \cos v,\ 0)$$

By definition,

$$E = \frac{\partial \vec{r}}{\partial u} \cdot \frac{\partial \vec{r}}{\partial u}$$

$$= a^2 \cos^2 u + C^2 \sin^2 u$$

$$G = \frac{\partial \vec{r}}{\partial v} \cdot \frac{\partial \vec{r}}{\partial v}$$

$$= a^2 \sin^2 u$$

$$F = \frac{\partial \vec{r}}{\partial u} \cdot \frac{\partial \vec{r}}{\partial v}$$

$$= 0$$

$F = 0$ implies that the u, v parametric curves are orthogonal to each other.

Let n be the unit vector normal to the surface.

$$n = \frac{\partial \vec{r}}{\partial u} \times \frac{\partial \vec{r}}{\partial v} \Big/ \left|\frac{\partial \vec{r}}{\partial u} \times \frac{\partial \vec{r}}{\partial v}\right|$$

$$= \frac{(bC\sin^2 u \cos v,\ aC\sin^2 u \sin v,\ ab\sin u \cos u)}{\sqrt{\{b^2C^2\sin^4 u \cos^2 v + a^2C^2\sin^4 u \sin^2 v + a^2b^2\sin^2 u \cos^2 u\}}}$$

$$\frac{\partial^2 \vec{r}}{\partial u^2} = (-a \sin u \cos v,\ -b \sin u \sin v,\ -C \cos u)$$

$$\frac{\partial^2 \vec{r}}{\partial v^2} = (-a \sin u \cos v,\ -b \sin u \sin v,\ 0)$$

$$n \cdot \frac{\partial^2 \vec{r}}{\partial u^2} = \frac{-aC}{\sqrt{\{C^2\sin^2 u + a^2\cos^2 u\}}}$$

$$n \cdot \frac{\partial^2 \vec{r}}{\partial v^2} = \frac{-aC\sin^2 u}{\sqrt{\{C^2\sin^2 u + a^2\cos^2 u\}}}$$

$$\frac{\partial^2 \vec{r}}{\partial v \partial u} = (-a \cos u \sin v,\ b \cos u \cos v,\ 0)$$

$$\hat{n} \cdot \frac{\partial^2 \vec{r}}{\partial v \partial u} = 0$$

By definition,

$$L = \hat{n} \cdot \frac{\partial^2 \vec{r}}{\partial u^2}$$

$$= \frac{-aC}{\sqrt{\{a^2\cos^2 u + C^2\sin^2 u\}}}$$

$$M = \hat{n} \cdot \frac{\partial^2 \vec{r}}{\partial v \partial u}$$

$$= 0$$

$$N = \hat{n} \cdot \frac{\partial^2 \vec{r}}{\partial v^2}$$

$$= \frac{- aC\sin^2 u}{\sqrt{\{a^2\cos^2 u + C^2\sin^2 u\}}}$$

$M = F = 0$ implies that the lines of curvatures are the u, v parametric curves chosen. Thus,

$$K_u = \frac{L}{E}$$

$$= \frac{- aC}{(a^2\cos^2 u + C^2\sin^2 u)^{3/2}}$$

$$K_v = \frac{M}{G}$$

$$= \frac{- C}{a\sqrt{\{a^2\cos^2 u + C^2\sin^2 u\}}}$$

and the Gaussian curvature

$$K = K_u\, K_v$$

$$= \frac{1}{a^4C^2\{\frac{x^2}{a^4} + \frac{y^2}{a^4} + \frac{z^2}{C^4}\}^2}$$

In terms of x, y and z,

$$K_u = \frac{- aC}{[\frac{C^2}{a^2}\, x^2 + \frac{C^2}{a^2}\, y^2 + \frac{a^2}{C^2}\, z^2]^{3/2}}$$

$$K_v = \frac{- C}{a[\frac{C^2}{a^2}\, x^2 + \frac{C^2}{a^2}\, y^2 + \frac{a^2}{C^2}\, z^2]^{1/2}}$$

Without loss of generality, consider the x-z plane:

The point P(x,z) with an aspect angle ϕ , as shown in Figure A(1), can be expressed in terms of ϕ, by solving

$$x = z \tan \phi$$

and $$\frac{x^2}{a^2} + \frac{z^2}{C^2} = 1$$

Thus,

$$z = \frac{aC}{\sqrt{\{C^2 \tan^2\phi + a^2\}}}$$

$$x = \frac{aC \tan \phi}{\sqrt{\{C^2 \tan^2\phi + a^2\}}}$$

Consequently,

$$K_u = \frac{-\ aC}{\left[\frac{C^4 \tan^2\phi + a^4}{C^2 \tan^2\phi + a^2}\right]^{3/2}}$$

$$K_v = \frac{-\ C}{a\sqrt{\left\{\frac{C^4 \tan^2\phi + a^4}{C^2 \tan^2\phi + a^2}\right\}}}$$

For a 2:1 prolate spheroid, C = 2a. As an example, suppose ϕ = 90 degrees, hence

$$K_u = -\ \frac{1}{4a}$$

$$K_v = -\ \frac{1}{a}$$

$$\frac{K_u - K_v}{2} = \frac{3}{8a}$$

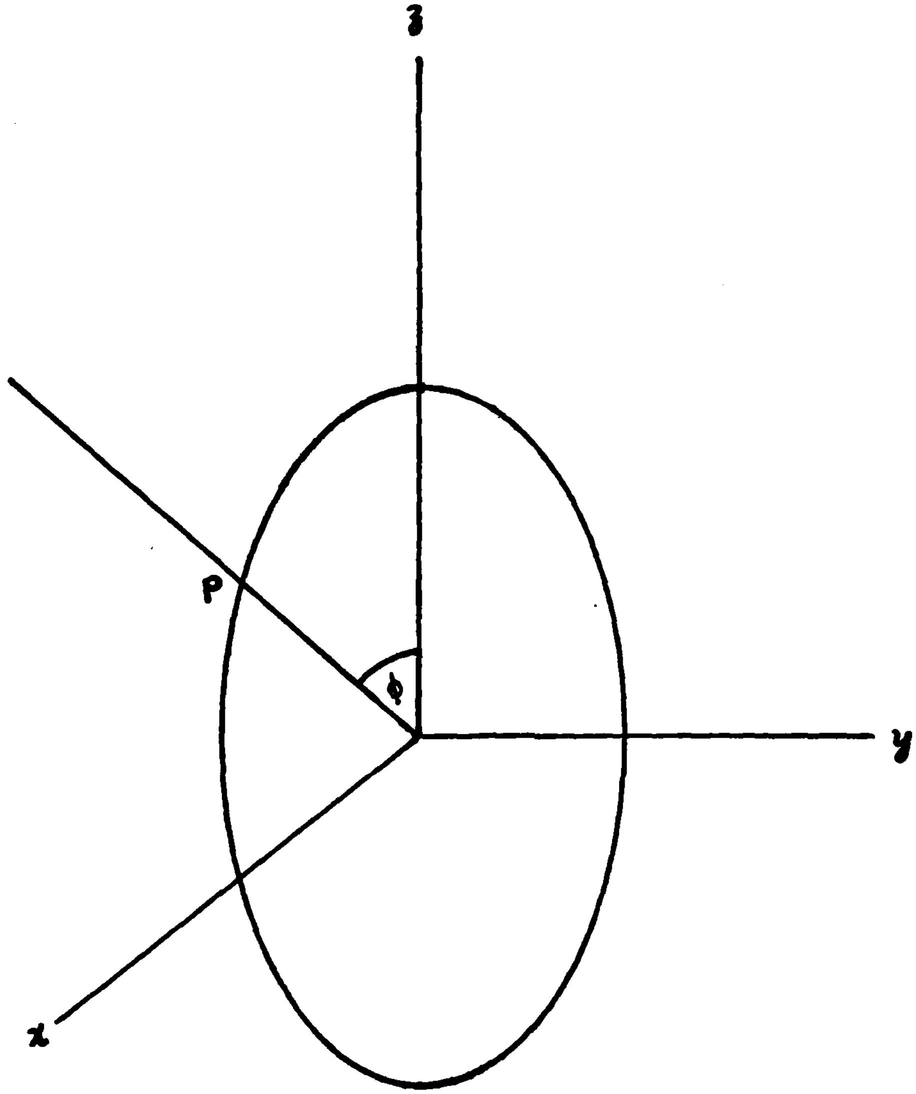

Figure A(1) Geometry of Prolate Spheroid for Curvature Calculation

Since k, the wave number, has been normalized in the phase-curvature relationship, a is set to unity here in conformity.

Thus,

$$\frac{K_u - K_v}{2} = 0.375$$

for broadside incidence.

Other values of curvature difference can be similarly evaluated once the aspect angle ϕ is specified.

APPENDIX II

COMPUTER PROGRAMS

(a) for computing curvature difference and plotting Figure 5.1(a)

(b) for plotting the scattering charts with theoretical and experimental data

(c) for plotting the scattering ratio D

```
C THEORETICAL VERIFICATION. DATA FROM V90.THEORY.DATA
C    AND H90.THEORY.DATA
C HIGH FREQUENCY PHASE/CURVATURE RELATIONSHIP VERIFICATION
C FILE NAME:::::::::::::: CURV.THEORY.CNTL
C N = NO. OF FREQUENCIES OR DATA
C FOR PROLATE SPHEROID, A=2B=2C
C ASPECT = PHI
      DIMENSION PHIV(180), PHIH(180), RHS(182)
      REAL K(182), K0,KS
      C=1.
      B=C
      A=2.0*C
      N=180
      K0=0.1
      KS=0.1
      PI=4.0*ATAN(1.0)
      THIDEG=90.
      THI=THIDEG*(PI/180.)
      PHIDEG=90.
      PHI=PHIDEG*(PI/180.)
      READ (8,15) (PHIV(I), I=1,N)
      READ (9,15) (PHIH(I), I=1,N)
   15 FORMAT(3(10X,F10.3))
      PRINT 1
    1 FORMAT('0',10X, 'PHIV', 36X, 'PHIH', '      IN RAD')
      DO 3 I=1,N
    3 PRINT 4, PHIV(I), PHIH(I)
    4 FORMAT('0', 10X, F10.3, 30X, F10.3)
      ZT=SIN(THI)*COS(PHI)
      ET=SIN(THI)*SIN(PHI)
      AK=COS(THI)
      B1=B*B*SIN(PHI)*SIN(PHI)+A*A*COS(PHI)*COS(PHI)
      C1=(A*A-B*B)*SIN(PHI)*COS(PHI)
      D1=A*A*SIN(PHI)*SIN(PHI)+B*B*COS(PHI)*COS(PHI)
      G1=A*A*B*B/B1
      H1=C1*C1/(B1*B1)-D1/B1
      TAU=ABS(A*A*B*B*B1*SIN(THI)*SIN(THI)/(C1*C1-B1*D1)-C*C*COS(THI
     1)*COS(THI))
      TAU=SQRT(TAU)
      H1=ABS(H1)
      GG=G1*C/(A*SQRT(H1))
      GG=GG/(TAU**3)
      P=SQRT(A*A*ZT*ZT+B*B*ET*ET+C*C*AK*AK)
      D12=(((A*ZT)**2)*(B*B-C*C)+((B*ET)**2)*(A*A-C*C))**2
      D12=D12+(((B*ET)**2)*(A*A-C*C)+((C*AK)**2)*(A*A-B*B))**2
      D12=D12-((B*ET)**4)*((A*A-C*C)**2)-2*((A*ZT)**2)*((C*AK)**2)*(A*A-
     1B*B)*(B*B-C*C)
      D12=SQRT(D12)*P/((A*B*C)**2)
      C12=D12*B/2.
      PRINT 99, D12
   99 FORMAT('0', '  EXACT CURVATURE DIFFERENCE BY 2 IS  ', F10.6)
      PRINT 5
    5 FORMAT('0', 8X, 'NORMALIZED K', 30X, 'CURVATURE DIFFERENCE BY 2 FR
     COM PHASE')
      DO 6 I=1,N
      K(I)=K0+(I-1)*KS
      ARG=(PHIH(I) - PHIV(I))/2.
      RHS(I)=K(I)*TAN(ARG)
    6 CONTINUE
```

```
      DO 7 I=1,N
    7 PRINT 8, K(I), RHS(I)
    8 FORMAT('0', 10X, F9.2, 30X, F15.6)
      PRINT 9, PHIDEG
    9 FORMAT('0', 'THE ASPECT ANGLE HAS BEEN  ', F10.6, '  DEG')
      PRINT 12, THIDEG
   12 FORMAT('0','ANGLE THI =',F10.6, 'DEG')
      PRINT 10, KO, KS
   10 FORMAT('0','STARTING NORM K =  ',F10.5, ', STEP= ', F10.5)
      CALL BGNPLT(5,CURVA)
      CALL SCALE(K,12.0,180,1)
      CALL SCALE(RHS,8.0,180,1)
      CALL AXIS(0.0,0.0,'NORM K',-6,12.0,0.0,K(181),K(182))
      CALL AXIS(0.0,0.0,'RHS',3,8.0,90.0,RHS(181),RHS(182))
      CALL LINE(K,RHS,180,1,1,4)
      PRINT 2221,K(181),K(182),RHS(181),RHS(182)
 2221 FORMAT('0',4F15.5)
      CALL ENDPLT
  222 FORMAT('0',4F14.6)
      STOP
      END

EFFECT*   NOTERM,ID,EBCDIC,SOURCE,NOLIST,NODECK,LOAD,NOMAP,NOTEST
EFFECT*   NAME = MAIN     , LINECNT =        50
    SOURCE STATEMENTS =        70,PROGRAM SIZE =      5908
  NO DIAGNOSTICS GENERATED
```

```
1  RELEASE 2.0                    MAIN                    DATE = 82134            10/53/34

C CHAUDHURI'S SCATTERING CHART
C FILE NAME::::::::::::KCHART.THEORY.CNTL
C DATA TO BE READ FROM V90.THEORY.DATA AND H90.THEORY.DATA
C N = NO. OF FREQUENCIES OR DATA
C PROLATE SPHEROID
      DIMENSION AMPV(180), AMPH(180), PHIV(180), PHIH(180)
      REAL K(182),K0,KS, RP(182), IP(182), KRP(182), KIP(182)
      COMPLEX CJ, CMPLX, CEXP, RNUM, RDEN, F(180)
      N=180
      K0=0.1
      KS=0.1
      CJ=CMPLX(0.0, 1.0)
      PI=4.*ATAN(1.)
      THIDEG=90.
      PHIDEG=90.
      READ(8,1)(AMPV(I),PHIV(I),I=1,N)
      READ(9,1)(AMPH(I),PHIH(I),I=1,N)
    1 FORMAT(6F10.5)
      DO 2 I=1,N
      K(I)=K0+(I-1)*KS
      PDIFF=PHIH(I)-PHIV(I)
      AM=AMPH(I)/AMPV(I)
      RNUM=1.-AM*CEXP(CJ*PDIFF)
      RDEN=1.+AM*CEXP(CJ*PDIFF)
      F(I)=RNUM/RDEN
      RP(I)=REAL(F(I))
      IP(I)=AIMAG(F(I))
      KRP(I)=K(I)*RP(I)
      KIP(I)=K(I)*IP(I)
    2 CONTINUE
      PRINT 3
    3 FORMAT('0','NORMALIZED K',10X,'REAL',19X,'IMAGINARY',25X, 'KREAL'
     C10X, 'KIMAG')
      DO 4 I=1,N
    4 PRINT 5, K(I), RP(I), IP(I), KRP(I), KIP(I)
    5 FORMAT('0',F10.3,21X,F14.7,5X,F14.7,13X,F14.7,15X,F14.7)
      CALL BGNPLT(5, CHART)
C UNIFIED SCALE FOR ALL IMAGINARY-REAL CLUSTER PLOTS NOW USED
C OTHER PLOTS HAVE NO UNIFIED SCALE
C TO REMOVE UNIFIED SCALE FOR IMAG-REAL CLUSTER PLOTS,
C JUST DELETE THE FOLLOWING 4 FORTRAN STATEMENTS,
C AND INSERT 2 SUBROUTINE SCALE, AS FOLLOWS:
C CALL SCALE(KRP,8.0,180,1)
C CALL SCALE(KIP,8.0,180,1)
      KRP(181)=-2.0
      KIP(181)=-2.0
      KRP(182)=0.5
      KIP(182)=0.5
      CALL AXIS(0.0,4.0,'KREAL',-5,8.0,0.0,KRP(181),KRP(182))
      CALL AXIS(4.0,0.0,'KIMAG',5,8.0,90.0,KIP(181),KIP(182))
      CALL LINE(KRP,KIP,180,1,0,4)
      CALL ENDPLT
      CALL BGNPLT(5, REALPT)
      CALL SCALE(K,12.0,180,1)
      CALL SCALE(KRP,8.0,180,1)
      CALL AXIS(0.0,0.0,'NORM K',-6,12.0,0.0,K(181),K(182))
      CALL AXIS(0.0,0.0,'KRE',3,8.0,90.0,KRP(181),KRP(182))
      CALL LINE(K,KRP,180,1,0,4)
      CALL ENDPLT
```

```
      CALL BGNPLT(4, IMAG)
      CALL SCALE(K,12.0,180,1)
      CALL SCALE(KIP,8.0,180,1)
      CALL AXIS(0.0,0.0,'NORM K',-6,12.0,0.0,K(181),K(182))
      CALL AXIS(0.0,0.0,'KIM',3,8.0,90.0,KIP(181),KIP(182))
      CALL LINE(K,KIP,180,1,0,4)
      CALL ENDPLT
      PRINT 553, THIDEG
  553 FORMAT('0', 'ANGLE THI =',F8.3, ' DEGREES')
      PRINT 555, PHIDEG
  555 FORMAT('0','THE ASPECT ANGLE = ',F8.3,' DEGREES')
      PRINT 556, K0,KS
  556 FORMAT('0','STARTING NORMALIZED K =',F10.5,' STEP=',F10.5)
      PRINT 991
  991 FORMAT('0', 'THE ORIGINAL VERTICAL POLARIZATION DATA:')
      PRINT 992,(AMPV(I),PHIV(I),I=1,N)
  992 FORMAT('0', 10F10.3)
      PRINT 993
  993 FORMAT('0', 'THE ORIGINAL HORIZONTAL POLARIZATION DATA:')
       PRINT 994,(AMPH(I),PHIH(I),I=1,N)
  994 FORMAT('0', 10F10.3)
      STOP
      END

*  EFFECT*  NOTERM,ID,EBCDIC,SOURCE,NOLIST,NODECK,LOAD,NOMAP,NOTEST
*  EFFECT*  NAME = MAIN    , LINECNT =       50
*      SOURCE STATEMENTS =       69,PROGRAM SIZE =    10786
*  NO DIAGNOSTICS GENERATED
```

```
C CHAUDHURI'S SCATTERING CHART
C FILE NAME:::::::::::::KCHART.CNTL
C N = NO. OF FREQUENCIES OR DATA
C PROLATE SPHEROID
      DIMENSION AMPV(200), AMPH(200), PHIV(200), PHIH(200)
      REAL K(202), RP(202), IP(202), KRP(202), KIP(202)
      COMPLEX CJ, CMPLX, CEXP, RNUM, RDEN, F(200)
      N=200
      CIN=3.
      C=CIN*2.54/100.
      B=C
      A=2.*C
      AIN=2.*CIN
      F0=2.
      S=0.01
      CJ=CMPLX(0.0, 1.0)
      PI=4.*ATAN(1.)
      THIDEG=90.
      PHIDEG=90.
      READ(3,1)(AMPV(I),PHIV(I),I=1,N)
      READ(9,1)(AMPH(I),PHIH(I),I=1,N)
    1 FORMAT(10F10.3)
      DO 2 I=1,N
      K(I)=(2.*PI/0.3)*(F0+(I-1)*S)*B
      PDIFF=PHIH(I)-PHIV(I)
      AM=10.**((AMPH(I)-AMPV(I))/10.)
      RNUM=1.-AM*CEXP(CJ*PDIFF)
      RDEN=1.+AM*CEXP(CJ*PDIFF)
      F(I)=RNUM/RDEN
      RP(I)=REAL(F(I))
      IP(I)=AIMAG(F(I))
      KRP(I)=K(I)*RP(I)
      KIP(I)=K(I)*IP(I)
    2 CONTINUE
      PRINT 3
    3 FORMAT('0','NORMALIZED K',19X,'REAL',19X,'IMAGINARY',25X, 'KREAL',
     C19X, 'KIMAG')
      DO 4 I=1,N
    4 PRINT 5, K(I), RP(I), IP(I), KRP(I), KIP(I)
    5 FORMAT('0',F10.5,21X,F14.7,5X,F14.7,13X,F14.7,15X,F14.7)
      CALL BGNPLT(5, CHART)
C UNIFIED SCALE FOR ALL IMAGINARY-REAL CLUSTER PLOTS NOW USED
C OTHER PLOTS HAVE NO UNIFIED SCALE
C TO REMOVE UNIFIED SCALE FOR IMAG-REAL CLUSTER PLOTS,
C JUST DELETE THE FOLLOWING 4 FORTRAN STATEMENTS,
C AND INSERT 2 SUBROUTINE SCALE, AS FOLLOWS:
C CALL SCALE(KRP,8.0,200,1)
C CALL SCALE(KIP,8.0,200,1)
      KRP(201)=-8.0
      KIP(201)=-8.0
      KRP(202)=2.0
      KIP(202)=2.0
      CALL AXIS(0.0,4.0,'KREAL',-5,8.0,0.0,KRP(201),KRP(202))
      CALL AXIS(4.0,0.0,'KIMAG',5,8.0,90.0,KIP(201),KIP(202))
      CALL LINE(KRP,KIP,200,1,0,4)
      CALL ENDPLT
      CALL BGNPLT(6, REALPT)
      CALL SCALE(K,12.0,200,1)
      CALL SCALE(KRP,3.0,200,1)
```

```
      CALL AXIS(0.0,0.0,'NORM K',-6,12.0,0.0,K(201),K(202))
      CALL AXIS(0.0,0.0,'KRE',3,8.0,90.0,KRP(201),KRP(202))
      CALL LINE(K,KRP,200,1,-1,4)
      CALL ENDPLT
      CALL BGNPLT(4, IMAG)
      CALL SCALE(K,12.0,200,1)
      CALL SCALE(KIP,3.0,200,1)
      CALL AXIS(0.0,0.0,'NORM K',-6,12.0,0.0,K(201),K(202))
      CALL AXIS(0.0,0.0,'KIM',3,8.0,90.0,KIP(201),KIP(202))
      CALL LINE(K,KIP,200,1,-1,4)
      CALL ENDPLT
      PRINT 554, CIN,AIN
  554 FORMAT('0','PROLATE SPHEROID, B=C=',F7.3,' A=',F7.3,' INS')
      PRINT 553, THIDEG
  553 FORMAT('0', 'ANGLE THI =',F8.3, ' DEGREES')
      PRINT 555, PHIDEG
  555 FORMAT('0','THE ASPECT ANGLE = ',F8.3,' DEGREES')
      PRINT 556, F0,S
  556 FORMAT('0','STARTING FREQ =',F10.5,' STEP=',F10.5,' GHZ')
      PRINT 991
  991 FORMAT('0', 'THE ORIGINAL VERTICAL POLARIZATION DATA:')
      PRINT 992,(AMPV(I),PHIV(I),I=1,N)
  992 FORMAT('0', 10F10.3)
      PRINT 993
  993 FORMAT('0', 'THE ORIGINAL HORIZONTAL POLARIZATION DATA:')
       PRINT 994,(AMPH(I),PHIH(I),I=1,N)
  994 FORMAT('0', 10F10.3)
      STOP
      END

 EFFECT*   NOTERM,ID,EBCDIC,SOURCE,NOLIST,NODECK,LOAD,NOMAP,NOTEST
 EFFECT*   NAME = MAIN     , LINECNT =       50
*     SOURCE STATEMENTS =        76,PROGRAM SIZE =      11910
*   NO DIAGNOSTICS GENERATED
```

```
C ROC 'S SCATTERING RATIO
C FILE NAME::::::::::::::RATIO.THEORY.CNTL
C DATA TO BE READ FROM V90.THEORY.DATA AND H90.THEORY.DATA
C N = NO. OF FREQUENCIES OR DATA
C PROLATE SPHEROID
      DIMENSION AMPV(180), AMPH(180), PHIV(180), PHIH(180)
      REAL K(182),K0,KS, RP(182), IP(182), AMP(182), PHASE(182)
      COMPLEX CJ, CMPLX, CEXP, RNUM, RDEN, RATIO(180)
      N=180
      K0=0.1
      KS=0.1
      CJ=CMPLX(0.0, 1.0)
      PI=4.*ATAN(1.)
      THIDEG=90.
      PHIDEG=90.
      READ(8,1)(AMPV(I),PHIV(I),I=1,N)
      READ(9,1)(AMPH(I),PHIH(I),I=1,N)
    1 FORMAT(6F10.6)
      PRINT 988
  988 FORMAT('0','NORMALIZED K',3X,'REAL',15X,'IMAGINARY',10X,'PHASE'
     C,14X,'AMPLITUDE')
      DO 2 I=1,N
      K(I)=K0+(I-1)*KS
      RNUM=AMPH(I)*CEXP(CJ*PHIH(I))*AMPV(I)*CEXP(CJ*PHIV(I))
      RDEN=AMPH(I)**2+AMPV(I)**2
      RATIO(I)=RNUM/RDEN
      RP(I)=REAL(RATIO(I))
      IP(I)=AIMAG(RATIO(I))
      AMPSQ=RP(I)**2+IP(I)**2
      AMP(I)=SQRT(AMPSQ)
      TAN=IP(I)/RP(I)
      PHASE(I)=ATAN(TAN)
      PRINT 999,K(I),RP(I),IP(I),PHASE(I),AMP(I)
    2 CONTINUE
  999 FORMAT('0',F10.3,4(5X,F14.7))
      CALL BGNPLT(5,RATIO)
      RP(181)=-1.0
      IP(181)=-1.0
      RP(182)=0.25
      IP(182)=0.25
      CALL AXIS(0.0,4.0,'REAL',-4,8.0,0.0,RP(181),RP(182))
      CALL AXIS(4.0,0.0,'IMAG',4,8.0,90.0,IP(181),IP(182))
      CALL LINE(RP,IP,180,1,1,4)
      CALL ENDPLT
      CALL BGNPLT(3,RAT)
      AMP(181)=0.0
      AMP(182)=0.5
      K(181)=0.0
      K(182)=2.5
      CALL AXIS(0.0,0.0,'NORM K',-6,8.0,0.0,K(181),K(182))
      CALL AXIS(0.0,0.0,'AMPLITUDE',9,2.0,90.0,AMP(181),AMP(182))
      CALL LINE(K,AMP,180,1,0,4)
      CALL ENDPLT
      PRINT 553, THIDEG
  553 FORMAT('0', 'ANGLE THI =',F8.3, ' DEGREES')
      PRINT 555, PHIDEG
  555 FORMAT('0','THE ASPECT ANGLE = ',F8.3,' DEGREES')
      PRINT 556, K0,KS
  556 FORMAT('0','STARTING NORMALIZED K =',F10.5,' STEP=',F10.5)
```

```
      PRINT 991
  991 FORMAT('0', 'THE ORIGINAL VERTICAL POLARIZATION DATA:')
      PRINT 992,(AMPV(I),PHIV(I),I=1,N)
  992 FORMAT('0', 10F10.3)
      PRINT 993
  993 FORMAT('0','THE ORIGINAL HORIZONTAL POLARIZATION DATA:')
      PRINT 994,(AMPH(I),PHIH(I),I=1,N)
  994 FORMAT('0', 10F10.3)
      STOP
      END

EFFECT*   NOTERM,ID,EBCDIC,SOURCE,NOLIST,NODECK,LOAD,NOMAP,NOTEST
EFFECT*   NAME = MAIN     , LINECNT =        50
    SOURCE STATEMENTS =        63,PROGRAM SIZE =     10518
  NO DIAGNOSTICS GENERATED
```

APPENDIX III

THEORETICAL DATA

(obtained from Dr. Sujeet Kumar Chaudhuri,
Department of Electrical Engineering,
University of Waterloo,
Waterloo, Ontario,
Canada, 1981)

```
THE ASPECT ANGLE =    90.000 DEGREES
STARTING NORMALIZED K =    0.10000 STEP=    0.10000
THE ORIGINAL VERTICAL POLARIZATION DATA:
```

0.027	-3.060	0.091	-3.077	0.194	-3.079	0.326	-3.076	0.481	-3.072
0.646	-3.065	0.410	-3.057	0.962	-3.072	1.091	-3.080	1.159	-3.094
1.246	-3.117	1.263	3.122	1.238	3.081	1.176	3.008	1.085	2.903
0.982	2.755	0.836	2.552	0.822	2.293	0.811	2.001	0.854	1.725
0.932	1.494	1.020	1.310	1.098	1.162	1.151	1.034	1.172	0.915
1.160	0.794	1.119	0.663	1.059	0.505	0.991	0.320	0.933	0.100
0.900	-0.149	0.902	-0.435	0.934	-0.649	0.985	-0.864	1.039	-1.051
1.082	-1.214	1.105	-1.365	1.105	-1.512	1.051	-1.665	1.041	-1.832
0.992	-2.020	0.947	-2.232	0.917	-2.467	0.911	-2.712	0.929	-2.952
0.964	3.109	1.006	2.901	1.043	2.728	1.067	2.561	1.073	2.399
1.062	2.235	1.037	2.065	1.003	1.875	0.970	1.669	0.945	1.447
0.938	1.216	0.948	0.986	0.972	0.767	1.003	0.553	1.032	0.375
1.053	0.198	1.061	0.039	1.056	-0.143	1.037	-0.320	1.012	-0.508
0.985	-0.709	0.963	-0.921	0.953	-1.145	0.956	-1.370	0.971	-1.588
0.993	-1.795	1.016	-1.930	1.034	-2.174	1.043	-2.353	1.041	-2.530
1.028	-2.711	1.009	-2.931	0.988	-3.100	0.971	2.973	0.961	2.756
0.962	2.536	0.972	2.320	0.990	2.111	1.009	1.914	1.025	1.724
1.034	1.540	1.035	1.353	1.028	1.175	1.014	0.986	0.997	0.789
0.982	0.583	0.973	0.371	0.971	0.156	0.978	-0.057	0.993	-0.265
1.005	-0.466	1.019	-0.633	1.027	-0.846	1.029	-1.031	1.024	-1.217
1.014	-1.408	1.000	-1.604	0.987	-1.807	0.977	-2.016	0.974	-2.229
0.978	-2.441	0.987	-2.649	0.999	-2.851	1.011	-3.047	1.019	3.045
1.023	2.856	1.020	2.663	1.013	2.477	1.002	2.281	0.991	2.080
0.983	1.873	0.979	1.663	0.981	1.453	0.998	1.246	0.995	1.043
1.008	0.845	1.016	0.652	1.020	0.461	1.019	0.272	1.014	0.080
1.005	-0.115	0.996	-0.315	0.988	-0.519	0.984	-0.727	0.984	-0.935
0.988	-1.142	0.996	-1.346	1.004	-1.545	1.012	-1.741	1.016	-1.933
1.016	-2.124	1.012	-2.317	1.005	-2.512	0.997	-2.711	0.990	-2.914
0.985	-3.120	0.985	2.935	0.988	2.748	0.994	2.544	1.001	2.344
1.008	2.147	1.013	1.951	1.014	1.760	1.012	1.567	1.007	1.372
1.000	1.174	0.994	0.972	0.989	0.768	0.988	0.562	0.990	0.355

0.994	0.152	1.000	-0.053	1.007	-0.247	1.011	-0.443	1.013	-0.635
1.011	-0.830	1.007	-1.033	1.002	-1.223	0.996	-1.424	0.991	-1.627
0.989	-1.832	0.990	-2.019	0.993	-2.242	0.998	-2.444	1.004	-2.643
1.008	-2.839	1.010	-3.031	1.010	3.054	1.007	2.859	1.002	2.662
0.997	2.462	0.993	2.233	0.990	2.055	0.990	1.850	0.993	1.646

THE ORIGINAL HORIZONTAL POLARIZATION DATA:

0.059	1.316	0.238	-2.969	0.490	-2.857	0.806	-2.762	1.144	-2.572
1.463	-2.587	1.725	-2.503	1.897	-2.439	1.960	-2.383	1.905	-2.347
1.744	-2.342	1.505	-2.383	1.239	-2.520	1.026	-2.779	0.955	3.140
1.039	2.814	1.186	2.605	1.307	2.483	1.356	2.402	1.318	2.327
1.205	2.227	1.049	2.069	0.907	1.817	0.843	1.479	0.885	1.145
0.986	0.897	1.084	0.730	1.135	0.607	1.124	0.493	1.058	0.357
0.962	0.173	0.880	-0.082	0.856	-0.387	0.901	-0.679	0.987	-0.910
1.068	-1.081	1.114	-1.213	1.113	-1.348	1.068	-1.495	1.001	-1.679
0.943	-1.911	0.924	-2.176	0.954	-2.436	1.014	-2.658	1.075	-2.836
1.111	-2.986	1.109	-3.123	1.072	3.002	1.015	2.819	0.963	2.598
0.939	2.348	0.954	2.099	0.996	1.873	1.042	1.684	1.072	1.519
1.072	1.364	1.043	1.201	0.997	1.013	0.954	0.795	0.933	0.552
0.944	0.306	0.979	0.031	1.019	-0.116	1.048	-0.289	1.053	-0.453
1.034	-0.623	1.000	-0.813	0.967	-1.023	0.950	-1.255	0.958	-1.491
0.987	-1.713	1.022	-1.911	1.048	-2.089	1.055	-2.257	1.042	-2.429
1.014	-2.614	0.985	-2.823	0.967	-3.043	0.959	3.011	0.990	2.792
1.017	2.591	1.039	2.409	1.046	2.233	1.036	2.058	1.012	1.972
0.985	1.665	0.967	1.449	0.966	1.223	0.981	1.004	1.004	0.799
1.024	0.610	1.032	0.433	1.026	0.251	1.008	0.063	0.985	-0.139
0.970	-0.354	0.968	-0.577	0.980	-0.795	1.001	-1.001	1.020	-1.194
1.030	-1.376	1.027	-1.557	1.014	-1.745	0.995	-1.943	0.981	-2.154
0.977	-2.372	0.986	-2.587	1.002	-2.794	1.019	-2.988	1.029	3.110
1.028	2.927	1.016	2.740	1.000	2.543	0.985	2.336	0.979	2.121
0.984	1.906	0.997	1.693	1.012	1.501	1.021	1.312	1.021	1.127
1.012	0.938	0.998	0.742	0.985	0.536	0.978	0.322	0.982	0.108

0.993	-0.100	1.006	-0.300	1.016	-0.491	1.019	-0.679	1.013	-0.969
1.001	-1.063	0.989	-1.267	0.983	-1.478	0.985	-1.690	0.994	-1.899
1.007	-2.099	1.016	-2.282	1.020	-2.480	1.016	-2.669	1.006	-2.863
0.995	-3.065	0.987	3.013	0.987	2.800	0.994	2.591	1.004	2.393
1.013	2.195	1.017	2.005	1.014	1.815	1.005	1.621	0.995	1.420
0.987	1.213	0.986	1.003	0.991	0.795	1.000	0.592	1.008	0.393
1.013	0.203	1.011	0.011	1.005	-0.183	0.996	-0.383	0.989	-0.588
0.987	-0.797	0.991	-1.005	0.999	-1.209	1.007	-1.406	1.013	-1.600
1.013	-1.791	1.007	-1.985	0.999	-2.183	0.993	-2.387	0.990	-2.595
0.993	-2.802	0.999	-3.005	1.007	3.079	1.012	2.885	1.013	2.693
1.008	2.499	1.001	2.301	0.994	2.099	0.990	1.892	0.992	1.685

APPENDIX IV

EXPERIMENTAL DATA

(obtained from Dr. Jonathan D. Young,
Electro-Science Laboratory,
Department of Electrical Engineering,
Ohio State University,
Columbus, Ohio, 1982)

THE ASPECT ANGLE = 90.000 DEGREES
STARTING FREQ = 2.00000 STEP= 0.01000 GHZ
THE ORIGINAL VERTICAL POLARIZATION DATA:

28.111	0.513	28.119	0.517	28.143	0.529	28.155	0.549	28.253	0.574
28.353	0.600	28.481	0.625	28.627	0.647	28.782	0.667	28.935	0.693
29.084	0.695	29.218	0.703	29.333	0.709	29.421	0.713	29.473	0.718
29.490	0.725	29.479	0.735	29.447	0.752	29.402	0.774	29.350	0.799
29.299	0.825	29.253	0.854	29.216	0.884	29.194	0.915	29.186	0.947
29.185	0.978	29.180	1.003	29.168	1.039	29.148	1.068	29.122	1.096
29.090	1.122	29.049	1.141	29.000	1.174	28.946	1.202	29.887	1.233
28.826	1.259	28.770	1.233	28.717	1.319	28.653	1.351	28.572	1.385
28.476	1.423	28.373	1.471	28.267	1.520	28.165	1.572	28.074	1.523
27.999	1.677	27.939	1.728	27.902	1.774	27.886	1.816	27.986	1.952

27.893	1.882	27.900	1.903	27.909	1.930	27.915	1.951	27.916	1.971
27.910	1.991	27.901	2.013	27.895	2.038	27.893	2.068	27.897	2.103
27.908	2.134	27.926	2.170	27.944	2.206	27.964	2.242	27.990	2.279
28.022	2.315	28.063	2.352	28.110	2.388	28.168	2.422	28.213	2.455
28.298	2.488	28.361	2.513	28.422	2.549	28.479	2.578	28.529	2.605
28.573	2.634	28.621	2.661	28.669	2.687	28.712	2.714	28.747	2.741
28.779	2.769	28.806	2.793	28.828	2.829	28.849	2.860	28.871	2.891
28.891	2.921	28.910	2.953	28.925	2.983	28.935	3.013	28.937	3.043
28.931	3.073	28.918	3.102	28.897	3.130	28.875	-3.127	28.853	-3.102
28.835	-3.080	28.839	-3.060	28.882	-3.040	28.956	-3.021	29.052	-3.001
29.160	-2.982	29.269	-2.960	29.365	-2.938	29.436	-2.913	29.478	-2.885
29.489	-2.856	29.469	-2.825	29.418	-2.791	29.343	-2.756	29.250	-2.719
29.144	-2.681	29.032	-2.643	28.920	-2.605	28.822	-2.568	28.742	-2.533
28.680	-2.500	28.637	-2.470	28.598	-2.442	28.549	-2.413	28.487	-2.384
28.413	-2.354	28.336	-2.324	28.256	-2.293	28.172	-2.262	28.093	-2.229
28.028	-2.194	27.980	-2.153	27.947	-2.120	27.930	-2.081	27.933	-2.042
27.953	-2.002	27.976	-1.968	27.995	-1.928	28.009	-1.893	28.009	-1.859
27.994	-1.825	27.969	-1.791	27.942	-1.756	27.918	-1.720	27.896	-1.683
27.883	-1.646	27.886	-1.603	27.903	-1.571	27.934	-1.533	27.982	-1.496
28.047	-1.460	28.118	-1.425	28.188	-1.392	28.260	-1.359	28.326	-1.329
28.378	-1.302	28.412	-1.277	28.431	-1.253	28.437	-1.230	28.435	-1.207
28.427	-1.184	28.418	-1.161	28.415	-1.136	28.425	-1.109	28.447	-1.081
28.483	-1.051	28.535	-1.020	28.600	-0.987	28.672	-0.954	28.749	-0.921
28.826	-0.888	28.898	-0.857	28.959	-0.826	29.002	-0.797	29.021	-0.770
29.029	-0.745	29.031	-0.720	29.030	-0.698	29.023	-0.676	29.013	-0.655
28.998	-0.635	28.974	-0.614	28.941	-0.592	28.899	-0.570	28.845	-0.544
28.778	-0.516	28.701	-0.485	28.621	-0.453	28.543	-0.418	28.473	-0.383
28.411	-0.347	28.359	-0.310	28.319	-0.274	28.290	-0.238	28.271	-0.204
28.253	-0.171	28.234	-0.137	28.214	-0.102	28.188	-0.066	28.160	-0.030
28.135	0.005	28.119	0.035	28.112	0.063	28.108	0.084	28.103	0.097

THE ORIGINAL HORIZONTAL POLARIZATION DATA:

29.022	0.354	29.006	0.355	28.964	0.364	28.901	0.378	28.819	0.397
28.730	0.421	28.649	0.441	28.592	0.478	28.566	0.508	29.559	0.537
28.560	0.563	28.576	0.585	28.611	0.609	28.665	0.631	28.732	0.654
28.798	0.678	28.855	0.705	28.904	0.736	28.950	0.770	28.999	0.808
29.049	0.846	29.105	0.882	29.171	0.916	29.246	0.948	29.317	0.977
29.373	1.000	29.408	1.013	29.418	1.032	29.399	1.045	29.348	1.058
29.278	1.073	29.199	1.092	29.114	1.116	29.026	1.144	28.943	1.175
28.874	1.208	28.825	1.241	28.799	1.271	28.796	1.297	28.812	1.317
28.839	1.331	28.873	1.341	28.904	1.349	28.920	1.357	28.906	1.369
28.861	1.386	28.790	1.410	28.700	1.441	28.601	1.482	28.503	1.530
28.414	1.585	28.340	1.645	28.287	1.709	28.255	1.773	28.242	1.835
28.245	1.892	28.260	1.944	28.280	1.988	28.299	2.024	28.310	2.053
28.307	2.079	28.285	2.102	28.246	2.124	28.196	2.149	28.139	2.175
28.084	2.205	28.040	2.239	28.022	2.276	28.028	2.317	28.057	2.359
28.107	2.402	28.172	2.442	28.245	2.477	28.313	2.506	28.370	2.528
28.409	2.543	28.436	2.553	28.453	2.560	28.458	2.556	28.454	2.575
28.444	2.589	28.432	2.603	28.424	2.635	28.422	2.667	28.429	2.704
28.452	2.747	28.490	2.794	28.537	2.842	28.583	2.890	28.621	2.938
28.649	2.983	28.667	3.026	28.673	3.066	28.663	3.105	28.641	3.141
28.610	-3.109	28.570	-3.080	28.514	-3.052	28.445	-3.026	28.371	-3.000
28.293	-2.975	28.213	-2.943	28.135	-2.919	28.066	-2.989	28.012	-2.855
27.974	-2.819	27.958	-2.781	27.965	-2.738	27.995	-2.694	28.045	-2.652
28.111	-2.611	28.180	-2.574	28.236	-2.540	28.270	-2.509	28.274	-2.480
28.249	-2.452	28.206	-2.424	28.156	-2.394	28.107	-2.363	28.065	-2.330
28.039	-2.294	28.033	-2.257	28.047	-2.220	28.078	-2.195	28.120	-2.152
28.166	-2.122	28.210	-2.096	28.247	-2.072	28.270	-2.049	28.275	-2.026
28.264	-2.000	28.244	-1.971	28.217	-1.936	28.188	-1.898	28.167	-1.858
28.154	-1.818	28.180	-1.791	28.208	-1.744	28.242	-1.711	28.280	-1.681
28.317	-1.652	28.345	-1.625	28.361	-1.598	28.368	-1.570	28.374	-1.541
29.392	-1.509	28.422	-1.474	28.461	-1.438	28.507	-1.402	29.552	-1.369
28.587	-1.335	28.608	-1.304	28.609	-1.275	28.593	-1.249	28.556	-1.222

28.504	-1.196	28.443	-1.169	28.377	-1.140	28.312	-1.108	28.253	-1.074
28.201	-1.040	28.154	-1.006	28.116	-0.974	28.087	-0.943	28.067	-0.914
28.055	-0.885	28.046	-0.857	28.043	-0.828	28.058	-0.800	28.094	-0.770
28.151	-0.741	28.221	-0.714	28.290	-0.689	28.352	-0.664	28.395	-0.640
28.416	-0.617	28.412	-0.592	28.387	-0.566	28.346	-0.538	28.295	-0.508
28.258	-0.475	28.246	-0.433	28.267	-0.400	28.318	-0.358	28.398	-0.315
28.496	-0.273	28.593	-0.232	28.674	-0.194	28.733	-0.158	28.764	-0.124
28.764	-0.091	28.730	-0.053	28.666	-0.025	28.581	0.006	28.484	0.036
28.384	0.063	28.287	0.087	28.200	0.106	28.134	0.120	28.093	0.128

THE ASPECT ANGLE =   0.0   DEGREES
STARTING FREQ =   2.00000 STEP=   0.01000 GHZ
THE ORIGINAL VERTICAL POLARIZATION DATA:

15.676	1.310	15.746	1.313	15.949	1.324	16.258	1.339	16.633	1.354
17.026	1.368	17.421	1.373	17.823	1.389	18.209	1.400	18.544	1.413
18.811	1.[illegible]30	19.023	1.452	19.207	1.478	19.381	1.508	19.563	1.541
19.762	1.575	19.976	1.613	20.214	1.643	20.468	1.674	20.721	1.702
20.956	1.725	21.152	1.745	21.269	1.760	21.267	1.770	21.138	1.778
20.885	1.783	20.505	1.793	19.996	1.800	19.371	1.816	18.655	1.839
17.866	1.871	17.091	1.911	16.125	1.962	15.184	2.025	14.207	2.104
13.210	2.198	12.204	2.303	11.253	2.437	10.445	2.586	9.844	2.750
9.503	2.928	9.522	3.116	9.930	-2.983	10.674	-2.824	11.589	-2.702
12.553	-2.619	13.522	-2.554	14.457	-2.513	15.324	-2.488	16.106	-2.470

16.787	-2.451	17.334	-2.421	17.744	-2.386	18.034	-2.337	18.221	-2.279
18.317	-2.212	18.364	-2.135	18.401	-2.055	18.454	-1.974	18.533	-1.938
18.638	-1.832	18.744	-1.771	18.842	-1.739	18.913	-1.713	18.924	-1.702
18.855	-1.702	18.694	-1.711	18.440	-1.723	18.134	-1.733	17.816	-1.733
17.502	-1.719	17.191	-1.631	16.899	-1.644	16.623	-1.587	16.374	-1.519
16.182	-1.440	16.050	-1.353	15.950	-1.267	15.875	-1.177	15.813	-1.082
15.748	-0.984	15.685	-0.873	15.649	-0.764	15.652	-0.641	15.731	-0.510
15.903	-0.378	16.176	-0.251	16.537	-0.141	16.944	-0.045	17.336	0.039
17.674	0.117	17.960	0.195	18.199	0.274	18.396	0.355	18.563	0.437
18.720	0.520	18.875	0.603	19.048	0.680	19.247	0.745	19.457	0.796
19.671	0.831	19.881	0.851	20.070	0.852	20.233	0.842	20.364	0.822
20.490	0.799	20.622	0.773	20.750	0.762	20.857	0.757	20.932	0.767
20.968	0.792	20.958	0.821	20.889	0.874	20.752	0.925	20.545	0.979
20.269	1.034	19.942	1.087	19.574	1.135	19.156	1.177	18.582	1.217
18.160	1.254	17.597	1.293	17.006	1.337	16.407	1.390	15.825	1.457
15.306	1.541	14.836	1.642	14.409	1.763	14.044	1.903	13.777	2.063
13.644	2.237	13.688	2.414	13.843	2.589	14.155	2.753	14.570	2.903
15.036	3.036	15.520	-3.123	16.017	-3.035	16.523	-2.956	17.025	-2.894
17.508	-2.848	17.961	-2.814	18.375	-2.790	18.745	-2.774	19.048	-2.764
19.274	-2.759	19.426	-2.756	19.523	-2.753	19.563	-2.751	19.542	-2.745
19.465	-2.737	19.338	-2.722	19.177	-2.701	18.988	-2.674	18.778	-2.643
18.550	-2.609	18.309	-2.572	18.045	-2.532	17.745	-2.487	17.396	-2.437
16.971	-2.380	16.470	-2.314	15.917	-2.236	15.348	-2.143	14.799	-2.043
14.330	-1.911	14.016	-1.779	13.892	-1.644	13.923	-1.512	14.064	-1.390
14.262	-1.275	14.475	-1.131	14.679	-1.093	14.851	-1.012	14.986	-0.935
15.106	-0.858	15.226	-0.731	15.357	-0.701	15.500	-0.620	15.562	-0.541
15.862	-0.467	16.088	-0.402	16.327	-0.343	16.583	-0.289	16.853	-0.237
17.127	-0.187	17.399	-0.142	17.656	-0.098	17.897	-0.056	18.120	-0.015
18.313	0.021	18.458	0.053	18.545	0.078	18.586	0.101	18.595	0.121
18.575	0.138	18.526	0.151	18.460	0.160	18.392	0.168	18.345	0.172

THE ORIGINAL HORIZONTAL POLARIZATION DATA:

14.989	1.419	15.126	1.416	15.487	1.409	15.998	1.406	16.563	1.409
17.154	1.416	17.765	1.423	18.360	1.446	18.917	1.468	19.410	1.495
19.835	1.523	20.192	1.551	20.476	1.578	20.679	1.601	20.789	1.621
20.792	1.636	20.715	1.651	20.583	1.665	20.410	1.678	20.205	1.596
19.954	1.692	19.675	1.703	19.383	1.712	19.107	1.730	18.858	1.755
18.642	1.787	18.452	1.826	18.272	1.872	18.097	1.924	17.917	1.984
17.699	2.049	17.411	2.122	17.050	2.203	16.626	2.293	16.159	2.393
15.671	2.502	15.174	2.623	14.681	2.750	14.240	2.896	13.956	3.058
13.875	-3.058	13.965	-2.891	14.251	-2.728	14.734	-2.582	15.347	-2.457
15.993	-2.355	16.600	-2.273	17.147	-2.204	17.628	-2.142	18.037	-2.085
18.367	-2.032	18.629	-1.982	18.842	-1.938	19.026	-1.900	19.204	-1.869
19.376	-1.848	19.549	-1.833	19.744	-1.825	19.963	-1.821	20.195	-1.819
20.417	-1.816	20.619	-1.813	20.785	-1.809	20.896	-1.802	20.936	-1.789
20.903	-1.770	20.800	-1.745	20.632	-1.714	20.396	-1.678	20.098	-1.639
19.748	-1.601	19.361	-1.566	18.941	-1.537	18.484	-1.512	17.985	-1.492
17.440	-1.471	16.853	-1.447	16.220	-1.418	15.527	-1.379	14.764	-1.328
13.948	-1.259	13.116	-1.165	12.331	-1.040	11.689	-0.882	11.319	-0.597
11.317	-0.499	11.670	-0.303	12.303	-0.138	13.087	0.002	13.988	0.115
14.661	0.205	15.385	0.277	16.053	0.334	16.668	0.378	17.237	0.411
17.751	0.434	18.213	0.451	18.608	0.467	18.938	0.483	19.211	0.502
19.435	0.527	19.610	0.558	19.739	0.595	19.825	0.638	19.874	0.686
19.890	0.740	19.878	0.797	19.831	0.854	19.746	0.908	19.615	0.958
19.438	1.003	19.220	1.041	18.954	1.074	18.638	1.104	18.269	1.137
17.863	1.174	17.436	1.220	16.977	1.277	16.489	1.344	15.989	1.423
15.495	1.513	15.020	1.614	14.576	1.724	14.718	1.843	13.841	1.973
13.561	2.107	13.364	2.245	13.283	2.382	13.337	2.515	13.541	2.638
13.869	2.749	14.291	2.847	14.780	2.935	15.296	3.009	15.779	3.070
16.206	3.120	16.586	-3.113	16.928	-3.079	17.223	-3.043	17.463	-3.010
17.653	-2.978	17.809	-2.945	17.937	-2.915	18.038	-2.882	18.123	-2.848
18.189	-2.814	18.236	-2.773	18.264	-2.742	18.274	-2.703	18.268	-2.561
18.246	-2.615	18.202	-2.563	18.133	-2.512	18.045	-2.455	17.954	-2.393

17.888	-2.328	17.839	-2.261	17.781	-2.193	17.695	-2.126	17.599	-2.059
17.500	-1.995	17.387	-1.934	17.246	-1.876	17.067	-1.819	16.837	-1.762
16.558	-1.704	16.243	-1.641	15.897	-1.573	15.525	-1.497	15.159	-1.414
14.825	-1.319	14.559	-1.213	14.375	-1.099	14.280	-0.978	14.295	-0.852
14.438	-0.724	14.707	-0.5[illegible]9	15.080	-0.483	15.529	-0.380	16.024	-0.295
15.522	-0.223	16.998	-0.15[illegible]	17.433	-0.114	17.805	-0.074	18.100	-0.040
18.325	-0.013	18.491	0.012	18.606	0.035	18.678	0.060	18.715	0.085
18.732	0.111	18.737	0.14[illegible]	18.745	0.172	18.777	0.205	18.835	0.237
18.914	0.267	19.006	0.2[illegible]	19.100	0.315	19.182	0.329	19.237	0.337

THE ASPECT ANGLE = 45.000 DEGREES

STARTING FREQ = 2.00000 STEP= 0.01000 GHZ

THE ORIGINAL VERTICAL POLARIZATION DATA:

23.572	-2.107	23.563	-2.137	23.533	-2.107	23.479	-2.105	23.429	-2.100
23.410	-2.091	23.412	-2.075	23.411	-2.049	23.415	-2.013	23.410	-1.970
23.393	-1.922	23.370	-1.872	23.339	-1.820	23.293	-1.769	23.220	-1.722
23.099	-1.680	22.917	-1.642	22.662	-1.602	22.327	-1.556	21.943	-1.501
21.558	-1.436	21.211	-1.363	20.948	-1.278	20.789	-1.200	20.722	-1.130
20.705	-1.071	20.705	-1.023	20.693	-0.985	20.656	-0.955	20.594	-0.927
20.522	-0.897	20.426	-0.864	20.301	-0.825	20.148	-0.777	19.972	-0.717
19.824	-0.643	19.767	-0.554	19.846	-0.456	20.046	-0.356	20.378	-0.263
20.723	-0.181	21.039	-0.114	21.286	-0.061	21.471	-0.018	21.617	0.017
21.734	0.045	21.822	0.063	21.881	0.093	21.922	0.119	21.959	0.149

21.999	0.175	22.057	0.234	22.136	0.221	22.253	0.227	22.428	0.222
22.665	0.208	22.927	0.185	23.171	0.162	23.356	0.140	23.503	0.122
23.578	0.113	23.586	0.114	23.511	0.128	23.353	0.160	23.140	0.211
22.897	0.281	22.652	0.363	22.436	0.467	22.260	0.571	22.112	0.573
21.963	0.764	21.787	0.846	21.578	0.920	21.357	0.990	21.128	1.057
20.887	1.123	20.637	1.132	20.391	1.263	20.159	1.335	19.985	1.405
19.849	1.468	19.748	1.542	19.687	1.574	19.652	1.616	19.639	1.649
19.595	1.680	19.516	1.712	19.414	1.752	19.299	1.798	19.190	1.852
19.110	1.912	19.089	1.933	19.160	2.053	19.320	2.128	19.537	2.203
19.788	2.277	20.059	2.343	20.337	2.418	20.610	2.483	20.854	2.543
21.056	2.589	21.220	2.653	21.356	2.700	21.464	2.747	21.542	2.792
21.614	2.838	21.712	2.887	21.846	2.936	21.996	2.983	22.151	3.027
22.301	3.065	22.434	3.099	22.538	3.130	22.605	-3.127	22.619	-3.104
22.571	-3.082	22.460	-3.061	22.286	-3.038	22.047	-3.015	21.749	-2.989
21.414	-2.960	21.079	-2.927	20.773	-2.889	20.513	-2.846	20.319	-2.799
20.213	-2.749	20.171	-2.691	20.154	-2.646	20.136	-2.593	20.123	-2.540
20.117	-2.484	20.117	-2.425	20.120	-2.367	20.122	-2.308	20.119	-2.248
20.101	-2.189	20.063	-2.130	20.012	-2.072	19.954	-2.014	19.900	-1.957
19.848	-1.902	19.788	-1.851	19.717	-1.798	19.644	-1.744	19.555	-1.591
19.445	-1.636	19.306	-1.573	19.158	-1.513	19.020	-1.444	18.901	-1.372
18.808	-1.298	18.750	-1.224	18.733	-1.150	18.765	-1.079	18.944	-1.010
18.962	-0.945	19.111	-0.885	19.280	-0.830	19.461	-0.782	19.638	-0.737
19.810	-0.694	19.980	-0.652	20.150	-0.611	20.308	-0.571	20.444	-0.531
20.568	-0.493	20.685	-0.457	20.787	-0.424	20.860	-0.393	20.901	-0.363
20.925	-0.333	20.933	-0.301	20.922	-0.272	20.884	-0.241	20.811	-0.209
20.711	-0.173	20.585	-0.135	20.442	-0.096	20.283	-0.055	20.113	-0.011
19.943	0.036	19.779	0.095	19.627	0.138	19.487	0.192	19.365	0.248
19.276	0.306	19.225	0.363	19.199	0.419	19.176	0.473	19.148	0.529
19.132	0.585	19.136	0.543	19.164	0.700	19.208	0.757	19.268	0.813
19.341	0.867	19.421	0.914	19.492	0.950	19.548	0.977	19.586	0.993

THE ORIGINAL HORIZONTAL POLARIZATION DATA:

22.852	-2.596	22.837	-2.591	22.799	-2.576	22.749	-2.554	22.671	-2.525
22.556	-2.495	22.416	-2.461	22.271	-2.422	22.107	-2.379	21.904	-2.333
21.676	-2.283	21.452	-2.221	21.244	-2.168	21.069	-2.103	20.943	-2.035
20.844	-1.966	20.765	-1.891	20.724	-1.816	20.736	-1.737	20.786	-1.660
20.841	-1.584	20.896	-1.509	20.951	-1.434	21.016	-1.360	21.110	-1.285
21.243	-1.212	21.408	-1.144	21.595	-1.080	21.796	-1.019	22.015	-0.963
22.253	-0.913	22.483	-0.853	22.863	-0.830	22.852	-0.793	23.004	-0.758
23.147	-0.724	23.276	-0.693	23.382	-0.662	23.459	-0.631	23.535	-0.597
23.579	-0.561	23.597	-0.525	23.581	-0.488	23.530	-0.451	23.447	-0.413
23.340	-0.375	23.222	-0.334	23.098	-0.302	22.969	-0.270	22.834	-0.240
22.693	-0.211	22.552	-0.183	22.419	-0.156	22.293	-0.129	22.169	-0.103
22.035	-0.075	21.887	-0.043	21.723	-0.004	21.540	0.042	21.326	0.097
21.081	0.162	20.817	0.236	20.574	0.318	20.370	0.404	20.212	0.494
20.110	0.585	20.073	0.675	20.097	0.760	20.169	0.839	20.286	0.911
20.439	0.973	20.597	1.024	20.737	1.067	20.853	1.108	20.947	1.150
21.022	1.196	21.084	1.243	21.127	1.307	21.164	1.373	21.217	1.444
21.314	1.516	21.458	1.585	21.641	1.645	21.844	1.698	22.095	1.743
22.279	1.779	22.492	1.303	22.693	1.831	22.878	1.849	23.040	1.863
23.172	1.877	23.277	1.832	23.370	1.911	23.454	1.934	23.520	1.959
23.566	1.986	23.580	2.015	23.550	2.049	23.481	2.085	23.376	2.123
23.233	2.164	23.061	2.210	22.873	2.260	22.689	2.314	22.514	2.369
22.344	2.425	22.178	2.481	22.017	2.535	21.863	2.589	21.725	2.642
21.606	2.695	21.505	2.749	21.408	2.803	21.301	2.863	21.200	2.929
21.123	2.995	21.083	3.073	21.078	-3.135	21.100	-3.063	21.150	-2.995
21.226	-2.933	21.312	-2.879	21.389	-2.829	21.443	-2.785	21.484	-2.734
21.519	-2.700	21.557	-2.655	21.615	-2.608	21.698	-2.557	21.817	-2.501
21.980	-2.442	22.184	-2.383	22.414	-2.326	22.650	-2.275	22.861	-2.231
23.023	-2.193	23.129	-2.153	23.179	-2.125	23.170	-2.019	23.105	-2.058
22.998	-2.022	22.866	-1.383	22.723	-1.940	22.589	-1.895	22.477	-1.849
22.392	-1.802	22.338	-1.757	22.310	-1.712	22.305	-1.667	22.315	-1.620
22.318	-1.572	22.297	-1.513	22.252	-1.461	22.187	-1.396	22.104	-1.323

22.019	-1.245	21.944	-1.164	21.881	-1.086	21.825	-1.013	21.769	-0.947
21.705	-0.891	21.622	-0.844	21.517	-0.806	21.389	-0.777	21.251	-0.755
21.130	-0.737	21.031	-0.723	20.947	-0.701	20.863	-0.676	20.767	-0.641
20.658	-0.593	20.542	-0.533	20.434	-0.455	20.349	-0.369	20.309	-0.277
20.332	-0.184	20.425	-0.097	20.579	-0.018	20.771	0.050	20.979	0.107
21.179	0.150	21.354	0.183	21.499	0.208	21.611	0.227	21.592	0.243
21.736	0.259	21.742	0.283	21.721	0.307	21.691	0.342	21.655	0.382
21.614	0.429	21.574	0.473	21.540	0.531	21.513	0.582	21.497	0.628
21.486	0.668	21.481	0.702	21.485	0.729	21.490	0.750	21.489	0.763

THE ASPECT ANGLE = 90.000 DEGREES

STARTING FREQ = 4.00000 STEP= 0.02000 GHZ

THE ORIGINAL VERTICAL FCLARIZATION DATA:

28.369	0.262	28.348	0.263	28.290	0.285	28.213	0.314	28.130	0.352
28.057	0.400	28.004	0.453	27.980	0.516	27.985	0.581	28.021	0.649
28.063	0.718	28.104	0.787	28.141	0.858	28.183	0.929	28.229	1.002
28.277	1.075	28.320	1.143	28.349	1.223	28.369	1.298	28.384	1.370
28.396	1.440	28.413	1.505	28.436	1.566	28.461	1.623	28.482	1.676
28.502	1.728	28.519	1.773	28.525	1.828	28.512	1.877	28.476	1.925
28.419	1.978	28.344	2.032	28.260	2.088	28.171	2.147	28.085	2.209
28.010	2.275	27.956	2.343	27.926	2.414	27.917	2.483	27.930	2.550
27.964	2.613	28.013	2.673	28.071	2.728	28.127	2.780	28.174	2.829
28.211	2.876	28.233	2.923	28.235	2.971	28.213	3.022	28.172	3.078

28.131	3.139	28.108	-3.077	28.107	-3.010	28.142	-2.938	28.215	-2.865
28.319	-2.793	28.444	-2.722	28.576	-2.653	28.697	-2.587	28.790	-2.522
28.850	-2.459	28.884	-2.395	28.887	-2.334	28.861	-2.270	28.815	-2.207
28.761	-2.143	28.701	-2.073	28.636	-2.013	28.564	-1.948	28.484	-1.883
28.393	-1.818	28.235	-1.753	28.202	-1.687	28.124	-1.621	28.063	-1.555
28.023	-1.489	28.005	-1.422	28.013	-1.355	28.039	-1.288	28.084	-1.221
28.144	-1.155	28.213	-1.091	28.287	-1.027	28.361	-0.965	28.428	-0.906
28.489	-0.849	28.542	-0.793	28.583	-0.738	28.607	-0.683	28.614	-0.628
28.608	-0.575	28.583	-0.525	28.540	-0.477	28.483	-0.430	28.417	-0.383
28.351	-0.333	28.288	-0.233	28.234	-0.222	28.192	-0.160	28.162	-0.095
28.151	-0.027	28.158	0.041	28.177	0.111	28.206	0.180	28.245	0.245
28.286	0.311	28.321	0.373	28.347	0.433	28.361	0.499	28.357	0.543
28.349	0.596	28.344	0.643	28.343	0.704	28.343	0.761	28.350	0.821
28.364	0.833	28.376	0.943	28.377	1.017	28.369	1.087	28.363	1.158
28.360	1.229	28.362	1.297	28.371	1.365	28.381	1.429	28.388	1.492
28.391	1.553	28.390	1.614	28.379	1.674	28.356	1.734	28.353	1.795
28.328	1.856	28.311	1.923	28.309	1.985	28.318	2.052	28.336	2.118
28.355	2.183	28.372	2.247	28.382	2.310	28.379	2.371	28.374	2.430
28.372	2.486	28.370	2.541	28.376	2.594	28.380	2.647	28.382	2.698
28.371	2.751	28.328	2.804	28.254	2.860	28.150	2.919	28.018	2.982
27.867	3.051	27.713	3.121	27.584	-3.084	27.489	-3.006	27.439	-2.932
27.429	-2.865	27.469	-2.801	27.555	-2.748	27.685	-2.698	27.837	-2.654
27.999	-2.611	28.169	-2.563	28.335	-2.524	28.487	-2.477	28.610	-2.427
28.693	-2.373	28.729	-2.315	28.704	-2.257	28.619	-2.193	28.478	-2.126
28.291	-2.055	28.085	-1.973	27.886	-1.900	27.719	-1.820	27.599	-1.742
27.564	-1.688	27.608	-1.603	27.700	-1.539	27.812	-1.483	27.922	-1.428
28.017	-1.371	28.082	-1.313	28.105	-1.252	28.087	-1.186	28.039	-1.116
27.972	-1.042	27.897	-0.965	27.831	-0.889	27.778	-0.813	27.745	-0.739
27.723	-0.663	27.711	-0.591	27.700	-0.519	27.710	-0.447	27.760	-0.378
27.848	-0.314	27.966	-0.253	28.101	-0.212	28.227	-0.179	28.320	-0.159

THE ORIGINAL HORIZONTAL POLARIZATION DATA:

28.210	0.404	28.202	0.413	28.182	0.430	28.155	0.462	28.120	0.505
28.080	0.558	28.046	0.617	28.024	0.681	28.010	0.747	28.006	0.814
28.010	0.881	28.019	0.946	28.030	1.008	28.041	1.067	28.049	1.125
28.049	1.182	28.045	1.239	28.049	1.295	28.069	1.350	28.104	1.406
28.148	1.461	28.206	1.513	28.272	1.575	28.341	1.634	28.404	1.597
28.464	1.761	28.521	1.824	28.575	1.887	28.616	1.947	28.633	2.005
28.620	2.063	28.581	2.122	28.523	2.182	28.446	2.245	28.347	2.312
28.232	2.363	28.106	2.457	27.979	2.534	27.861	2.614	27.758	2.696
27.677	2.781	27.628	2.867	27.613	2.954	27.634	3.040	27.679	3.123
27.728	-3.081	27.795	-3.003	27.879	-2.940	27.979	-2.876	28.088	-2.815
28.204	-2.761	28.312	-2.708	28.404	-2.657	28.473	-2.606	28.512	-2.554
28.527	-2.502	28.521	-2.449	28.505	-2.394	28.489	-2.337	28.479	-2.278
28.478	-2.216	28.486	-2.154	28.503	-2.090	28.522	-2.025	28.534	-1.961
28.532	-1.898	28.517	-1.835	28.490	-1.772	28.451	-1.709	28.397	-1.645
28.331	-1.582	28.252	-1.513	28.170	-1.457	28.088	-1.397	28.014	-1.341
27.951	-1.286	27.898	-1.234	27.851	-1.181	27.816	-1.129	27.799	-1.075
27.797	-1.020	27.802	-0.961	27.817	-0.905	27.841	-0.848	27.863	-0.791
27.878	-0.734	27.890	-0.673	27.897	-0.615	27.904	-0.552	27.910	-0.487
27.911	-0.419	27.904	-0.343	27.884	-0.276	27.858	-0.199	27.831	-0.118
27.815	-0.035	27.815	0.053	27.832	0.135	27.867	0.218	27.919	0.299
27.977	0.376	28.027	0.443	28.067	0.518	28.107	0.584	28.160	0.648
28.220	0.708	28.281	0.765	28.342	0.819	28.391	0.870	28.424	0.921
28.434	0.972	28.417	1.024	28.368	1.077	28.286	1.133	28.176	1.190
28.048	1.250	27.909	1.312	27.777	1.377	27.633	1.442	27.572	1.509
27.510	1.577	27.476	1.644	27.461	1.710	27.457	1.776	27.454	1.843
27.452	1.911	27.458	1.982	27.473	2.065	27.502	2.131	27.547	2.207
27.604	2.284	27.677	2.361	27.762	2.437	27.849	2.512	27.925	2.585
27.992	2.658	28.055	2.727	28.109	2.792	28.153	2.855	28.196	2.917
28.239	2.978	28.280	3.033	28.317	3.100	28.351	-3.123	28.372	-3.064
28.375	-3.005	28.365	-2.945	28.341	-2.886	28.306	-2.826	28.264	-2.765
28.221	-2.703	28.182	-2.643	28.167	-2.578	28.180	-2.519	28.205	-2.464

28.231	-2.412	28.247	-2.360	28.253	-2.307	28.250	-2.251	28.241	-2.193
28.223	-2.130	28.191	-2.062	28.154	-1.991	28.126	-1.918	28.107	-1.942
28.101	-1.767	28.113	-1.692	28.146	-1.620	28.201	-1.551	28.271	-1.487
28.347	-1.428	28.410	-1.374	28.445	-1.324	28.452	-1.275	28.430	-1.224
28.389	-1.168	28.332	-1.103	28.259	-1.042	28.182	-0.973	28.114	-0.902
28.057	-0.830	28.023	-0.753	28.013	-0.689	28.022	-0.624	28.044	-0.562
28.071	-0.504	28.090	-0.450	28.089	-0.397	28.066	-0.341	28.026	-0.283
27.973	-0.220	27.912	-0.152	27.854	-0.079	27.818	-0.004	27.822	0.070
27.863	0.140	27.925	0.203	27.992	0.255	28.047	0.294	28.087	0.317

THE ASPECT ANGLE = 0.0 DEGREES

STARTING FREQ = 4.00000 STEP= 0.02000 GHZ

THE ORIGINAL VERTICAL POLARIZATION DATA:

15.159	1.421	16.062	1.436	15.773	1.481	15.348	1.559	14.870	1.674
14.462	1.824	14.230	1.993	14.227	2.182	14.410	2.360	14.706	2.525
15.032	2.678	15.338	2.827	15.626	2.958	15.887	3.088	16.123	-3.067
15.364	-2.943	16.600	-2.822	16.822	-2.709	16.992	-2.605	17.080	-2.508
17.069	-2.419	16.942	-2.336	16.703	-2.255	16.351	-2.174	15.837	-2.088
15.366	-1.993	14.785	-1.834	14.174	-1.755	13.574	-1.606	13.041	-1.433
12.645	-1.242	12.468	-1.035	12.578	-0.828	12.960	-0.639	13.521	-0.478
14.114	-0.344	14.682	-0.221	15.161	-0.140	15.519	-0.060	15.734	0.012
15.794	0.080	15.715	0.151	15.505	0.226	15.191	0.313	14.799	0.416
14.357	0.537	13.908	0.671	13.500	0.842	13.157	1.019	12.890	1.208

12.717	1.407	12.666	1.603	12.769	1.812	13.051	2.008	13.489	2.187
14.040	2.343	14.637	2.477	15.229	2.586	15.744	2.674	16.152	2.744
16.429	2.800	16.549	2.847	16.508	2.892	16.294	2.941	15.905	2.999
15.354	3.071	14.650	-3.123	13.825	-2.998	12.933	-2.846	12.053	-2.661
11.293	-2.445	10.746	-2.202	10.529	-1.945	10.677	-1.688	11.143	-1.447
11.869	-1.235	12.763	-1.058	13.732	-0.916	14.689	-0.806	15.552	-0.725
16.283	-0.664	16.864	-0.619	17.275	-0.577	17.513	-0.538	17.560	-0.494
17.417	-0.442	17.088	-0.373	16.581	-0.297	15.915	-0.192	15.145	-0.055
14.363	0.119	13.737	0.335	13.428	0.579	13.535	0.828	13.974	1.059
14.580	1.261	15.234	1.415	15.853	1.586	16.398	1.718	16.855	1.839
17.216	1.350	17.490	2.057	17.699	2.163	17.843	2.269	17.929	2.376
17.954	2.483	17.921	2.583	17.821	2.693	17.639	2.793	17.361	2.892
17.009	2.993	16.583	3.103	16.108	-3.065	15.606	-2.936	15.125	-2.793
14.716	-2.635	14.433	-2.466	14.302	-2.294	14.339	-2.127	14.493	-1.969
14.719	-1.822	14.946	-1.684	15.155	-1.549	15.364	-1.412	15.603	-1.272
15.850	-1.134	16.112	-1.003	16.373	-0.875	16.598	-0.761	16.761	-0.526
16.830	-0.558	16.793	-0.463	16.633	-0.367	16.344	-0.264	15.943	-0.147
15.443	-0.011	14.925	0.143	14.525	0.333	14.369	0.525	14.474	0.707
14.763	0.867	15.108	0.993	15.393	1.103	15.567	1.190	15.600	1.266
15.493	1.339	15.238	1.413	14.843	1.492	14.347	1.582	13.806	1.682
13.325	1.800	12.978	1.933	12.792	2.072	12.713	2.210	12.648	2.340
12.507	2.465	12.200	2.583	11.679	2.723	10.901	2.881	9.934	3.079
8.946	-2.948	8.293	-2.621	8.451	-2.262	9.417	-1.942	10.778	-1.594
12.166	-1.509	13.405	-1.372	14.414	-1.264	15.175	-1.174	15.731	-1.594
15.085	-1.020	16.271	-0.947	16.291	-0.875	16.172	-0.796	15.930	-0.705
15.596	-0.596	15.219	-0.467	14.894	-0.320	14.669	-0.159	14.494	0.005
14.356	0.167	14.267	0.317	14.197	0.462	14.165	0.592	14.213	0.709
14.337	0.808	14.482	0.833	14.654	0.962	14.832	1.018	15.006	1.067
15.144	1.116	15.237	1.154	15.239	1.211	15.166	1.260	15.017	1.314
14.825	1.372	14.559	1.433	14.262	1.508	14.021	1.572	13.865	1.620

THE ORIGINAL HORIZONTAL POLARIZATION DATA:

17.121	0.976	17.079	0.986	16.951	1.015	16.732	1.064	15.427	1.134
16.049	1.227	15.631	1.344	15.238	1.487	14.933	1.652	14.767	1.931
14.743	2.018	14.887	2.203	15.193	2.377	15.611	2.531	16.059	2.664
16.474	2.777	16.798	2.875	17.026	2.963	17.170	3.045	17.240	3.125
17.241	-3.079	17.184	-2.999	17.076	-2.915	16.924	-2.829	15.713	-2.743
16.409	-2.655	15.999	-2.551	15.479	-2.432	14.925	-2.287	14.420	-2.113
14.063	-1.913	13.929	-1.695	14.060	-1.477	14.427	-1.271	14.938	-1.089
15.507	-0.935	16.072	-0.805	16.548	-0.695	16.896	-0.599	17.137	-0.510
17.294	-0.423	17.384	-0.377	17.428	-0.250	17.470	-0.162	17.511	-0.077
17.533	0.005	17.491	0.087	17.365	0.174	17.136	0.272	16.828	0.382
16.474	0.509	16.104	0.655	15.781	0.820	15.576	1.002	15.532	1.191
15.673	1.378	15.971	1.552	16.370	1.707	16.789	1.841	17.161	1.954
17.451	2.051	17.649	2.137	17.748	2.215	17.740	2.289	17.651	2.363
17.481	2.439	17.224	2.517	16.864	2.603	16.419	2.698	15.902	2.806
15.329	2.929	14.724	3.073	14.125	-3.052	13.593	-2.870	13.200	-2.667
13.016	-2.448	13.093	-2.225	13.411	-2.010	13.900	-1.814	14.490	-1.637
15.123	-1.482	15.744	-1.347	16.305	-1.228	16.768	-1.122	17.095	-1.025
17.280	-0.934	17.321	-0.846	17.229	-0.755	17.020	-0.660	16.707	-0.558
16.302	-0.449	15.834	-0.330	15.329	-0.201	14.826	-0.060	14.353	0.093
13.958	0.259	13.699	0.493	13.619	0.625	13.728	0.810	14.002	0.981
14.387	1.135	14.842	1.263	15.294	1.383	15.673	1.482	15.946	1.569
16.088	1.648	16.096	1.723	15.969	1.796	15.719	1.872	15.359	1.952
14.896	2.024	14.323	2.142	13.675	2.257	13.000	2.392	12.334	2.550
11.753	2.734	11.371	2.941	11.261	-3.119	11.471	-2.894	11.963	-2.686
12.637	-2.506	13.388	-2.354	14.134	-2.229	14.811	-2.125	15.363	-2.037
15.783	-1.958	16.091	-1.883	16.291	-1.809	16.386	-1.736	16.378	-1.562
16.263	-1.586	16.037	-1.505	15.684	-1.421	15.198	-1.330	14.591	-1.230
13.853	-1.115	13.033	-0.974	12.229	-0.801	11.574	-0.591	11.247	-0.352
11.359	-0.105	11.874	0.123	12.685	0.313	13.522	0.453	14.329	0.577
15.012	0.664	15.536	0.733	15.896	0.795	16.086	0.853	16.106	0.991
15.940	0.974	15.581	1.343	15.028	1.123	14.306	1.221	13.458	1.342

12.569	1.492	11.741	1.677	11.161	1.896	10.967	2.132	11.171	2.357
11.630	2.552	12.167	2.715	12.666	2.852	13.111	2.972	13.502	3.081
13.864	-3.103	14.218	-3.003	14.540	-2.916	14.827	-2.826	15.069	-2.735
15.261	-2.645	15.371	-2.554	15.384	-2.462	15.288	-2.367	15.097	-2.265
14.826	-2.154	14.490	-2.028	14.101	-1.882	13.741	-1.712	13.529	-1.520
13.522	-1.322	13.731	-1.130	14.085	-0.958	14.481	-0.811	14.830	-0.695
15.081	-0.574	15.228	-0.473	15.259	-0.375	15.157	-0.276	14.939	-0.171
14.628	-0.055	14.281	0.075	13.947	0.220	13.699	0.376	13.587	0.533
13.635	0.682	13.824	0.803	14.086	0.908	14.327	0.978	14.486	1.019

THE ASPECT ANGLE = 45.000 DEGREES

STARTING FREQ = 4.00000 STEP= 0.02000 GHZ

THE ORIGINAL VERTICAL POLARIZATION DATA:

18.122	1.812	18.136	1.826	18.188	1.865	18.269	1.928	18.383	2.008
18.534	2.101	18.727	2.203	18.965	2.300	19.214	2.398	19.526	2.489
19.790	2.576	20.017	2.657	20.196	2.733	20.328	2.805	20.400	2.875
20.406	2.943	20.351	3.011	20.237	3.086	20.070	-3.121	19.850	-3.038
19.584	-2.947	19.298	-2.843	19.014	-2.733	18.769	-2.612	18.575	-2.485
18.433	-2.358	18.351	-2.227	18.337	-2.095	18.395	-1.961	18.545	-1.826
18.795	-1.694	19.118	-1.561	19.486	-1.455	19.871	-1.353	20.246	-1.262
20.580	-1.182	20.835	-1.111	20.997	-1.045	21.070	-0.982	21.064	-0.915
21.008	-0.845	20.924	-0.767	20.823	-0.681	20.719	-0.586	20.529	-0.487
20.560	-0.386	20.534	-0.293	20.530	-0.187	20.537	-0.093	20.625	0.008

20.460	0.106	20.327	0.207	20.135	0.313	19.918	0.426	19.702	0.546
19.517	0.670	19.392	0.756	19.330	0.921	19.322	1.044	19.357	1.164
19.419	1.280	19.511	1.395	19.627	1.509	19.741	1.617	19.847	1.719
19.925	1.811	19.961	1.895	19.944	1.974	19.870	2.052	19.729	2.132
19.523	2.215	19.235	2.302	18.881	2.393	18.467	2.486	19.014	2.587
17.553	2.695	17.119	2.811	16.765	2.943	16.521	3.079	16.389	-3.061
16.379	-2.920	16.478	-2.783	16.687	-2.653	16.982	-2.535	17.314	-2.431
17.637	-2.339	17.921	-2.256	18.158	-2.182	18.339	-2.114	18.450	-2.045
18.495	-1.981	18.476	-1.311	18.392	-1.834	18.265	-1.749	19.105	-1.657
17.934	-1.557	17.767	-1.450	17.608	-1.338	17.472	-1.221	17.365	-1.101
17.290	-0.981	17.258	-0.862	17.256	-0.748	17.268	-0.639	17.276	-0.536
17.272	-0.438	17.258	-0.345	17.236	-0.257	17.228	-0.170	17.239	-0.083
17.273	0.006	17.312	0.093	17.358	0.199	17.409	0.304	17.484	0.413
17.588	0.522	17.725	0.630	17.886	0.737	18.047	0.843	18.214	0.949
18.372	1.052	18.512	1.151	18.624	1.252	18.706	1.351	18.745	1.448
18.734	1.543	18.662	1.638	18.531	1.735	18.345	1.837	18.130	1.946
17.920	2.062	17.743	2.193	17.618	2.300	17.561	2.420	17.582	2.535
17.679	2.647	17.846	2.753	18.063	2.846	18.298	2.936	18.516	3.020
18.713	3.101	18.857	-3.101	18.938	-3.018	18.964	-2.930	18.941	-2.837
18.877	-2.738	18.780	-2.635	18.649	-2.528	18.490	-2.419	18.320	-2.309
18.154	-2.201	17.997	-2.095	17.841	-1.994	17.684	-1.898	17.518	-1.807
17.338	-1.720	17.138	-1.633	16.920	-1.557	16.701	-1.475	16.483	-1.388
16.275	-1.294	16.106	-1.189	15.973	-1.079	15.880	-0.966	15.833	-0.845
15.864	-0.722	15.978	-0.593	16.196	-0.479	16.478	-0.369	16.791	-0.271
17.066	-0.183	17.333	-0.103	17.561	-0.026	17.731	0.047	17.833	0.122
17.858	0.199	17.773	0.283	17.602	0.373	17.361	0.475	17.095	0.593
16.821	0.717	16.587	0.852	16.380	0.990	16.233	1.129	16.124	1.262
16.013	1.385	15.837	1.493	15.563	1.603	15.196	1.709	14.743	1.824
14.275	1.956	13.898	2.105	13.747	2.270	13.903	2.446	14.402	2.611
15.113	2.749	15.871	2.855	16.507	2.934	16.978	2.985	17.258	3.013

THE ORIGINAL HORIZONTAL POLARIZATION DATA:

20.298	1.322	20.262	1.333	20.178	1.365	20.072	1.415	19.983	1.492
19.931	1.563	19.921	1.655	19.956	1.754	20.028	1.857	20.119	1.962
20.220	2.069	20.329	2.177	20.458	2.287	20.622	2.399	20.816	2.511
21.030	2.622	21.258	2.733	21.475	2.833	21.659	2.931	21.787	3.026
21.844	3.118	21.819	-3.073	21.713	-2.984	21.542	-2.889	21.335	-2.790
21.109	-2.683	20.905	-2.586	20.750	-2.448	20.670	-2.329	20.661	-2.212
20.711	-2.103	20.789	-2.003	20.876	-1.912	20.961	-1.829	21.034	-1.753
21.072	-1.680	21.074	-1.608	21.054	-1.536	21.007	-1.461	20.930	-1.382
20.826	-1.298	20.696	-1.205	20.565	-1.107	20.483	-1.001	20.471	-0.891
20.529	-0.781	20.634	-0.676	20.774	-0.577	20.914	-0.486	21.034	-0.398
21.106	-0.312	21.126	-0.223	21.084	-0.135	20.998	-0.040	20.883	0.061
20.771	0.166	20.665	0.276	20.581	0.389	20.542	0.507	20.555	0.624
20.600	0.740	20.655	0.851	20.694	0.957	20.698	1.058	20.572	1.158
20.617	1.259	20.551	1.362	20.483	1.467	20.441	1.576	20.427	1.688
20.436	1.803	20.456	1.923	20.485	2.037	20.516	2.154	20.542	2.273
20.576	2.394	20.658	2.516	20.773	2.634	20.903	2.748	21.043	2.858
21.187	2.965	21.316	3.068	21.429	-3.116	21.528	-3.021	21.594	-2.929
21.620	-2.838	21.609	-2.745	21.582	-2.651	21.577	-2.554	21.599	-2.455
21.653	-2.360	21.728	-2.267	21.800	-2.178	21.852	-2.094	21.866	-2.012
21.819	-1.933	21.722	-1.852	21.600	-1.767	21.475	-1.677	21.355	-1.581
21.251	-1.479	21.181	-1.372	21.160	-1.263	21.194	-1.153	21.301	-1.043
21.452	-0.937	21.616	-0.837	21.761	-0.741	21.875	-0.648	21.954	-0.554
21.994	-0.457	22.007	-0.355	22.003	-0.251	21.986	-0.142	21.970	-0.031
21.962	0.079	21.960	0.173	21.965	0.295	21.975	0.402	21.988	0.507
21.993	0.609	21.981	0.703	21.948	0.806	21.884	0.901	21.791	0.995
21.674	1.092	21.544	1.192	21.418	1.295	21.312	1.403	21.244	1.513
21.222	1.623	21.241	1.732	21.285	1.836	21.337	1.937	21.393	2.033
21.428	2.128	21.479	2.221	21.537	2.314	21.605	2.408	21.682	2.503
21.767	2.597	21.861	2.693	21.955	2.783	22.052	2.874	22.152	2.961
22.253	3.045	22.336	3.127	22.390	-3.076	22.398	-2.996	22.354	-2.913
22.268	-2.824	22.158	-2.733	22.043	-2.629	21.933	-2.523	21.836	-2.411

21.757	-2.294	21.712	-2.173	21.705	-2.051	21.731	-1.928	21.790	-1.806
21.871	-1.685	21.964	-1.567	22.060	-1.451	22.159	-1.339	22.252	-1.231
22.378	-1.126	22.502	-1.025	22.615	-0.931	22.707	-0.841	22.761	-0.755
22.767	-0.670	22.731	-0.584	22.672	-0.497	22.610	-0.405	22.549	-0.312
22.492	-0.213	22.448	-0.111	22.434	-0.005	22.466	0.101	22.542	0.205
22.665	0.307	22.810	0.405	22.956	0.498	23.073	0.584	23.154	0.566
23.195	0.745	23.189	0.822	23.144	0.898	23.077	0.975	22.997	1.055
22.906	1.136	22.801	1.219	22.686	1.306	22.590	1.394	22.542	1.481
22.538	1.563	22.570	1.636	22.623	1.695	22.680	1.738	22.725	1.764

REFERENCES

[1] A. J. Poelman, "A Study of Controllable Polarization Applied to Radar", Proceedings Military Microwaves 80 Conference, The Cunard International Hotel, London, England, pp. 389-404, Oct. 1980. [Microwave Exhibitions and Publishers Ltd., Temple House, 36 High Street, Sevenoaks, Kent, England, TN13 1JG.]

[2] S. K. Chaudhuri and W.-M. Boerner, "Polarization utilization in profile inversion of a perfectly conducting prolate spheroid", IEEE Trans. Antennas Propagation, Vol. AP-25, pp. 505-511, July 1977.

[3] W.-M. Boerner, M. B. El-Arini, C. Y. Chan, and P. M. Mastoris, "Polarization dependence in electromagnetic inverse problem", IEEE Trans. Antennas Propagation (Special issue on inverse methods in electromagnetics), Vol. AP-29, pp. 262-269, March, 1981.

[4] J. R. Huynen, "Phenomenological theory of radar targets", Ph.D. dissertation, Technical University, Delft, The Netherlands, 1970.

[5] W.-M. Boerner, M. B. El-Arini, S. Saatchi, M. Davidovitz, J. Nespor, W.-S. Ip, "Polarization utilization in radar target reconstruction", Final Report on Contract No. NAV-AIR-N00019-80-C-0620, Sept. 15, 1981.

[6] W.-M. Boerner, "Polarization utilization in electromagnetic inverse scattering", Chapter 7 in Inverse Scattering Problems in Optics, H. P. Baltes, Ed., Topics in Current Physics, Vol. 20, New York: Springer, 1980, pp. 237-290.

[7] D. B. Kanareykin, N. F. Pavlov, and U. A. Potekhin, The Polarization of Radar Signals, Sovyetskoye Radio, Moscow, 1966. English translation of Chapters 10-12: Radar Polarization Effects, New York: Macmillan

[8] C. L. Bennett, A. M. Auckenthaler, R. S. Smith, J. D. DeLorenzo, "Space-time integral equation approach to the large body scattering problems", Sperry Research Center, Sudbury, MA, Final Report on Contract No. F30602-71-C-0162, AD 763794, May, 1973.

[9] C. L. Bennett, "Time domain inverse scattering", IEEE Trans. Antennas Propagations (Special issue on inverse methods in electromagnetics), Vol. AP-29, pp. 213-219, March, 1981.

[10] E. M. Kennaugh and R. L. Cosgriff, "The use of impulse response in electromagnetic scattering problems", IRE National Convention Record, Part I, pp. 72-77, 1958.

[11] Yu N. Barabenenkov, "Scattering of electromagnetic delta pulses by ideally conducting bodies of finite dimensions", Radiotekhonika i Electronika (USSR), Vol. 8, pp. 1069-1071, June 1963. C. C. Translation.

[12] E. M. Kennaugh and D. L. Moffatt, "Transient and impulse response approximation", IEEE Proc. Vol. 53 (8), 1965, pp. 893-901.

[13] D.J. Struik, "Lectures on classical differential geometry", Addison Wesley Publishing Company, Inc., Reading MA, U.S.A. and London, England, 1961.

[14] M.M. Lipschitz, "Theory and problem of differential geometry", McGraw-Hill Book Co., Inc., N.Y., 1969.

[15] S.K. Chaudhuri, "A time domain synthesis of electromagnetic backscattering by conducting ellipsoids", IEEE Trans. Antennas Propagations, Vol. AP-28, July 1980, pp. 523-530.

[16] C.L. Bennett, "A technique for computing approximate electromagnetic impulse responses of conducting bodies", Ph D. dissertation, Purdue University, Lafayette, Indiana, August, 1981.

[17] S.K. Chaudhuri and W-M. Boerner, "A monostatic inverse scattering model based on polarization utilization", Applied Physics, Vol. 11, No. 4, pp. 337-350, December 1976.

[18] E.M. Kennaugh, "Polarization properties of radar reflections", M.S. thesis, Dept. Elec. Eng., O.S.U., Columbus, 1952 (O.S.U. Antenna Lab., Rep. 389-12, March 1, 1952)

[19] J.D. Kraus, Radio Astronomy, New York: McGraw-Hill, 1966.

[20] E.M. Kennaugh, "Effects of type of polarization on echo characteristics", O.S.U., Antenna Lab., Columbus, OH, Reps. 389-1 to 389-24, 1949-1954.

[21] W-M. Boerner, "State of the Art Review--- Polarization Utilization in Electromagnetic Inverse Scattering", Communications Lab. Rept, 78-3, Oct. 1978.

[22] J.D. Young, "Target Imaging from Multiple-frequency radar returns", O.S.U., ESL Rept, 2768-6, June 1971.

[23] C.L. Bennett, R. Hieronymus and H. Mieras, "Impulse Response Target Study", Sperry Research Center, Final Rept, 1977.

[24] S.K. Chaudhuri, "Utilization of Polarization-Depolarization Characteristics in Electromagnetic Inverse Scattering", PhD thesis, Univ. of Manitoba, Winnipeg, Canada, 1977.

[25] W-M. Boerner, C-M. Ho, B.Y. Foo, "Use of Radon's Projection Theory in Electromagnetic Inverse Scattering", IEEE Trans Antennas Prop., Special Issue on Inverse Methods in Electromagnetics, Vol. AP-29, pp. 262-269, March 1981.

[26] C-M. Ho, "The Extension of Physical Optics Far-Field Inverse Scattering using Radon's Transform Theories and Polarization Utilization", M.S. thesis, Dept. of Information Eng., Univ. of Illinois at Chicago Circle, Chicago, 1980.

[27] M.W. Long, "Radar Reflectivity of Land and Sea", D.C. Heath & Company, 1975.

[28] E.A. Walton, "Analysis of Accuracy of a Radar Backscatter Measurement System using Phasor Compensation", OSU-ESL, Oct. 1981.

[29] G.C. McCormick and A.Hendry, "Techniques for the Determination of the Polarization Properties of Precipitation", Radio Science, Vol. 14, No. 6, pp. 1027-1040, Nov-Dec 1979.

[30] A.L. Maffett, "Scattering Matrices", in Methods of Radar Cross-Section Analysis, Ed. by J.W. Crispin, Jr. and K.M Siegal, Academic Press, NY, 1968.

[31] M.W. Long, "Backscattering for Circular Polarization", Electronics Letters, Vol. 2, pp. 351, Sept. 1966.

[32] L.E. Allan and G.C. McCormick, "Measurements of the Backscatter Matrix of Dielectric Spheroids", IEEE trans. Antennas & Prop., Vol. AP-26, No. 4, July 1978.

[33] L.E. Allan and G.C. McCormick, "Measurements of Backscatter Matrix of Dielectric Bodies", IEEE Trans. Antennas & Prop., Vol. AP-28, No. 2, March 1980.

[34] G.C. McCormick and A. Hendry, "Principles for the Radar Determination of the Polarization Properties of Precipitation", Radio Science, Vol. 10, pp. 421-434, April 1975.

[35] W-M. Boerner, M.B. El-Arini, C-Y. Chan, S. Saatchi, W-S. Ip, P.M. Mastoris, B-Y. Foo, "Polarization Utilization in Radar Target Reconstruction", Technical Rept., UICC CL-EMID-NANRAR-81-01, Jan. 1981.

[36] L.A. Morgan, S. Weisbrod, "RCS Matrix Studies of Sea Clutter", Teledyne Micronetics, Final Rept., San Diego, California, Mar. 1982.

[37] H. Mieras and C.L. Bennett, "Space-Time Integral Equation Approach to Dielectric Targets", IEEE Trans. Antennas & Prop., Vol. AP-30, No. 1, January 1982.

[38] S.H. Bickel, "Some Invariant Properties of the Polarization Scattering Matrix", Proc. IEEE, Vol. 53, pp. 1070-1072, Aug. 1965.

[39] C.D. Graves, "Radar Polarization Power Scattering Matrix", Proc. IRE, Vol. 44, pp. 248-252, Feb. 1956.

[40] J.S. Hollis, T.G. Hickman and T.J. Lyon, "Polarization Theory", in Microwave Antenna Measurements, Ed., by J.S. Hollis, T.J. Lyon and L. Clayton, Scientific-Atlanta, Inc., Atlanta, Georgia, July 1970.

[41] G. Sinclair, "Modification of the Radar Equation for Arbitrary Targets and Arbitrary Polarization", Rept. #302-19, Antenna Lab., OSU, Columbus, Ohio, 1948.

[42] J.R. Huynen, "Phenomenological Theory of Radar Targets", Ph.D Dissertation, Drukkerij Bronder-Offset, N.V., Rotterdom, 1970.

RESUME

Name : Thomas Bing-Yuen Foo
Address : 838 S. Miller St.,
Chicago, Illinois, 60607
Phone : (312) 829-7725 <Home>
: (312) 996-5140 <Office>

Date of Birth : January 25, 1956
Marital Status : Single
Status : visa student
Place of Birth/Citizenship : Hong Kong

EDUCATION :

June 80 - present

University of Illinois at Chicago
Degree : M. Sc. in information Engineering
Major : Electromagnetics, remote sensing
Cumulative Grade Point : 5.00 out of 5.00
Expected Graduation Date : around end of Mar. 82

Sept 79 - June 80

Ohio State University, Columbus, Ohio
Enrolled in Graduate School,
Department of Electrical Engineering
Major : Communications, Applied Electromagnetics
Cumulative Graduate Grade Point: 4.00 out of 4.00

Sept 74 - May 78

University of Manitoba, Winnipeg, Canada
Degree : B. Sc. in Civil Engineering
Major : Structural Analysis
Cumulative Grade Point : 3.74 out of 4.00

EXPERIENCE :

June 80 - present

Position - Research Assistant in Electromagnetic Imaging Group Communications Laboratory, UICC
Research/Thesis Adviser- Dr.Wolfgang-Martin Boerner
Research Area - Electromagnetic Inverse Scattering, Polarization Utilization in radar target identification and shape reconstruction

July 81

Temporarily involved in the balloon lauching project of NRCC in the investigation of powerline low frequency radiation to the earth 's atmosphere

Mar 81 - June 81

Position - Teaching Assistant in electromagnetic theories

ACADAMIC HONORS :

1974 - 1978

Dean's Honor List in Civil Engineering
University of Manitoba

PUBLICATIONS :

(1) W-M Boerner, Chuk-Min Ho and Bing-yuen Foo, " Use of Radon's Projection Theory in electromagnetic Inverse Scattering ", special issue, IEEE, vol. AP-29, Mar. 81
(2) W-M Boerner, M. B. El-Arini, C. Y. Chan, S. S. Saatchi, Bing-Yuen Foo " Polarization Utilization in Radar Classification and Imaging " Electromagnetic Imaging Division, Communications Laboratory, Information Engineering Dept., U.I.C.C., 1981
(3) W-M Boerner, M. B. El-Arini, C. Y. Chan, S. S. Saatchi, W. S. Ip, P. M. Mastoris, Bing-Yuen Foo " Polarization Utilization in Radar Target Reconstruction " Technical Report, UICC, CL-EMID-NANRAR-81-01 Jan. 81
(4) S. K. Chaudhuri, B-Y. Foo, W-M Boerner, "A High Frequency Inverse Scattering Model to Recover the Specular Point Curvature from Polarimetric Scattering Matrix Data", University of Waterloo, Canada /University of Illinois at Chicago, Dec. 1981, (In print)

PROFESSIONAL ACTIVITIES :

Dec 80 - present

Student member of IEEE

Jan 82 - present

Member of American Association for the Advancement of Science

HOBBIES :

Table Tennis, Tennis, Badminton

COLLEGE OF ENGINEERING

UNIVERSITY OF ILLINOIS AT CHICAGO CIRCLE

M.S. THESIS DEFENSE

DATE: Friday, May 21, 1982

TIME: 1:00 p.m.

PLACE: 1127 SEO

SPEAKER: Bing-Yuen (Thomas) Foo

TITLE: "A High Frequency Inverse Scattering Model to Recover the Specular Point Curvature from Polarimetric Scattering Data"

ABSTRACT: Based on the time-domain first order correction to the physical optics current approximation, a relationship between the phase factors of the polarimetric scattering matrix elements and the principal curvatures at the specular point of a scatterer is established.

The above phase-curvature relationship is tested by applying it to theoretical as well as experimental backscattering data obtained for a prolate spheroidal scatterer. The results of these tests not only determine the acceptability of the phase-curvature relationship, they also point out the range of kb values over which the first order correction to the physical optics currents is valid, and which serves as a compromise range between the high frequency condition required by the curvature recovery model and the drawback to lower frequencies required to prevent critical magnification of measurement errors.

Another curvature recovery equation is derived by transforming the linear polarization basis to the circular polarization basis. The curvature recovery model is proven to satisfy the image reconstruction identities of invariant transformation. A scattering ratio is defined and its behavior is investigated at high frequencies. Its plots on the complex plane provides a simple way to help judge the accuracy of polarimetric scattering measurement, regardless of whether a linear or a circular polarization basis is used.

DEPARTMENT OF INFORMATION ENGINEERING

FILMED

7-8